APPENDIX 3.9.1
DSC SHELL STRUCTURAL ANALYSIS

Table of Contents

List of Tables

List of Figures

3.9.1 DSC SHELL STRUCTURAL ANALYSIS

The purpose of this appendix is to present the structural evaluation of the shell assembly of the EOS-37PTH dry shielded canister (DSC) and the EOS-89BTH DSC under all applicable normal, off-normal and accident loading conditions during storage in the EOS horizontal storage module (HSM) and during transfer in the EOS transfer cask (TC). The EOS system consists of the EOS-HSM, the EOS-TC, the dual-purpose (transportable/storage) EOS-37PTH and EOS-89BTH DSC, and associated ancillary equipment.

The design of the DSC includes five design options: EOS-37PTH (short, medium and long) and EOS-89BTH (short and medium). The longest and heaviest EOS-37PTH DSC, which uses TC135 for transfer operations, is analyzed to bound all DSC design options in the NUHOMS® EOS System.

3.9.1.1 General Description

The DSC consists of a fuel basket and a shell assembly. The DSC pressure boundary consists of DSC shell with two cover plates at each end. Non-pressure boundary shield plugs are included at each end of the assembly. The inner bottom shield (IBS) is confined between the inner bottom cover plate (IBCP) and outer bottom cover plate (OBCP). The top shield plug (TSP) is confined by the inner top cover plate (ITCP) and four lifting lugs, which are welded to the inside of the DSC shell. The grapple ring support is welded to the OBCP using full penetration weld. The ITCP is welded along the top perimeter with partial penetration weld. The IBCP is welded using a full penetration weld. Grapple ring assembly connections are all made using full penetration welds.

The DSC shell thickness is 0.50 inch, and the top and bottom closure assemblies are 10.0 inches and 8.0 inches, respectively. The DSC shell is constructed entirely from stainless steel or duplex steel. There are no penetrations through the pressure boundary. The draining and venting systems are covered by the port plugs. The outer top cover plate (OTCP) and the ITCP are welded to the cylindrical shell with multilayer welds. The DSC cavity is pressurized above atmospheric pressure with helium. The DSC shell assembly geometry and the materials used for its analysis and fabrication are shown on drawings EOS01-1000-SAR, EOS01-1001-SAR, EOS01-1005-SAR and EOS01-1006-SAR included in Chapter 1.

3.9.1.2 DSC Shell Assembly Stress Analysis

An enveloping technique of combining various individual loads in a single analysis is used in this evaluation for several load combinations. This approach reduces the number of computer runs, while remaining conservative. For some load combinations, stress intensities under individual loads are added to obtain resultant stress intensities for the specified combined loads. This addition at the

stress intensity level for the combined loads, instead of at component stress level, is also a conservative method for reducing the number of analysis runs.

The stresses of all components are assessed by means of elastic analysis methodology for all load combinations, except *for most accident loading conditions*. Elastic-plastic analysis methodology is used to assess the stresses for Service Level D load *combinations, except for the end drop load combinations*.

A detailed description of each load combination is provided in Section 3.9.1.2.7.

3.9.1.2.1 Material Properties

For elastic analysis, temperature dependent material properties used for each component of DSC shell assembly are obtained from the American Society of Mechanical Engineers (ASME) code [3.9.1-2], and are summarized in Chapter 8. Material properties used for stress evaluations are conservatively taken at 500 °F.

For plastic analysis, a bilinear stress-strain curve with a 5% tangent modulus is used for steel components. The non-linear material properties at 500 °F for side drop analysis are shown in Table 3.9.1-3. Steel material (except shield plugs) is modeled by bilinear kinematic hardening method (TB, BKIN – [3.9.1-9]).

3.9.1.2.2 DSC Shell Stress Criteria

The calculated stresses in the DSC shell assembly structural components are compared with the allowable stresses set forth by ASME Boiler and Pressure Vessel (B&PV) Code, Section III, Subsection NB [3.9.1-3] under normal (Level A), and off-normal (Level B) loading conditions. Appendix F of the ASME B&PV Code is used to evaluate the calculated stresses in the DSC shell assembly under accident (Level D) loading conditions. Allowable stress limits for Levels A, B and D service loading conditions, as appropriate, are summarized in Table 3-1, and the corresponding allowable stress values at different temperatures are summarized in Table 3.9.1-5.

The OTCP-to-DSC shell weld and the ITCP-to-DSC shell weld, which are both partial penetration welds, are to be evaluated using a joint efficiency factor of 0.8. Per NUREG-1536 [3.9.1-7], the minimum inspection requirement for end closure welds is multi-pass dye penetrant testing (PT) using a stress (allowable) reduction factor of 0.8. The allowable weld stresses are summarized in Table 3.9.1-4.

Proprietary Information on Pages 3.9.1-3 through 3.9.1-7
Withheld Pursuant to 10 CFR 2.390

3.9.1.2.6 Load Cases for DSC Shell Stress Analysis

This section discusses the different load cases considered to evaluate the stresses generated in the EOS-37PTH DSC and EOS-89BTH DSC shell assembly during transfer operations and in storage conditions under normal, off-normal and accident loading. During fuel transfer, the DSC is oriented horizontally inside the EOS-TC, which is mounted to the transfer skid and transferred from the reactor or fuel building to the independent spent fuel storage installation (ISFSI). During storage, the DSC is in the horizontal position within EOS-HSM.

Each load case analysis utilizes the *FEM* that is described in Section 3.9.1.2.3, along with pertinent loads and boundary conditions. Bounding storage load cases, transfer load cases and load combinations used to evaluate the DSC shell assembly are tabulated in Table 2-5. In general, major loads (ram push/pull loading with internal/external pressure) are combined within the ANSYS analyses, while stress intensities from minor loads (i.e. dead weight and pressure) are added algebraically.

3.9.1.2.6.1 *Dead Weight*

The dead weight is analyzed for the following three basic configurations:

- *When the DSC is vertical in the EOS-TC135,*
- *When the DSC is horizontal in the EOS-TC135,*
- *When the DSC is horizontal in the EOS-HSM.*

The model for the EOS-TC135 and EOS-HSM differ in boundary conditions representing support rails.

Vertical in EOS-TC

The DSC shell supports the entire weight of the top end components in addition to its self-weight. The weight of the fuel is assumed to be uniformly distributed over the area of the IBCP. The fuel load and the weight of the bottom end components are transferred directly to the ground through bearing between the IBCP, IBS, and OBCP.

The bottom end surface of the EOS-TC135 is constrained in the vertical direction. The contact elements are generated between DSC shell and OBCP outermost nodes (excluding the surface of OBCP, which is bounded by the grapple ring support) and the EOS-TC135 surface. The payload of 105 kips is applied as uniform pressure acting on the IBCP.

Horizontal in EOS-TC

When the DSC is in a horizontal position, the end components and basket assembly bear against the DSC shell.

The inertial loads for DSC internals are accounted for by applying an equivalent pressure on the inside surface of the DSC represented by the projection of first 6.5° support rail only. This pressure is determined based on the payload of 105 kips and the projected area of the DSC shell that is in interface with the EOS-TC135 support rail. Figure 3.9.1-7 shows the pressure load and boundary conditions applied to the FEM.

The interface between the DSC and the EOS-TC135 support rails is modeled through node-to-node contact elements (CONTA178). Nodes that interface with the rails are selected and copied, creating new nodes that are restrained in all DOF and connected to the original nodes belonging to the DSC shell through the CONTA178 contact elements.

Three sets of rails, at 6.5°,17.5° and 25.5°, are modeled in the FEM. The 6.5° rail is modeled as contacts with closed gaps between the DSC shell and the EOS-TC135 rail. For the second and third rail, at 17.5° and 25.5°, respectively, from the plane of symmetry, contact elements between the rail nodes and the DSC shell nodes are created through the same type of contact element, but the real constant of these elements is modified to the true geometric gap value between the DSC shell and the EOS-TC135 rail.

Horizontal Position in EOS-HSM

When stored in the EOS-HSM, the DSC shell is supported by two, 3-inch wide EOS-HSM slide rails at ±30° from the bottom centerline. The inertial loads for DSC internals are accounted for by applying equivalent pressure onto the inner surface of DSC shell representing the EOS-HSM support rail only. The magnitude of the pressure is determined based on the payload of 105 kips and projected area that are in interface with the EOS-HSM support rail.

The interface between the DSC and the EOS-HSM support rail is modeled through node-to-node contact elements (CONTA178). Nodes that interface with the EOS-HSM support rail are selected and copied, creating new nodes. Each row of nodes represents the width of the EOS-HSM support rail (there are three nodes across the width of the rail). Each node of the row is coupled with its neighboring node in all DOF using CERIG command, creating a rigid platform. Figure 3.9.1-7 shows the pressure load and boundary conditions applied to the FEM.

Each middle node of this platform is connected in the axial direction of the DSC through BEAM188 element. Finally, these new nodes representing the EOS-HSM are connected to the original nodes belonging to the DSC shell through the CONTA178 contact elements. Gaps are set to zero, placing the DSC shell and the EOS-HSM support rail in initial contact. Nodes representing the EOS-HSM support rail are constrained in all DOF along a length of 16.5 inches from bottom end and 20.5 inches from the top end. The BEAM188 elements have the properties of the wide-flange steel beam that supports the DSC when inside the EOS-HSM. Therefore, the flexibility of the support beam is considered in the analysis.

3.9.1.2.6.2 Fabrication Pressure and Leak Testing

Pressurization and leak testing is performed on the DSC shell and IBCP during fabrication. No other DSC components are in place during this test. A seal plate is placed on the open top of the DSC shell and preloaded through the application of torque on eight bolts that are connected with a flange at the bottom of the DSC shell. The resulting preload to be considered in the evaluation is 155 kips. The DSC is then evacuated to a partial vacuum (simplified to full vacuum) and then re-pressurized with helium. Therefore, two load conditions are evaluated for the DSC shell and IBCP:

1. *Leak Test: 155 kip axial compression + 14.7 psi external pressure (full vacuum) on the DSC shell between the top edge and the IBCP + 14.7 psi external pressure on the IBCP. Note that the vacuum will add axial load to the 155 kips preload.*

2. *Pressure Test: 155 kip axial compression + 23.0 psig internal pressure on the DSC shell between the top edge and the IBCP + 23.0 psig internal pressure on the IBCP. Note that the internal pressure will not affect the reaction on the DSC shell due to the preload.*

In order to simulate the leak testing conditions, the OTCP, ITCP and OBCP, TSP and IBS, grapple ring and its support are removed from the FEM, including all contact pair elements.

The bottom surface of the DSC shell surface is constrained in the vertical direction. The 155 kips load is represented by equivalent pressure that is applied at the top surface of the DSC shell.

External pressure is applied at all external nodes of the DSC shell-IBCP assembly with the exception of the top surface of the DSC shell that is loaded with the 155 kips preload. Internal pressure is applied at all nodes on the inside surface of the DSC shell-IBCP assembly. Two load steps are performed, one for the internal pressure and the second one for the external pressure as stated above.

3.9.1.2.6.3 Internal and External Pressure

The DSC pressure boundary is defined by the DSC shell, the IBCP, the ITCP and the associated welds. Since there are no gaps between the top end plate components, the ITCP bears against the OTCP. Since the ITCP meets the leaktight requirements of ANSI N14.5, no leakage is feasible and, therefore, the pressure load is shared by the two plates according to their relative stiffness. Similarly, the absence of gaps between the bottom end components allows the IBCP to bear against the IBS, which, in turn, bears against the OBCP.

Normal (Level A)	*15 psig (Elastic)*
Off-Normal (Level B)	*20 psig (Elastic)*
Accident (Level D)	*130 psig (Elastic-plastic)*

A bounding pressure of 30 psig was used for normal and off-normal conditions. Two load cases were analyzed: one with an internal pressure of 30 psig and the second with an internal pressure of 130 psig.

All of the nodes of the inner surface of DSC shell confined by ITCP and IBCP are selected for application of internal pressure. A node of the grapple is constrained in axial (z-direction) and vertical (x-direction) directions and a node of the OTCP is also constrained in the vertical direction to prevent rigid body motion. Figure 3.9.1-6 shows the internal pressure applied onto the inside of the DSC cavity.

In addition to the internal pressure loads listed above, the DSC will be subjected to hydrostatic, blowdown, vacuum, and test pressures during the fuel loading and draining/drying processes. Prior to loading fuel and without the top end components in place, the TC/DSC annulus is filled with water resulting in a hydrostatic external load on the DSC shell. The hydrostatic load is then balanced by filling the DSC with water.

After the fuel is loaded, the TSP and ITCP are installed and an internal blowdown pressure of 15 psig is applied to evacuate the DSC of water. The DSC internals are then dried under vacuum conditions. The DSC is backfilled with helium at 20 psig. The pressure is then reduced to 3.5 psig and the OTCP is welded in place.

External pressure is applied at all external nodes of the DSC at a level below 12 inches from the top of the DSC. Internal pressure is applied at all surface nodes inside the DSC from the inside of the IBCP up to the ITCP-DSC shell weld. Nodes in contact between the lifting lugs and the DSC shell are not subject to pressure load. Contact elements are modeled on the lateral surface of the shell and the bottom of the OBCP.

Two load steps are performed for the blowdown/pressure test and the vacuum drying with combinations of internal and external pressures without the OTCP installed. Figure 3.9.1-14 and Figure 3.9.1-15 show the stress results for normal and accident internal pressure load cases.

3.9.1.2.6.4 EOS-HSM Loading/Unloading

To load the DSC into the EOS-HSM, the DSC is pushed out of the EOS-TC using a hydraulic ram. The load is applied at the center of the OBCP within the diameter of the grapple ring support. Based on the relative stiffnesses of the cover plates and the IBS, a portion of the insertion load will be transferred through the IBS to the IBCP and associated welds.

Loading is defined as:

Level A/B/C/D: 135 kips (Ram Push)

Unloading (grapple) loads are defined as:

Level A/B: 80 kips (Grapple Pull)

Level C/D: 135 kips (Grapple Pull)

To unload the EOS-HSM, the DSC is pulled using grapple hooks, which engage the grapple ring. The loads applied by the hydraulic ram are balanced by friction between the DSC shell and the EOS-TC135 and/or EOS-HSM rails.

For the grapple push simulation, the cask is modeled by copying the outer surface nodes of the DSC, creating a new pattern of nodes representing the cask inner surface. These new nodes are restrained in all DOF and connected to the original nodes belonging to the DSC shell through the CONTA178 contact elements. Furthermore, gaps are set to zero at the first rail placing the DSC and the first rail in initial contact. Real constants of contact elements at the second and third rail are set to the gap calculated based on the nodal coordinates of the contact element nodes on both the DSC side and the rail side.

The outer top nodes of the DSC shell are constrained in the axial direction and a node of the ITCP is constrained in the vertical direction to aid in convergence. The insertion force is modeled through a uniform pressure applied within the inner diameter of the grapple support. Three load cases were analyzed: one with a push load of 135 kips, the second with an internal pressure of 30 psig and a push load of 135 kips, and the third with a 130 psig accident pressure and a push load of 135 kips. Table 3.9.1-12 lists the load conditions. Figure 3.9.1-10 shows the load and boundary conditions applied to the FEM.

For the grapple pull simulation, the outer top nodes of the DSC shell are constrained in the axial direction and a node of ITCP is constrained in the vertical direction to aid in convergence. The extraction force is modeled through nodal forces applied on selected nodes within the footprint of the grapple hook. Five load cases were analyzed combining pressure loads and are described in the table below. Refer to Table 3.9.1-12 for load combinations. Figure 3.9.1-9 shows the load and boundary conditions applied to the FEM.

Internal Pressure	***Pull Force (kips)***	***Analysis Type***
0	*80*	*Elastic*
30	*80*	*Elastic*
0	*135*	*Elastic-plastic*
30	*135*	*Elastic-plastic*
30	*80*	*Limit Load Elastic-perfectly plastic*

*For the normal condition pull load cases, a limit load analysis is performed to show that the stresses at the junction between the grapple ring support and the outer bottom cover plate are secondary stresses. The limit load analysis is described in NB-3228.1 [3.9.1-2]. The grapple ring assembly is acceptable for the normal pull load if the lower bound limit load (LL) is equal to or greater than 1.5 times the normal pull load (2/3 * LL) without any excessive deformation and plastic strain. The lower bound limit load is determined using elastic-perfect plastic material properties with a yield strength defined as $1.5S_m$. The last converged load step for the limit load analysis corresponds to a 200 kip axial pull load, which is greater than 1.5*80 kip = 120 kip.*

3.9.1.2.6.5 *Transfer/Handling Load*

The same model described in Section 3.9.2.1.6.1 is used and updated to reflect the effect of the vertical 1g load, transverse 1g load, axial 1g load and internal pressure of 30 psig.

Two runs were performed for this load:

1. *Deadweight +1g vertical + 1g transverse + 1g axial with the weight of DSC internals modeled by equivalent pressure application on TSP with addition of internal pressure of 30 psig.*

2. *Deadweight +1g vertical + 1g transverse + 1g axial with the weight of DSC internals modeled by equivalent pressure application on IBCP with addition of internal pressure of 30 psig.*

3.9.1.2.6.6 Seismic Load during Storage

The same model described in Section 3.9.1.2.6.1 for dead weight in EOS-HSM is used and updated to reflect the effect of the vertical 3g load, transverse 3g load, axial 3g load and internal pressure of 30 psig.

Two elastic-plastic runs are performed for this load:

1. *3g vertical + 3g transverse + 3g axial with the weight of DSC internals modeled by equivalent pressure application on TSP with addition of internal pressure of 30 psig.*

2. *3g vertical + 3g transverse + 3g axial with the weight of DSC internals modeled by equivalent pressure application on IBS with addition of internal pressure of 30 psig.*

The dead weight and 3g vertical and 3g transverse effect is modeled by multiplying the pressure projected at the EOS-HSM support rail through the DSC shell by factor of 5 = SQRT[$(3g+1g)^2$ + $(3g)^2$].

DSC support within an EOS-HSM is provided by two, 3.00-inch wide rails at ± 30° from the bottom centerline. Seismic axial forces toward the EOS-HSM door are resisted by the axial retainer. The retainer is a 4-inch x 2-inch steel bar located on the vertical centerline, at the edge of the DSC shell below the center of the DSC. The retainer bears against the edge of the DSC shell and OBCP. The nodes of DSC shell and OBCP, which bears against the area of the retainer bar, are restrained in the axial direction. Figure 3.9.1-13 shows the pressure load and boundary conditions applied to the FEM.

The DSC shell and the OBCP experience compressive bearing stress in the vicinity of the axial retainer. The bearing stresses experienced by the DSC shell and OBCP need not be evaluated for Service Level D loads.

Seismic axial forces away from the EOS-HSM door are resisted by the canister stop plates located at the ends of the support rails. The stop plates are 11 inches wide. Because the top cover plate is recessed from the edge of the DSC shell, the stop plates bear against the bottom edge of the DSC shell only. The nodes of the top end of DSC shell, which come into contact with the DSC stop plate, are restrained in the axial direction. Figure 3.9.1-18 shows the stress results for seismic load acting towards the stop plates of the EOS-HSM support rails.

3.9.1.2.6.7 Cask Drop

Side and end drop accelerations of 75g are applied. Drops are only postulated for the DSC when positioned inside of the EOS-TC135. The following accident drops are analyzed:

- *65-inch side drop of the TC onto a concrete pad above a generic soil profile.*
- *A corner drop from a height of 65 inches at an angle of 30° to the horizontal, onto the top or bottom corner of the TC (two cases) using the bounding deceleration based on a 65-inch drop.*

The top end drop and bottom end drop are not credible events under 10 CFR Part 72; therefore, these drop analyses are not required. However, consideration of end drops (for 10 CFR Part 71 conditions) and the 65-inch side drop is performed to conservatively envelope the effects of a corner drop.

In summary, three drop conditions are considered in the analyses:

- *75g bottom end drop*
- *75g top end drop*
- *75g side drop*

End Drop

For the bottom end drop, the interface between the bottom surface of DSC shell and OBCP (excluding the OBCP surface, which falls inside the grapple ring support) with the EOS-TC135 is modeled through CONTA178 node-to-node contact elements. The nodes of the EOS-TC135 are constrained in the vertical direction representing TC as a rigid surface. The payload is applied as a load of 105 kips multiplied by 75. The inertial load of the basket assembly and fuel is applied as uniform pressure acting on the IBCP. An elastic material model is used in the analysis. In addition to pressure representing the payload inertia load, conservative internal pressure of 30 psig is added.

For the bottom end drop, the couplings (CP) representing the welds between the lug plate and the DSC shell are deleted from the model and these welds are modeled by spring elements (COMBIN14). Figure 3.9.1-12 shows the pressure load and boundary conditions applied to the FEM.

Two load cases are performed for bottom end drop:

- *Bottom end drop without internal pressure*
- *Bottom end drop with internal pressure*

For the top end drop, the interface between the top surface of the DSC and the EOS-TC135 is modeled through CONTA178 node-to-node contact elements. The nodes of the EOS-TC135 (node position 2 of CONTA178 elements) are constrained in all directions representing TC as a rigid surface. The payload is applied as a total load of 105 kips multiplied by 75g. The inertial load of the basket assembly and fuel is applied as uniform pressure acting on the bottom side of the TSP. An elastic material model is used in the analysis. In addition to pressure representing the payload inertial load, this load case includes a 30 psig internal pressure in the model, as opposed to adding the internal pressure load case later.

Two load cases are performed for top end drop:

- *Top end drop without internal pressure*
- *Top end drop with internal pressure*

Figure 3.9.1-17 shows the stress results for end drop without internal pressure.

Side Drop

The side drop analysis of the DSC shell assembly is simplified by considering the distribution of the basket load to the DSC as uniform. The basket is flexible enough to deform under the action of 75g deceleration of its contents and, therefore, during an accident side drop, the basket will tend to bend under the action of the higher g-loads on its contents. This results in a uniform radial pressure load applied to the inner surface of the DSC to represent the basket load.

An elastic-plastic analysis was performed for side drop analysis. For elastic-plastic analyses, the steel components (except shield plugs) are modeled by a bilinear kinematic hardening method. At the specified yield stress, the curve continues along the second slope defined by the plastic modulus. It is assumed that the plastic modulus is 5% of the elastic modulus, except for shield plugs, which are modeled with elastic material properties.

Side Drop on Cask Rails

A uniform pressure load is applied to the DSC inner surface. The inner nodes of the DSC are selected from 0° to 45° and a uniform pressure is applied. The interface between the DSC and the EOS-TC135 is modeled through node-to-node contact elements CONTA178. Nodes that interface with the DSC are selected and copied, creating new pattern of nodes. These new nodes are restrained in all DOF and connected to the original nodes belonging to the DSC shell through the CONTA178 contact elements. Gaps are set to zero at the 6.5° and 17.5° rail, placing the DSC and the 6.5° and 17.5° rail in initial contact. Real constants of contact elements at the 25.5° rail are set to a gap calculated based on the nodal coordinates of the contact element node at the DSC side and the rail side. The small radial gaps between the shield plugs and the DSC shell are set to zero, since during a side drop event these gaps will close.

In addition to pressure representing the payload inertial load, this load case includes a 30 psig internal pressure in the model, as opposed to adding the internal pressure load case later.

Two load cases are analyzed for the side drop onto the cask rail:

- *Side drop onto the cask rail without internal pressure*
- *Side drop onto the cask rail with internal pressure*

Side Drop Away From Cask Rails

The interface between the DSC and the EOS-TC135 is modeled through node-to-node contact elements CONTA178. Nodes that interface with the DSC are selected and copied, creating new pattern of nodes. These new nodes are restrained in all DOF and connected to the original nodes belonging to the DSC shell through the CONTA178 contact elements. Gaps between the DSC shell and the cask inner surface are set to the gap calculated based on nodal coordinates of the contact element node at the DSC side and the cask side. At the point where the DSC contacts the rigid cask, the initial contact gap is zero. Circumferentially away from this initial contact point, the initial contact gap increases. The small radial gap between the shield plugs and the DSC shell is set to zero since during a side drop event, this gap will close.

In addition to pressure representing the payload inertial load, this load case includes a 30 psig internal pressure in the model, as opposed to adding the internal pressure load case later. Figure 3.9.1-11 shows the load and boundary conditions applied to the FEM.

Two load cases are analyzed for side drop away from the cask rail:

- *Side drop away from the cask rail without internal pressure*
- *Side drop away from the cask rail with internal pressure*

Figure 3.9.1-16 shows the stress results for side drop away from cask rails without internal pressure.

3.9.1.2.6.8 *Thermal Loads*

Per Chapter 4, the thermal storage load cases have lower temperature gradients in the DSC shell compared to thermal transfer load cases. Therefore, only bounding off-normal thermal transfer load cases have been selected for thermal stress analysis of the EOS-37PTH DSC.

For thermal stress analysis, temperature profiles and maximum component temperatures are based on the thermal analyses of the EOS-37PTH DSC in TC125 for transfer conditions, which is discussed in Chapter 4. Only the off-normal load cases with higher temperature gradients in the DSC shell are taken for thermal stress analysis.

Since the TC125 is shorter than TC135, there is a higher temperature distribution in TC125. Therefore, the thermal analysis of the EOS-37PTH in TC125 bounds the thermal analysis of EOS-37PTH in TC135. The thermal conditions have been evaluated separately to minimize the number of analyses to be performed. For all DSC components, the thermal stresses have been combined by adding the maximum stress intensities of components from thermal load runs to the primary membrane plus bending stresses of components from mechanical load runs.

Thermal stresses are classified as secondary stresses per the ASME Code, [3.9.1-3]. These secondary stresses are a result of dissimilar material properties, primarily differential thermal growth of a structure due to material thermal expansion coefficient differences between different materials used for construction of the structure, or differential temperature distribution throughout the structure, or a combination of both.

Nodal temperature from thermal analyses is transferred to the structural model described in Section 3.9.1.2.3. The structural model is solved and stresses of thermal load of each load step are post-processed and the largest stresses for all the transfer cases are selected. Only the largest selected stresses are used for further stress evaluation and stress combination.

3.9.1.2.7 Load Combinations

The bounding load combinations, along with the applicable ASME service level, are listed in *Chapter 2,* Table 2-5 for the shell assembly. Stresses generated by applied loads described in Section *3.9.1.2.6.1* are combined in a manner that bounds all load conditions under consideration. *The methodologies for combining the load cases into their corresponding load combinations are described in the following sections.*

Load Combination 1

Load Combination 1 (LC1) addresses the DSC when it is in a vertical position. LC1 is developed by adding the linearized stress intensities of a vertical dead weight load case, an internal pressure of 30 psig within the DSC and the maximum stress intensities due to thermal loading.

Load Combinations 2 and 3

Load Combinations 2 and 3 (LC23) addresses the DSC when it is in a horizontal position. LC23 is developed by adding linearized stress intensities from a model comprised of the dead weight, an internal pressure of 30 psig within the DSC and handling loads with thermal loads.

Load Combination 4

Load Combination 4 (LC4) addresses the DSC when it is in a horizontal position. LC4 describes a hydraulic ram push case. The stress intensities from the dead weight load case, the 135-kip insertion load cases and thermal load cases are determined independently and subsequently added together to develop the maximum stress intensity on the DSC components and welds. The 135-kip insertion model evaluates the system with and without a 30-psig internal pressure load.

Load Combination 5

Load Combination 5 (LC5) addresses the DSC when it is in a horizontal position. LC5 describes a hydraulic ram pull case. The stress intensities from the dead weight load case, the 80-kip retrieval load cases and thermal load cases are determined independently and subsequently added to develop the maximum stress intensity on the DSC component and weld. The 80-kip retrieval model evaluates the system with and without a 30-psig internal pressure load.

Load Combination 6

Load Combination 6 (LC6) addresses the DSC when it is in a horizontal position. LC6 describes a hydraulic ram pull case. The stress intensities from the dead weight load case and the 135-kip retrieval load cases are determined independently and subsequently added to develop the maximum stress intensity on the DSC component and weld. The 135-kip retrieval model evaluates the system with and without a 30 psig internal pressure load.

Load Combination 7A

Load Combination 7A (LC7A) addresses the DSC when it is in a horizontal position. LC7A describes the 65-inch accident drop condition. LC7A is developed by post-processing the stresses from a FEM that includes the 30-psig off-normal internal pressure load and the 75g side drop load.

Load Combination 7B

Load Combination 7B (LC7B) addresses the DSC when it is in a vertical position. LC7B describes the 65-inch accident drop condition. LC7B is developed by post-processing the stresses from a FEM that includes the 30-psig off-normal internal pressure load and the 75g end drop load.

Load Combination 8

Load Combination 8 (LC8) addresses the DSC when it is in the horizontal position. LC8 describes the accident internal pressure load case. The stress intensities from the dead weight load case and the 130-psig internal pressure load case are determined independently and subsequently added to develop the maximum stress intensity on the DSC component and weld.

Load Combination 9

Load Combination 9 (LC9) addresses the DSC when it is in the horizontal position. LC9 describes the off-normal internal pressure load case. The stress intensities from the dead weight load case, 30-psig internal pressure load case and thermal load cases are determined independently and subsequently added to develop the maximum stress intensity on the DSC component and weld.

Load Combination 10

Load Combination 10 (LC10) addresses the DSC when it is in the horizontal position. LC10 describes the seismic load case. LC10 is developed by post-processing the stresses from an FEM that includes the internal off-normal pressure loads and the seismic loads.

Load Combination 11

Load Combination 11 (LC11) addresses the DSC when it is in the vertical position. LC11 describes the fabrication pressure and leak testing loads. LC11 is developed by post-processing the stresses from stresses from the fabrication pressure/leak test load case.

3.9.1.3 DSC Shell Buckling Evaluation

An FE plastic analysis with large displacement option is performed to monitor occurrence of canister shell buckling under the specified loads.

The bottom end drop envelopes the top end drop because the top end structure is heavier than the bottom end structure, which will impose a larger load on the *DSC shell*. A drop on the bottom end is therefore chosen for buckling analysis.

The buckling analysis uses the same model as the end drop simulation.

The inertia load of the basket assembly and fuel is applied as uniform pressure acting on the IBCP. Elastic-plastic bilinear kinematic hardening material model is used at a uniform temperature of 500 °F with a plastic tangent modulus conservatively taken at 1% of the elastic modulus for buckling. Conservatively, no internal pressure that could have a stabilizing effect is applied. Large deformation effect NLGEOM is enabled in the ANSYS model.

Uniform pressure at the IBCP that represents the payload is multiplied by acceleration as g-factor that is incrementally increased by 5g with every load step. 50 load steps are defined, which correspond to total load of 250g. The last converged load step represents the stability limit load.

Load step # 27 corresponding to 130g load is the last saved converged solution. Two thirds of the maximum compressive load of 130g is equal to 87g limit load per F-1331.5 of Appendix F, [3.9.1-3], which is higher than required load of 75g. It is therefore concluded that buckling of the DSC will not occur during a hypothetical accident end drop.

3.9.1.4 DSC Fatigue Analysis

Fatigue effects on the EOS-37PTH DSC is addressed using NB-3222.4 criteria of [3.9.1-3]. Fatigue effects need not be specifically evaluated, provided the criteria contained in NB-3222.4(d) are met. A summary of the six criteria and their application to the DSC is presented below:

A. The first criterion states that the DSC is adequate for fatigue effects, provided that the total number of atmospheric-to-operating pressure cycles during normal operation (including startup and shutdown) does not exceed the number of cycles on the applicable fatigue curve corresponding to a S_a value of three times the S_m value of the material at operating temperatures. This condition is satisfied for the DSC since the pressure is not cycled during its design life. The pressure established at the time that the DSC is sealed following fuel loading and DSC closure operations is maintained during normal storage in the EOS-HSM.

B. The second criterion states that DSC is adequate for fatigue effects, provided that the specified full range of pressure fluctuations during normal operation does not exceed the quantity (1/3) x design pressure x (S_a/S_m), where S_a is the value obtained from the applicable fatigue curve for the total specified number of significant pressure fluctuations, and S_m is the allowable stress intensity for the material at operating temperatures.

Significant pressure fluctuations are those for which the total excursion exceeds (1/3) x design pressure x (S/S_m), where S equals the value of S_a for 10^6 cycles. Using a design pressure of 20.0 psig, an S_m value of 17,500 psi, and an S value of 28,200 psi, the total range for a significant pressure fluctuation is 10.7 psig. This pressure fluctuation is not expected to occur during normal storage as a result of seasonal ambient temperature changes.

Ambient temperature cycles significant enough to cause a measurable pressure fluctuation are assumed to occur five times per year for 80 years. The number of fluctuations with this pressure range is expected to be 400 for the DSC. The value of S_a associated with this number of cycles is 170 ksi. Therefore, the value of (1/3) x design pressure x (S_a/S_m) is equal to 64.76 psig. Clearly, this value will not be exceeded during the pressure fluctuation of the DSC. Therefore, the second criterion is satisfied for the DSC.

C. The third criterion states that the DSC is adequate for fatigue effects, provided that the temperature differences between any two adjacent points on the DSC during normal operation do not exceed $S_a/2E\alpha$, where S_a is the value obtained from the applicable fatigue curve for the specified number of startup-shutdown cycles, α is the instantaneous coefficient of thermal expansion at the mean value of the temperatures at the two points, and E is the modulus of elasticity at the mean value of the temperatures at the two points.

   For an operational cycle of the DSC, thermal gradients occur during fuel loading, DSC closure, transport to the EOS-HSM, and transfer of the DSC to the EOS-HSM. This half-cycle is approximately reversed for DSC unloading operations. However, this normal operational cycle occurs only once in the design service life of a DSC. Since there is only one startup-shutdown cycle associated with the DSC, the value of S_a is very large (>800 ksi). Therefore, the value of $S_m/2E\alpha$ is very large (>1500°F). This is far greater than the temperature difference between any two adjacent points on the dry shielded canister. Therefore, the third criterion is satisfied for the DSC.

D. The fourth criterion states that the DSC is adequate for fatigue effects, provided that the temperature difference between any two adjacent points on the DSC does not change during normal operation by more than the quantity $S_a/2E\alpha$, where S_a is the value obtained from the applicable fatigue curve for the total specified number of significant temperature difference fluctuations.

   A temperature difference fluctuation is considered to be significant if its total algebraic range exceeds the quantity S/2Eα where S is value of S_a (28,200 psi) obtained from the applicable fatigue curve for 10^6 cycles if the number of cycles is 10^6 or less.

Small fluctuations in the DSC thermal gradients during normal storage in the EOS-HSM occur as a result of seasonal ambient temperature changes. Ambient temperature cycles significant enough to cause a measurable thermal gradient fluctuation are assumed to occur five times per year for 80 years. The temperature gradient fluctuation is 250 cycles. Since this is less than 10^6 cycles, the value of $S/2E\alpha$ at 10^6 cycles is 112.7 °F.

The most significant fluctuation in normal operating temperature occurs during a change in ambient temperature from -20° F to 100 °F. A review of thermal evaluation of EOS-HSM loaded with EOS-37PTH DSC storage load cases in Chapter 4 concluded that the temperature difference between adjacent points in the DSC does not exceed the quantity 112.7 °F, therefore the fourth condition is satisfied for the DSC.

E. The fifth criterion states that for components fabricated from materials of differing moduli of elasticity or coefficients of thermal expansion, the total algebraic range of temperature fluctuation experienced by the component during normal operation must not exceed the magnitude $S_a/2(E_1\alpha_1 - E_2\alpha_2)$, where S_a is the value obtained from the applicable fatigue curve for the total specified number of significant temperature fluctuations, E_1 and E_2 are the moduli of elasticity, and α_1 and α_2 are the values of the instantaneous coefficients of thermal expansion at the mean temperature value involved for the two materials of construction.

A temperature fluctuation is considered to be significant if its total excursion exceeds the quantity $S/2(E_1\alpha_1 - E_2\alpha_2)$, where S is the value of S_a obtained from the applicable fatigue curve for 10^6 cycles. If the two materials have different applicable design fatigue curves, the lower value of S_a has to be used. Since the structural material used to construct the DSC shell is 240 Type 304 and shield plug is A-36, therefore taking the values of $E_1 = 25.9 \times 10^6$ psi, $E_2 = 27.3 \times 10^6$, $\alpha_1 = 10.5 \times 10^{-6}$ and $\alpha_2 = 8.0 \times 10^{-6}$ (Section II, Part D, [3.9.1-2]), the quantity $S/2(E_1\alpha_1 - E_2\alpha_2) = 268.6$°F.

Since the DSC experiences temperature fluctuation from -20 °F to 100 °F, the range of temperature fluctuation is 120°F which is less than 268.6 °F. Therefore, the fifth criterion is satisfied for the DSC.

F. The sixth criterion states that the DSC is adequate for fatigue effects, provided that the specified full range of mechanical loads does not result in a stress range that exceeds the S_a value obtained from the applicable fatigue curve for the total specified number of significant load fluctuations. If the total specified number of significant load fluctuations exceeds 10^6, the S_a value at $N = 10^6$ can be used.

A load fluctuation is considered to be significant if the total excursion of stresses exceed the value of S_a obtained from the applicable fatigue curve for 10^6 cycles. The only mechanical loads that affect the DSC are those associated with handling loads and a seismic event. One handling load cycle and a major seismic event are postulated during the design life of the DSC. The DSC stresses resulting from these mechanical load fluctuations are small since the structural capacity of the DSC is designed for extreme accident loads such as a postulated cask drop.

The number of significant cycles associated with mechanical load fluctuations is conservatively assumed to be 1,000. The value of S_a associated with this number of cycles is 120 ksi. Since the maximum stress range intensity permitted by the code is 3.0 S_m, or 52.5 ksi for SA-240, Type 304 stainless steel at 500 °F, this sixth condition is satisfied for the DSC.

The evaluation presented in the preceding paragraphs demonstrates that the six criteria contained in NB-3222.4(d) are satisfied for all components of the EOS-37PTH DSC.

3.9.1.5 DSC Weld Flaw Size Evaluation

EOS-37PTH DSC is considered as the bounding DSC for weld flaw evaluation because the weight of EOS-37PTH DSC (long) is greater than the weight of EOS-89BTH DSC.

3.9.1.5.1 Methodology

It is stipulated that the critical flaw configuration is a circumferential weld flaw exposed to the tensile component radial stress. The determination of the allowable surface and sub-surface flaw depth is accomplished by means of the methodology outlined below.

- *Determine the tensile radial membrane stresses in the weld. Evaluate membrane radial stresses occurring at the weld between the OTCP and the DSC shell for all individual loads.*
- *Determine limiting membrane radial stresses in the OTCP weld for all load combinations, for Service levels A, B, C, and D.*
- *L*imiting stresses are multiplied by safety factors SF_m for the corresponding service levels.
- Since OTCP weld is gas tungsten arc welding (GTAW) (non-flux weld), according to ASME Code Sec XI, Division 1, Figure C-4210-1 [3.9.1-4], maximum allowable flaw depth is estimated using limit load criteria.

The allowable membrane stress, S_t, in the flawed section for each service level is determined from Article C-5322, Appendix C [3.9.1-4] where the relation between the applied membrane stress and flaw depth at incipient stress is given.

3.9.1.5.2 Flaw Size Calculation

For 3D, half-symmetric model, as described in Section 3.9.1.2.3*, the tensile radial membrane stresses in the weld are evaluated by the stress linearization method explained in Section 3.9.1.2.5*.

Radial stresses for controlling load combination are calculated by adding individual load cases. Bounding radial tensile stresses in OTCP weld for all load combinations for Service Level A, B, and D are assessed. The allowable flaw depths, calculated by means of the methodology described in previous Section and are shown in Table 3.9.1-13.

Based on the evaluation, requirements for welding and weld inspections should be based on limiting the weld critical depth for surface and subsurface flaws to the following values:

- Surface Crack: 0.38 inch.
- Subsurface Crack: 0.38 inch.

3.9.1.6 Conclusions

Table 3.9.1-7 through Table 3.9.1-12 summarize the stress intensities in different components of DSC shell assembly and compared with ASME code stress intensity allowables. *Figure 3.9.1-20 and Figure 3.9.1-21 show the linearized component stresses for the DSC shell.*

The maximum ratio of induced load to allowable load for a confinement boundary area is 0.83, in the weld between the ITCP and the DSC shell during a side drop event. However, the maximum ratio of 0.90 is located separate from the confinement boundary welds in the DSC shell during extraction from the HSM (maximum of level A and B). The DSC assembly is, therefore, structurally adequate under all anticipated load conditions for service during storage and transfer.

Initial gaps between cover plates and shell do not close in any load cases. The margin exceeds any anticipated change in the results due to element size/density variations.

3.9.1.7 References

3.9.1-1 Title 10, Code of Federal Regulations, Part 72, "Licensing Requirements for the Independent Storage of Spent Nuclear Fuel, High-Level Radioactive Waste, and Reactor-Related Greater than Class C Waste."

3.9.1-2 American Society of Mechanical Engineers, ASME Boiler and Pressure Vessel Code, Section II, Part D, 2010 Edition through 2011 Addenda.

3.9.1-3 American Society of Mechanical Engineers, ASME Boiler and Pressure Vessel Code, Section III, 2010 Edition through 2011 Addenda.

3.9.1-4 American Society of Mechanical Engineers, ASME Boiler and Pressure Vessel Code, Section XI, Division 1, Appendix C, 2010 Edition Addenda through 2011 Addenda.

3.9.1-5 ANSI N14.5, "Leakage Tests on Packages for Shipment of Radioactive Materials," 1997.

3.9.1-6 ANSI N14.6 – 1993, "American National Standard for Radioactive Materials – Special Lifting Devices for Shipping Containers Weighing 10000 pounds (4500 kg) or More," American National Standards Institute, Inc., New York.

3.9.1-7 NUREG-1536, "Standard Review Plan for Spent Fuel Dry Cask Storage Systems at a General License Facility," Revision 1, U.S. Nuclear Regulatory Commission, July 2010.

3.9.1-8 U.S. Nuclear Regulatory Commission, Regulatory Guide 1.60, "Design Response Spectra for Seismic Design of Nuclear Power Plants," Revision 1, 1973.

3.9.1-9 ANSYS Computer Code and User's Manual, Release 14.0.

Table 3.9.1-1
EOS37PTH DSC Major Dimensions

Component	Dimensions
Outer Diameter of DSC Shell	75.50 inches
DSC Shell Thickness	0.5 inch
DSC Length	219 inches(1)
OTCP Thickness	2 inches
ITCP Thickness	2 inches
TSP Thickness	6 inches
OBCP Thickness	2 inches
IBCP Thickness	2 inches
IBS	4 inches

(1) Indicated length is for longest EOS-37PTH DSC

Table 3.9.1-2
Material of EOS DSC Components

DSC Shell	ASME SA-240 Type 304
OTCP	ASTM A240 Type 304
ITCP	*ASME SA-240 Type 304*
TSP	ASTM A36
OBCP	*ASTM A240 Type 304*
IBCP	ASME SA-240 Type 304
IBS	ASTM A36
Grapple Ring Support	*ASTM A240 Type 304*
Grapple Ring	*ASTM A240 Type 304*
Lifting Lug Plate	*ASTM A240 Type 304*
Lifting Lug	*ASTM A240 Type 304*

Table 3.9.1-3
Elastic-Plastic Material Properties

Material Property	SA-240 Type 304 at 500 °F	SA-36 at 500 °F
Elastic Modulus (psi)	25.9×10^6	27.3×10^6
Yield Strength (psi)	19,400	29,300
Tangent Modulus, E_t (psi)	5% of $E = 1.295 \times 10^6$	5% of $E = 1.365 \times 10^6$

Table 3.9.1-4
Allowable Weld Stresses for Pressure Boundary Partial Penetration Welds, Material Type 304

Service Level	Stress Region / Category	Stress Criteria	Allowable Stress Value at 500 °F [ksi]
Level A / Level B	*Primary Local Membrane Stress, P_L*	*$P_L = 0.8\ [1.5\ S_m]$*	*21.0*
	Primary Local Membrane + Bending Stress, $P_L + P_b$	*$P_L + P_b = 0.8\ [1.5\ S_m]$*	*21.0*
	Primary + Secondary Stress, P+Q	*$P_L + P_b + Q = 0.8\ [3.0\ S_m]$*	*42.0*
Level D (Elastic)	*Primary Local Membrane Stress, P_L*	*$0.8\ [Min(3.6\ S_m,\ S_u)]$*	*50.4*
	Primary Local Membrane + Bending Stress, $P_L + P_b$	*$0.8\ [Min(3.6\ S_m,\ S_u)]$*	*50.4*
Level D (Elastic Plastic)	*Primary Local Membrane Stress, P_L*	*$0.8\ [0.9\ S_u]$*	*45.6*
	Primary Local Membrane + Bending Stress, $P_L + P_b$	*$0.8\ [0.9\ S_u]$*	*45.6*

Table 3.9.1-5
SA-240/SA-479 304 & SA-182 F304 -Stress Allowables

Temp (°F)	S_m (ksi)	S_y (ksi)	S_u (ksi)	Level A/B			Level D (Elastic)		Level D (Plastic)	
				P_m	$P_m + P_b$	$P_m + P_b + Q$	P_m	$P_m + P_b$	P_m	$P_m + P_b$
70	20	30	75	20.0	30.0	60.0	48.0	72.0	52.5	67.5
200	20	25	71	20.0	30.0	60.0	48.0	71.0	49.7	63.9
300	20	22.4	66.2	20.0	30.0	60.0	46.3	66.2	46.3	59.6
400	18.6	20.7	64	18.6	27.9	55.8	44.6	64.0	44.8	57.6
500	17.5	19.4	63.4	17.5	26.3	52.5	42.0	63.0	44.4	57.1
600	16.6	18.4	63.4	16.6	24.9	49.8	39.8	59.8	44.4	57.1
700	15.8	17.6	63.4	15.8	23.7	47.4	37.9	56.9	44.4	57.1

Table 3.9.1-6
Allowable Base Metal Stresses for Non Pressure Boundary Partial Penetration & Fillet Welds Type 304 Base Metal

Temp. (°F)	S_y (ksi)	Level A $F_W = .40S_y$	Level B $F_W = .53S_y$	Level C $F_W = .60S_y$	Level D $F_W = .80S_y$
100	30	12	15.9	18	24
200	25	10	13.3	15	20
300	22.4	8.96	11.9	13.4	17.9
400	20.7	8.28	11	12.4	16.6
500	19.4	7.76	10.3	11.6	15.5
600	18.4	7.36	9.75	11	14.7
650	18	7.2	9.54	10.8	14.4
700	17.6	7.04	9.33	10.6	14.1

Table 3.9.1-7
DSC Shell Stress Results, *Confinement Boundary* – Load Combinations
2 Pages

Load Comb No.	Stress Category	Loads	Stress *Intensity* (ksi)	Allowable Stress (ksi)	Stress Ratio
1	P_m	DW_v + max($PI_{(30)}$, BD, VD)	*8.17*	17.50	*0.47*
	P_m+P_b	DW_v + max($PI_{(30)}$, BD, VD)	*16.62*	26.25	*0.63*
	P_m+P_b+Q	DW_v + max($PI_{(30)}$, BD, VD)+THTS6	*39.77*	52.50	*0.76*
2	P_m	DW_h + 1g axial + 1g transverse + 1g Vertical + $PI_{(30)}$	*8.65*	17.50	*0.49*
	P_m+P_b	DW_h + 1g axial + 1g transverse + 1g Vertical + $PI_{(30)}$	*14.71*	26.25	*0.56*
	P_m+P_b+Q	DW_h + 1g axial + 1g transverse + 1g Vertical + $PI_{(30)}$ + $THT_{(117\ °F)}$	*37.85*	52.50	*0.72*
3	P_m	DW_h + 1g axial + 1g transverse + 1g Vertical + $PI_{(30)}$	*8.65*	17.50	*0.49*
	P_m+P_b	DW_h + 1g axial + 1g transverse + 1g Vertical + $PI_{(30)}$	*14.71*	26.25	*0.56*
	P_m+P_b+Q	DW_h + 1g axial + 1g transverse + 1g Vertical + $PI_{(30)}$ + THTS6	*37.85*	52.50	*0.72*
4	P_m	DW_h + 135kips + $PI_{(30)}$	*8.67*	17.50	*0.50*
	P_m+P_b	DW_h + 135kips + $PI_{(30)}$	*17.85*	26.25	*0.68*
	P_m+P_b+Q	DW_h + 135kips + THTS6	*40.99*	52.50	*0.78*
5	P_m	DW_h + 80 kips + $PI_{(30)}$	*9.24*	17.50	*0.53*
	P_m+P_b	DW_h + 80 kips + $PI_{(30)}$	*16.70*	26.25	*0.64*
	P_m+P_b+Q	DW_h + 80 kips + THTS6	*39.84*	52.50	*0.76*
6	P_m	DW_h + 135 kips + $PI_{(30)}$	*9.63*	*44.38*	*0.22*
	P_m+P_b	DW_h + 135 kips + $PI_{(30)}$	*16.79*	*57.06*	*0.29*
7A	P_m	DW_h + max. (SD_AWAY_EP, SD_RAIL_EP) + $PI_{(30)}$	*33.73*	44.38	*0.76*
	P_m+P_b	DW_h + max. (SD_AWAY_EP, SD_RAIL_EP)+ $PI_{(30)}$	*38.60*	57.06	*0.68*
7B	P_m	DW_v + max. (TOP_ED, BOT_ED)+ $PI_{(30)}$	*23.75*	42.00	*0.57*
	P_m+P_b	DW_v + max. (TOP_ED, BOT_ED)+ $PI_{(30)}$	*42.34*	63.00	*0.67*

Table 3.9.1-7
DSC Shell Stress Results, *Confinement Boundary* – Load Combinations
2 Pages

Load Comb No.	Stress Category	Loads	Stress *Intensity* (ksi)	Allowable Stress (ksi)	Stress Ratio
8	P_m	$DW_h + PI_{(130)}$	*18.14*	*44.38*	*0.41*
	P_m+P_b	$DW_h + PI_{(130)}$	*35.36*	*57.06*	*0.62*
9	P_m	$DW_h + PI_{(30)}$	*11.58*	17.50	*0.66*
	P_m+P_b	$DW_h + PI_{(30)}$	*19.94*	26.25	*0.76*
	P_m+P_b+Q	$DW_h + PI_{(30)}$ + THTS6	*43.08*	52.50	*0.82*
10	P_m	DW_h + max.(HS_TOP, HS_BOT) + $PI_{(30)}$	*24.35*	*44.38*	*0.55*
	P_m+P_b	DW_h + max.(HS_TOP, HS_BOT) + $PI_{(30)}$	*37.58*	*57.06*	*0.66*
11	P_m	max. ($PI_{(23)}$ + 155 kips ,$PE_{(14.7)}$ + 155 kips)	*5.37*	17.50	*0.31*
	P_m+P_b	max. ($PI_{(23)}$ + 155 kips,$PE_{(14.7)}$ + 155 kips)	*11.35*	26.25	*0.43*
12	*External Pressure (psi)*		*21.7*	*45.1*	*0.48*

Table 3.9.1-7a
DSC Shell Stress Results, Non-Confinement Boundary – Load Combinations
2 Pages

Load Comb No.	Stress Category	Loads	Stress Intensity (ksi)	Allowable Stress (ksi)	Stress Ratio
1	P_m	DW_v + max($PI_{(30)}$,BD,VD)	1.58	17.50	0.09
	P_m+P_b	DW_v + max($PI_{(30)}$,BD,VD)	3.69	26.25	0.14
	P_m+P_b+Q	DW_v + max($PI_{(30)}$,BD,VD)+THTS6	26.84	52.50	0.51
2	P_m	DW_h + 1g axial + 1g transverse + 1g Vertical + $PI_{(30)}$	5.41	17.50	0.31
	P_m+P_b	DW_h + 1g axial + 1g transverse + 1g Vertical + $PI_{(30)}$	6.09	26.25	0.23
	P_m+P_b+Q	DW_h + 1g axial + 1g transverse + 1g Vertical + $PI_{(30)}$ + $THT_{(117\ °F)}$	29.23	52.50	0.56
3	P_m	DW_h + 1g axial + 1g transverse + 1g Vertical + $PI_{(30)}$	5.41	17.50	0.31
	P_m+P_b	DW_h + 1g axial + 1g transverse + 1g Vertical + $PI_{(30)}$	6.09	26.25	0.23
	P_m+P_b+Q	DW_h + 1g axial + 1g transverse + 1g Vertical + $PI_{(30)}$ + THTS6	29.23	52.50	0.56
4	P_m	DW_h + 135 kips + $PI_{(30)}$	6.19	17.50	0.35
	P_m+P_b	DW_h + 135 kips + $PI_{(30)}$	12.98	26.25	0.49
	P_m+P_b+Q	DW_h + 135 kips + THTS6	36.13	52.50	0.69
5	P_m	DW_h + 80 kips + $PI_{(30)}$	6.74	17.50	0.39
	P_m+P_b	DW_h + 80 kips + $PI_{(30)}$	23.69	26.25	0.90
	P_m+P_b+Q	DW_h + 80 kips + THTS6	46.84	52.50	0.89
6	P_m	DW_h + 135 kips + $PI_{(30)}$	9.90	44.38	0.22
	P_m+P_b	DW_h + 135 kips + $PI_{(30)}$	31.93	57.06	0.56
7A	P_m	DW_h + max.(SD_AWAY_EP, SD_RAIL_EP) + $PI_{(30)}$	24.59	44.38	0.55
	P_m+P_b	DW_h + max.(SD_AWAY_EP, SD_RAIL_EP) + $PI_{(30)}$	25.79	57.06	0.45
7B	P_m	DW_v + max.(TOP_ED, BOT_ED) + $PI_{(30)}$	15.48	42.00	0.37
	P_m+P_b	DW_v + max.(TOP_ED, BOT_ED) + $PI_{(30)}$	45.93	63.00	0.73

Table 3.9.1-7a
DSC Shell Stress Results, Non-Confinement Boundary – Load Combinations
2 Pages

Load Comb No.	***Stress Category***	***Loads***	***Stress Intensity (ksi)***	***Allowable Stress (ksi)***	***Stress Ratio***
8	P_m	$DW_h + PI_{(130)}$	*6.42*	*44.38*	*0.14*
	P_m+P_b	$DW_h + PI_{(130)}$	*15.49*	*57.06*	*0.27*
9	P_m	$DW_h + PI_{(30)}$	*2.40*	*17.50*	*0.14*
	P_m+P_b	$DW_h + PI_{(30)}$	*4.73*	*26.25*	*0.18*
	P_m+P_b+Q	$DW_h + PI_{(30)}$ + THTS6	*27.88*	*52.50*	*0.53*
10	P_m	DW_h + max.(HS_TOP, HS_BOT) + $PI_{(30)}$	*29.18*	*44.38*	*0.66*
	P_m+P_b	DW_h + max.(HS_TOP, HS_BOT)+$PI_{(30)}$	*34.02*	*57.06*	*0.60*
11	P_m	max. ($PI_{(23)}$+155 kips ,$PE_{(14.7)}$ + 155 kips)	*3.78*	*17.50*	*0.22*
	P_m+P_b	max. ($PI_{(23)}$+155 kips,$PE_{(14.7)}$ + 155 kips)	*10.09*	*26.25*	*0.38*
12	*External Pressure (psi)*		*21.7*	*45.1*	*0.48*

Table 3.9.1-8
OTCP Stress Results – Load Combinations
2 Pages

Load Comb No.	Stress Category	Loads	Stress *Intensity* (ksi)	Allowable Stress (ksi)	Stress Ratio
1	P_m	DW_v + max($PI_{(30)}$,BD,VD)	*2.53*	17.50	*0.14*
	P_m+P_b	DW_v + max($PI_{(30)}$,BD,VD)	*6.73*	26.25	*0.26*
	P_m+P_b+Q	DW_v + max($PI_{(30)}$,BD,VD)+ THTS6	*10.68*	52.50	*0.20*
2	P_m	DW_h + 1g axial + 1g transverse + 1g Vertical + $PI_{(30)}$	*3.21*	17.50	*0.18*
	P_m+P_b	DW_h + 1g axial + 1g transverse + 1g Vertical + $PI_{(30)}$	*10.62*	26.25	*0.40*
	P_m+P_b+Q	DW_h + 1g axial + 1g transverse + 1g Vertical + $PI_{(30)}$ + $THT_{(117\ °F)}$	*14.57*	52.50	*0.28*
3	P_m	DW_h + 1g axial + 1g transverse + 1g Vertical + $PI_{(30)}$	*3.21*	17.50	*0.18*
	P_m+P_b	DW_h + 1g axial + 1g transverse + 1g Vertical + $PI_{(30)}$	*10.62*	26.25	*0.40*
	P_m+P_b+Q	DW_h + 1g axial + 1g transverse + 1g Vertical + $PI_{(30)}$ + THTS6	*14.57*	52.50	*0.28*
4	P_m	DW_h + 135kips + $PI_{(30)}$	*2.72*	17.50	*0.16*
	P_m+P_b	DW_h + 135kips + $PI_{(30)}$	*6.66*	26.25	*0.25*
	P_m+P_b+Q	DW_h + 135kips + THTS6	*10.62*	52.50	*0.20*
5	P_m	DW_h + 80 kips + $PI_{(30)}$	*2.68*	17.50	*0.15*
	P_m+P_b	DW_h + 80 kips + $PI_{(30)}$	*7.52*	26.25	*0.29*
	P_m+P_b+Q	DW_h + 80 kips + THTS6	*11.48*	52.50	*0.22*
6	P_m	DW_h + 135 kips + $PI_{(30)}$	*2.67*	*44.38*	*0.06*

Table 3.9.1-8
OTCP Stress Results – Load Combinations
2 Pages

Load Comb No.	Stress Category	Loads	Stress *Intensity* (ksi)	Allowable Stress (ksi)	Stress Ratio
	P_m+P_b	DW_h+ 135 kips + $PI_{(30)}$	*7.75*	*57.06*	*0.14*
7A	P_m	DW_h + max. (SD_AWAY, SD_RAIL_EP, SD_TOP_RAIL_EP) + $PI_{(30)}$	*12.90*	44.38	*0.29*
	P_m+P_b	DW_h+ max. (SD_AWAY_EP, SD_RAIL_EP)+ $PI_{(30)}$	*29.19*	57.06	*0.51*
7B	P_m	DW_v + max. (TOP_ED, BOT_ED)+ $PI_{(30)}$	*7.32*	42.00	*0.17*
	P_m+P_b	DW_v + max. (TOP_ED, BOT_ED)+ $PI_{(30)}$	*21.16*	63.00	*0.34*
8	P_m	DW_h + $PI_{(130)}$	*10.78*	*44.38*	*0.24*
	P_m+P_b	DW_h + $PI_{(130)}$	*24.24*	*57.06*	*0.42*
9	P_m	DW_h+ $PI_{(30)}$	*3.04*	17.50	*0.17*
	P_m+P_b	DW_h + $PI_{(30)}$	*8.08*	26.25	*0.31*
	P_m+P_b+Q	DW_h + $PI_{(30)}$+ THTS6	*12.04*	52.50	*0.23*
10	P_m	DW_h + max. (HS_TOP, HS_BOT) + $PI_{(30)}$	*16.81*	*44.38*	*0.38*
	P_m+P_b	DW_h + max. (HS_TOP, HS_BOT) + $PI_{(30)}$	*24.90*	*57.06*	*0.44*
11	P_m	max. ($PI_{(23)}$ + 155 kips, $PE_{(14.7)}$ + 155 kips)	NA		
	P_m+P_b	max. ($PI_{(23)}$+155 kips, $PE_{(14.7)}$ + 155 kips)	NA		

Table 3.9.1-9
ITCP Stress Results – Load Combinations
2 Pages

Load Comb. No.	Stress Category	Loads	Stress *Intensity* (ksi)	Allowable Stress (ksi)	Stress Ratio
1	P_m	DW_v + max($PI_{(30)}$, BD, VD)	*4.12*	17.50	*0.24*
	P_m+P_b	DW_v + max($PI_{(30)}$, BD, VD)	*9.06*	26.25	*0.35*
	P_m+P_b+Q	DW_v + max($PI_{(30)}$, BD, VD) + THTS6	*16.01*	52.50	*0.30*
2	P_m	DW_h + 1g axial + 1g transverse + 1g Vertical + $PI_{(30)}$	*2.60*	17.50	*0.15*
	P_m+P_b	DW_h + 1g axial + 1g transverse + 1g Vertical + $PI_{(30)}$	*9.01*	26.25	*0.34*
	P_m+P_b+Q	DW_h + 1g axial + 1g transverse + 1g Vertical + $PI_{(30)}$ + $THT_{(117\ °F)}$	*15.96*	52.50	*0.30*
3	P_m	DW_h + 1g axial + 1g transverse + 1g Vertical + $PI_{(30)}$	*2.60*	17.50	*0.15*
	P_m+P_b	DW_h + 1g axial + 1g transverse + 1g Vertical + $PI_{(30)}$	*9.01*	26.25	*0.34*
	P_m+P_b+Q	DW_h + 1g axial + 1g transverse + 1g Vertical + $PI_{(30)}$ + THTS6	*15.96*	52.50	*0.30*
4	P_m	DW_h + 135kips + $PI_{(30)}$	*2.96*	17.50	*0.17*
	P_m+P_b	DW_h + 135kips + $PI_{(30)}$	*9.77*	26.25	*0.37*
	P_m+P_b+Q	DW_h + 135kips + THTS6	*16.72*	52.50	*0.32*
5	P_m	DW_h + 80 kips + $PI_{(30)}$	*2.86*	17.50	*0.16*
	P_m+P_b	DW_h + 80 kips + $PI_{(30)}$	*9.44*	26.25	*0.36*
	P_m+P_b+Q	DW_h + 80 kips + THTS6	*16.39*	52.50	*0.31*
6	P_m	DW_h + 135 kips + $PI_{(30)}$	*2.83*	*44.38*	*0.06*
	P_m+P_b	DW_h+ 135 kips + $PI_{(30)}$	*9.34*	*57.06*	*0.16*

Table 3.9.1-9
ITCP Stress Results – Load Combinations
2 Pages

Load Comb. No.	Stress Category	Loads	Stress *Intensity* (ksi)	Allowable Stress (ksi)	Stress Ratio
7A	P_m	DW_h + max. (SD_AWAY_EP, SD_RAIL_EP) + $PI_{(30)}$	*12.69*	44.38	*0.29*
	P_m+P_b	DW_h + max. (SD_AWAY_EP, SD_RAIL_EP) + $PI_{(30)}$	*32.72*	57.06	*0.57*
7B	P_m	DW_v + max. (TOP_ED, BOT_ED) + $PI_{(30)}$	*7.36*	42.00	*0.18*
	P_m+P_b	DW_v + max. (TOP_ED, BOT_ED) + $PI_{(30)}$	*23.93*	63.00	*0.38*
8	P_m	DW_h + $PI_{(130)}$	*10.75*	*44.38*	*0.24*
	P_m+P_b	DW_h + $PI_{(130)}$	*23.88*	*57.06*	*0.42*
9	P_m	DW_h + $PI_{(30)}$	*3.38*	17.50	*0.19*
	P_m+P_b	DW_h + $PI_{(30)}$	*10.79*	26.25	*0.41*
	P_m+P_b+Q	DW_h + $PI_{(30)}$+ THTS6	*17.75*	52.50	*0.34*
10	P_m	DW_h + max. (HS_TOP, HS_BOT)+$PI_{(30)}$	*12.77*	*44.38*	*0.29*
	P_m+P_b	DW_h + max. (HS_TOP, HS_BOT)+$PI_{(30)}$	*22.86*	*57.06*	*0.40*
11	P_m	max. ($PI_{(23)}$+155 kips, $PE_{(14.7)}$+155 kips)	NA		
	P_m+P_b	max. ($PI_{(23)}$+155 kips, $PE_{(14.7)}$+155 kips)	NA		

Table 3.9.1-10
IBCP Stress Results – Load Combinations
2 Pages

Load Comb. No.	Stress Category	Loads	Stress *Intensity* (ksi)	Allowable Stress (ksi)	Stress Ratio
1	P_m	DW_v + max. ($PI_{(30)}$, BD, VD)	*0.54*	17.50	*0.03*
	P_m+P_b	DW_v + max. ($PI_{(30)}$, BD, VD)	*1.18*	26.25	*0.05*
	P_m+P_b+Q	DW_v + max. ($PI_{(30)}$, BD, VD) + THTS6	*21.33*	52.50	*0.41*
2	P_m	DW_h + 1g axial + 1g transverse + 1g Vertical + $PI_{(30)}$	*0.39*	17.50	*0.02*
	P_m+P_b	DW_h + 1g axial + 1g transverse + 1g Vertical + $PI_{(30)}$	*0.92*	26.25	*0.03*
	P_m+P_b+Q	DW_h + 1g axial + 1g transverse + 1g Vertical + $PI_{(30)}$ + THTS6	*21.06*	52.50	*0.40*
3	P_m	DW_h + 1g axial + 1g transverse + 1g Vertical + $PI_{(30)}$	*0.39*	17.50	*0.02*
	P_m+P_b	DW_h + 1g axial + 1g transverse + 1g Vertical + $PI_{(30)}$	*0.92*	26.25	*0.03*
	P_m+P_b+Q	DW_h + 1g axial + 1g transverse + 1g Vertical + $PI_{(30)}$ + THTS6	*21.06*	52.50	*0.40*
4	P_m	DW_h+ 135kips + $PI_{(30)}$	*1.53*	17.50	*0.09*
	P_m+P_b	DW_h + 135kips + $PI_{(30)}$	*5.23*	26.25	*0.20*
	Pm+Pb+Q	DW_h + 135kips + THTS6	*25.38*	52.50	*0.48*
5	P_m	DW_h + 80 kips + $PI_{(30)}$	*0.68*	17.50	*0.04*
	P_m+P_b	DW_h + 80 kips + $PI_{(30)}$	*1.30*	26.25	*0.05*
	P_m+P_b+Q	DW_h + 80 kips + THTS6	*21.44*	52.50	*0.41*
6	P_m	DW_h + 135 kips + $PI_{(30)}$	*0.72*	*44.38*	*0.02*
	P_m+P_b	DW_h + 135 kips + $PI_{(30)}$	*1.49*	*57.06*	*0.03*
7A	P_m	DW_h + max. (SD_AWAY_EP, SD_RAIL_EP)+ $PI_{(30)}$	*17.50*	44.38	*0.39*
	P_m+P_b	DW_h + max. (SD_AWAY_EP, SD_RAIL_EP)+ $PI_{(30)}$	*23.28*	57.06	*0.41*

Table 3.9.1-10
IBCP Stress Results – Load Combinations
2 Pages

Load Comb. No.	Stress Category	Loads	Stress *Intensity* (ksi)	Allowable Stress (ksi)	Stress Ratio
7B	P_m	DW_v + max. (TOP_ED, BOT_ED) + $PI_{(30)}$	*6.32*	42.00	*0.15*
	P_m+P_b	DW_v + max. (TOP_ED, BOT_ED) + $PI_{(30)}$	*14.35*	63.00	*0.23*
8	P_m	DW_h + $PI_{(130)}$	*2.18*	*44.38*	*0.05*
	P_m+P_b	DW_h + $PI_{(130)}$	*4.85*	*57.06*	*0.09*
9	P_m	DW_h + $PI_{(30)}$	*0.96*	17.50	*0.05*
	P_m+P_b	DW_h + $PI_{(30)}$	*1.75*	26.25	*0.07*
	P_m+P_b+Q	DW_h + $PI_{(30)}$ + THTS6	*21.89*	52.50	*0.42*
10	P_m	DW_h + max.(HS_TOP, HS_BOT) + $PI_{(30)}$	*7.76*	*44.38*	*0.17*
	P_m+P_b	DW_h + max.(HS_TOP, HS_BOT) + $PI_{(30)}$	*23.70*	*57.06*	*0.42*
11	P_m	max. ($PI_{(23)}$ + 155 kips, $PE_{(14.7)}$ + 155 kips)	*2.44*	17.50	*0.14*
	P_m+P_b	max. ($PI_{(23)}$ + 155 kips, $PE_{(14.7)}$ + 155 kips)	*5.84*	26.25	*0.22*

Table 3.9.1-11
ITCP-DSC Shell Weld Stress Results – Load Combinations
2 Pages

Load Comb. No.	*Stress Category*	*Loads*	*Stress Intensity (ksi)*	*Allowable Stress (ksi)*	*Stress Ratio*
1	P_L	DW_v + max (PI(30),BD,VD)	4.74	21.00	0.23
	P_L+P_b	DW_v + max(PI(30),BD,VD)	11.35	21.00	0.54
	P_L+P_b+Q	DW_v + max(PI(30),BD,VD)+THTT3	20.02	42.00	0.48
2	P_L	DW_h + 1g axial + 1g transverse + 1g Vertical + $PI_{(30)}$	4.54	21.00	0.22
	P_L+P_b	DW_h + 1g axial + 1g transverse + 1g Vertical + $PI_{(30)}$	11.06	21.00	0.53
	P_L+P_b+Q	DW_h + 1g axial + 1g transverse + 1g Vertical + $PI_{(30)}$ + THTT3	19.74	42.00	0.47
3	P_L	DW_h + 1g axial + 1g transverse + 1g Vertical + $PI_{(30)}$	4.54	21.00	0.22
	P_L+P_b	DW_h + 1g axial + 1g transverse + 1g Vertical + $PI_{(30)}$	11.06	21.00	0.53
	P_L+P_b+Q	DW_h + 1g axial + 1g transverse + 1g Vertical + $PI_{(30)}$ + THTT3	19.74	42.00	0.47
4	P_L	DW_h + 135kips + $PI_{(30)}$	4.93	21.00	0.23
	P_L+P_b	DW_h + 135kips + $PI_{(30)}$	12.32	21.00	0.59
	P_L+P_b+Q	DW_h + 135kips + THTT3	21.00	42.00	0.50
5	P_L	DW_h + 80 kips + $PI_{(30)}$	5.08	21.00	0.24
	P_L+P_b	DW_h + 80 kips + $PI_{(30)}$	11.95	21.00	0.57
	P_L+P_b+Q	DW_h + 80 kips + THTT3	20.63	42.00	0.49

Table 3.9.1-11
ITCP-DSC Shell Weld Stress Results – Load Combinations
2 Pages

Load Comb. No.	*Stress Category*	*Loads*	*Stress Intensity (ksi)*	*Allowable Stress (ksi)*	*Stress Ratio*
6	P_L	DW_h + 135 kips + $PI_{(30)}$	*5.31*	*45.65*	*0.12*
	P_L+P_b	DW_h + 135 kips + $PI_{(30)}$	*11.92*	*45.65*	*0.26*
7A	P_L	DW_h + max. (SD_AWAY_EP, SD_RAIL_EP)+ $PI_{(30)}$	*36.76*	*45.65*	*0.81*
	P_L+P_b	DW_h + max. (SD_AWAY_EP, SD_RAIL_EP)+ $PI_{(30)}$	*37.72*	*45.65*	*0.83*
7B	P_L	DW_v + max. (TOP_ED, BOT_ED) + $PI_{(30)}$	*11.06*	*50.40*	*0.22*
	P_L+P_b	DW_v + max. (TOP_ED, BOT_ED) + $PI_{(30)}$	*30.26*	*50.40*	*0.60*
8	P_L	DW_h + $PI_{(130)}$	*12.36*	*45.65*	*0.27*
	P_L+P_b	DW_h + $PI_{(130)}$	*27.72*	*45.65*	*0.61*
9	P_L	DW_h + $PI_{(30)}$	*6.82*	*21.00*	*0.32*
	P_L+P_b	DW_h + $PI_{(30)}$	*14.42*	*21.00*	*0.69*
	P_L+P_b+Q	DW_h + $PI_{(30)}$ + THTT3	*23.09*	*42.00*	*0.55*
10	P_L	DWh + max. (HS_TOP, HS_BOT) + $PI_{(30)}$	*15.44*	*45.65*	*0.34*
	P_L+P_b	DW_h + max. (HS_TOP, HS_BOT) + $PI_{(30)}$	*18.97*	*45.65*	*0.42*

Note that $P_L + P_b$ stresses are secondary stresses; however, they are conservatively considered as primary stresses. Side drop (LC7A) P_L and $P_L + P_b$ stresses that occur at the impact location are conservatively included in the stress results that are compared to the allowable stresses. As shown in Figure 3.9.1-16, these compressive stresses dominate the results.

Table 3.9.1-12
OTCP-DSC _Shell_ Weld Stress Results – Load Combinations
2 Pages

Load Comb. No.	*Stress Category*	*Loads*	*Stress Intensity (ksi)*	*Allowable Stress (ksi)*	*Stress Ratio*
1	P_L	DW_v + max. ($PI_{(30)}$, BD, VD)	*5.30*	*21.00*	*0.25*
	$P_L + P_b$	DW_v + max. ($PI_{(30)}$, BD, VD)	*9.28*	*21.00*	*0.44*
	$P_L + P_b + Q$	DW_v+ max. ($PI_{(30)}$, BD, VD) + THTT3	*16.61*	*42.00*	*0.40*
2	P_L	DW_h + 1g axial + 1g transverse + 1g Vertical + $PI_{(30)}$	*8.57*	*21.00*	*0.41*
	$P_L + P_b$	DW_h+ 1g axial + 1g transverse + 1g Vertical + $PI_{(30)}$	*14.94*	*21.00*	*0.71*
	$P_L + P_b + Q$	DW_h + 1g axial + 1g transverse + 1g Vertical + $PI_{(30)}$ + THTT3	*22.27*	*42.00*	*0.53*
3	P_L	DW_h + 1g axial + 1g transverse + 1g Vertical + $PI_{(30)}$	*8.57*	*21.00*	*0.41*
	$P_L + P_b$	DW_h + 1g axial + 1g transverse + 1g Vertical + $PI_{(30)}$	*14.94*	*21.00*	*0.71*
	$P_L + P_b + Q$	DW_h + 1g axial + 1g transverse + 1g Vertical + $PI_{(30)}$ + THTT3	*22.27*	*42.00*	*0.53*
4	P_L	DW_h + 135kips + $PI_{(30)}$	*5.38*	*21.00*	*0.26*
	$P_L + P_b$	DW_h + 135kips + $PI_{(30)}$	*8.94*	*21.00*	*0.43*
	$P_L + P_b + Q$	DW_h + 135kips + THTT3	*16.27*	*42.00*	*0.39*
5	P_L	DW_h + 80 kips + $PI_{(30)}$	*5.85*	*21.00*	*0.28*
	$P_L + P_b$	DW_h + 80 kips + $PI_{(30)}$	*10.36*	*21.00*	*0.49*
	$P_L + P_b + Q$	DW_h + 80 kips + THTT3	*17.69*	*42.00*	*0.42*
6	P_L	DW_h + 135 kips + $PI_{(30)}$	*5.98*	*45.65*	*0.13*
	$P_L + P_b$	DW_h + 135 kips + $PI_{(30)}$	*10.76*	*45.65*	*0.24*

Table 3.9.1-12
OTCP-DSC _Shell_ Weld Stress Results – Load Combinations
2 Pages

Load Comb. No.	*Stress Category*	*Loads*	*Stress Intensity (ksi)*	*Allowable Stress (ksi)*	*Stress Ratio*
7A	P_L	DW_h + max. (SD_AWAY_EP, SD_RAIL_EP)+ $PI_{(30)}$	*27.02*	*45.65*	*0.59*
	$P_L + P_b$	DW_h + max. (SD_AWAY_EP, SD_RAIL_EP)+ $PI_{(30)}$	*30.62*	*45.65*	*0.67*
7B	P_L	DW_v + max. (TOP_ED, BOT_ED)+ $PI_{(30)}$	*16.45*	*50.40*	*0.33*
	$P_L + P_b$	DW_v + max. (TOP_ED, BOT_ED)+ $PI_{(30)}$	*28.97*	*50.40*	*0.57*
8	P_L	$DW_h + PI_{(130)}$	*12.84*	*45.65*	*0.28*
	$P_L + P_b$	$DW_h + PI_{(130)}$	*23.10*	*45.65*	*0.51*
9	P_L	DW_h + PI(30)	*6.35*	*21.00*	*0.30*
	$P_L + P_b$	$DW_h + PI_{(30)}$	*10.96*	*21.00*	*0.52*
	$P_L + P_b + Q$	$DW_h + PI_{(30)}$+ THTT3	*18.28*	*42.00*	*0.44*
10	P_L	DW_h + max. (HS_TOP, HS_BOT)+$PI_{(30)}$	*22.53*	*45.65*	*0.49*
	$P_L + P_b$	DW_h + max. (HS_TOP, HS_BOT)+$PI_{(30)}$	*24.40*	*45.65*	*0.53*

Note that $P_L + P_b$ stresses are secondary stresses. However, they are conservatively considered as primary stresses. Side drop (LC7A) P_L and $P_L + P_b$ stresses that occur at the impact location are conservatively included in the stress results that are compared to the allowable stresses. As shown in Figure 3.9.1-16, these compressive stresses dominate the results.

Table 3.9.1-13
Weld Flaw *Size* for Controlling Load Combination

Service Level	Controlling Load Combination	Tensile Radial Stress SX (ksi)	Safety Factor SF_m	Radial Stress including Safety Factor (Sx)x (SF_m)	Allowable a/t	Subsurface Flaws		Surface Flaws	
						Weld Thickness 2t (inch)	Flaw Depth, 2a (inch)	Weld Thickness t (inch)	Flaw Depth, a (inch)
A	4	*0.32*	2.7	*0.85*	(0.98) 0.75	0.50	0.38	0.50	0.38
B	4	*0.32*	2.4	*0.76*	(0.98) 0.75	0.50	0.38	0.50	0.38
D	7A	*4.79*	1.3	*6.23*	*(0.85)* 0.75	0.50	0.38	0.50	0.38

Table 3.9.1-14
Mesh Sensitivity Results Comparison with Mesh Refinement

Component	*Parameter*	*Six-element Through Thickness*	*Eight-element Through Thickness*
OTCP(1)	*Deflection (in.)*	*0.08403*	*0.08415*
	P_m (psi)	*2479.5*	*2479.4*
	$P_m + P_b$ (psi)	*6590.1*	*6276.8*
ITCP(1)	*Deflection (in)*	*0.08403*	*0.08415*
	P_m (psi)	*2658.3*	*2476.8*
	$P_m + P_b$ (psi)	*8899.3*	*8200.5*
DSC Shell	*P_m (psi)*	*7567.0*	*7946.2*
	$P_m + P_b$ (psi)	*15094.3*	*15703.1*
OTCP Weld	*P_L (psi)*	*5191.5*	*5101.0*
	$P_L + P_b$ (psi)	*9073.0*	*9134.4*
ITCP Weld	*P_L (psi)*	*4177.7*	*4190.9*
	$P_L + P_b$ (psi)	*11100.3*	*11858.4*

Note:

1) OTCP and ITCP have 12 elements through the thickness of the component for the six-element through thickness case and 16 elements through the thickness of the component for the eight-element through thickness.

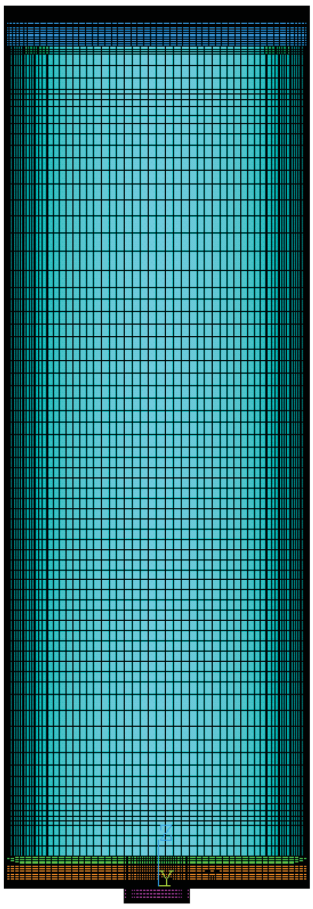

Figure 3.9.1-1
DSC *FEM*

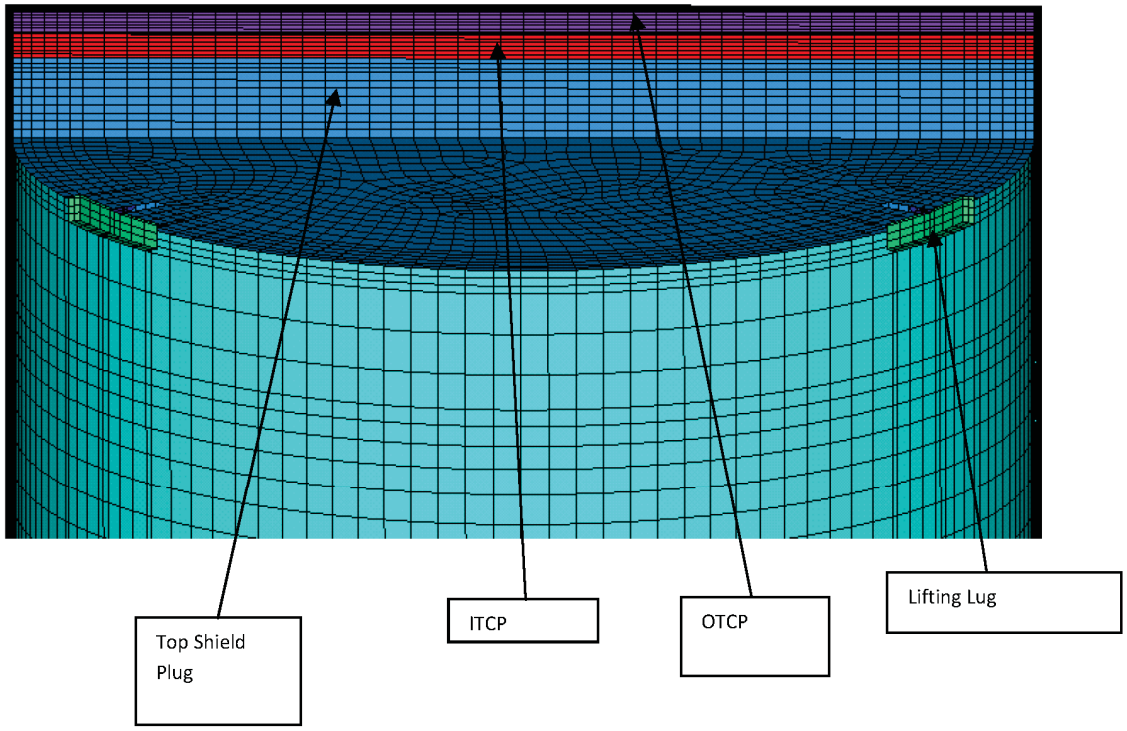

Figure 3.9.1-2
DSC *FEM*-Top End

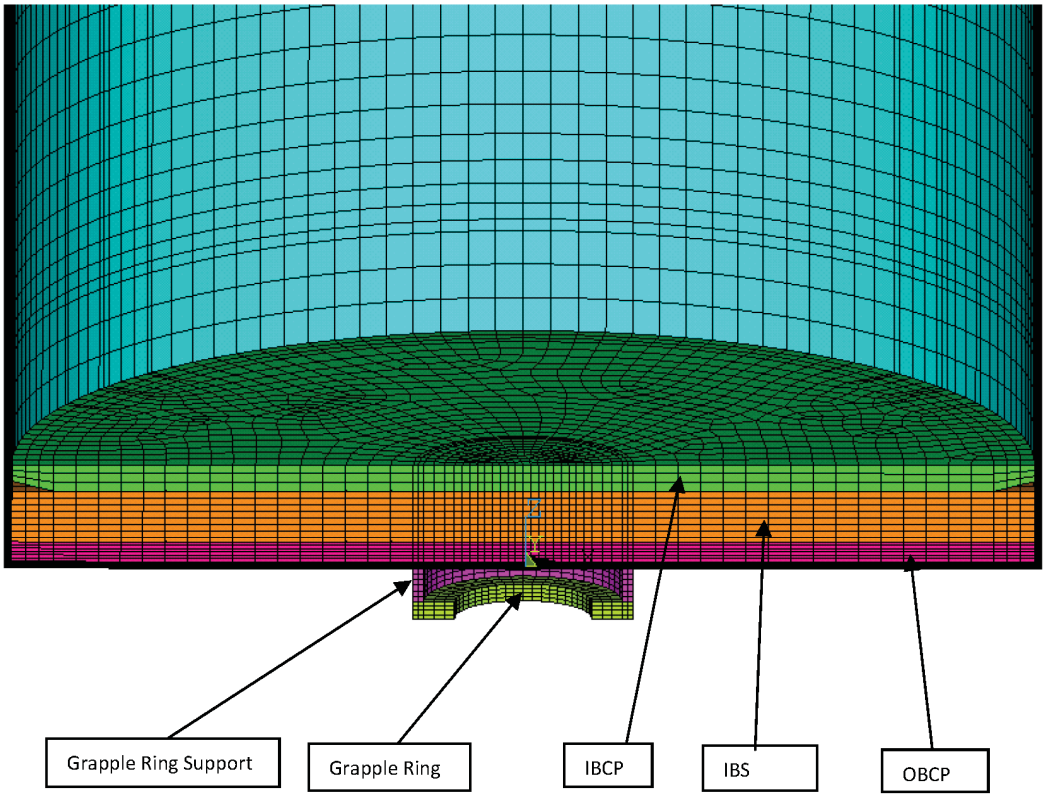

Figure 3.9.1-3
DSC *FEM*-Bottom End

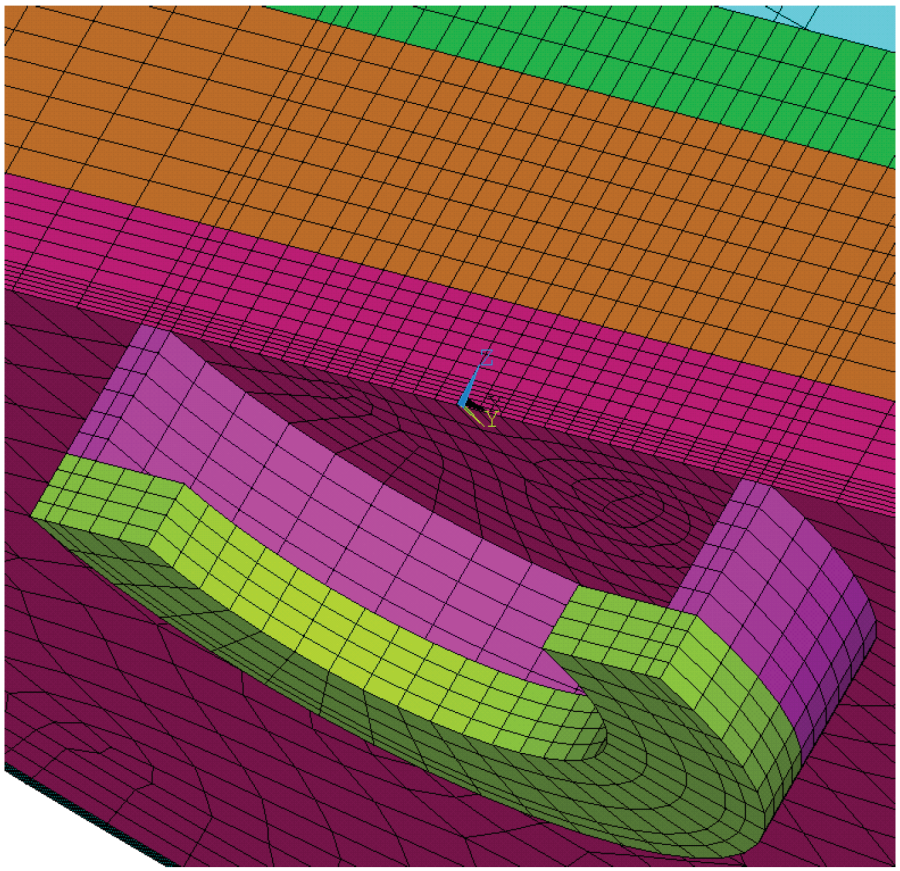

Figure 3.9.1-4
Mesh detail – Grapple Assembly

Proprietary Information on This Page
Withheld Pursuant to 10 CFR 2.390

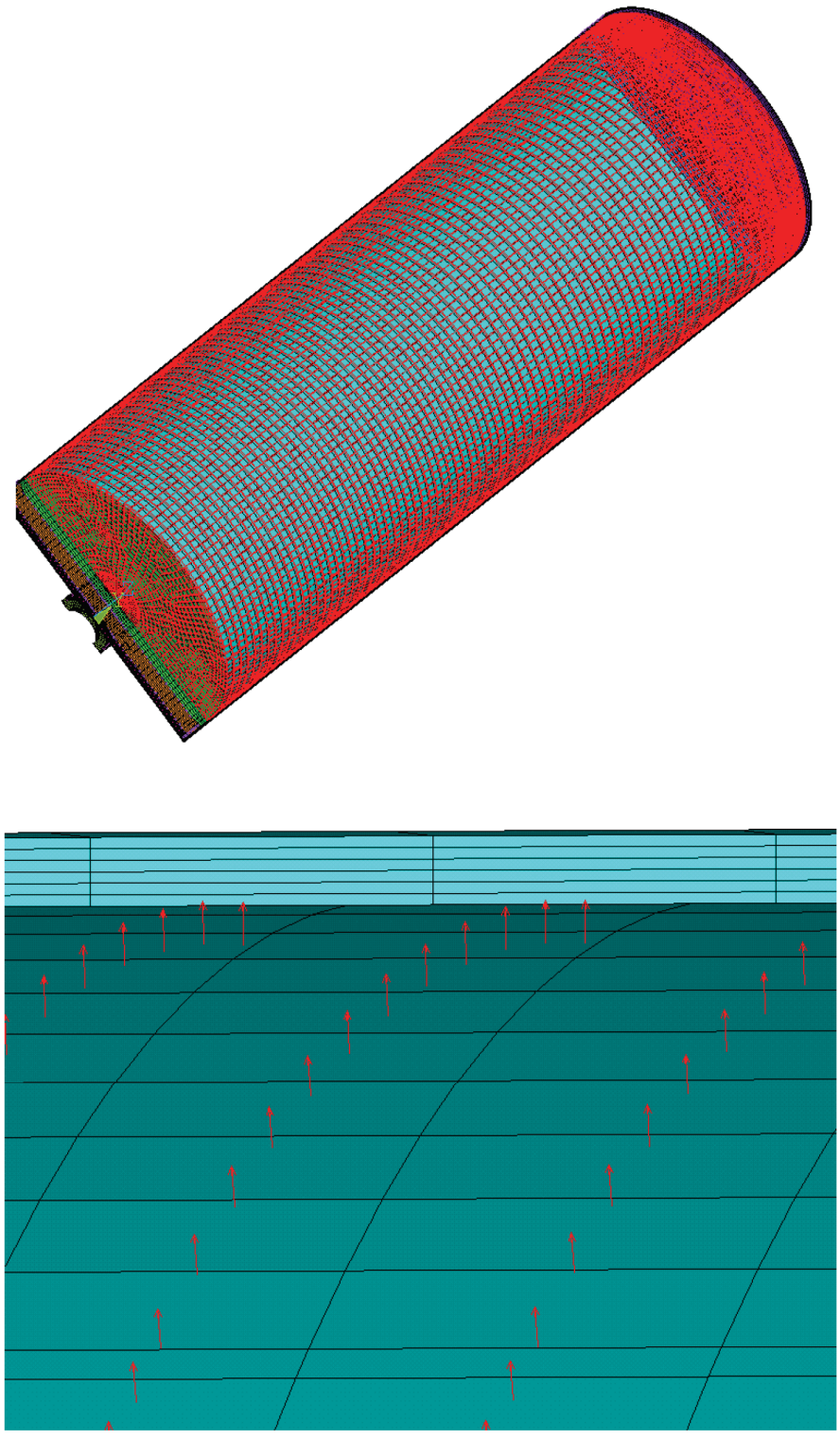

Figure 3.9.1-6
Internal Pressure – Load Application

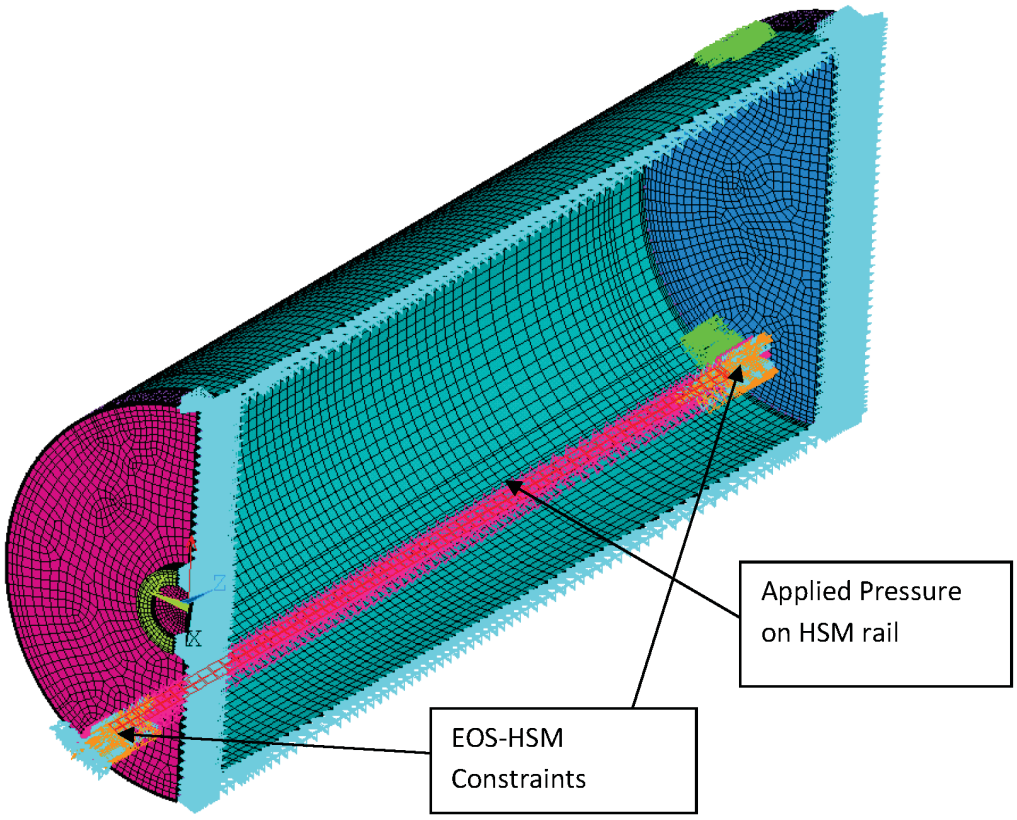

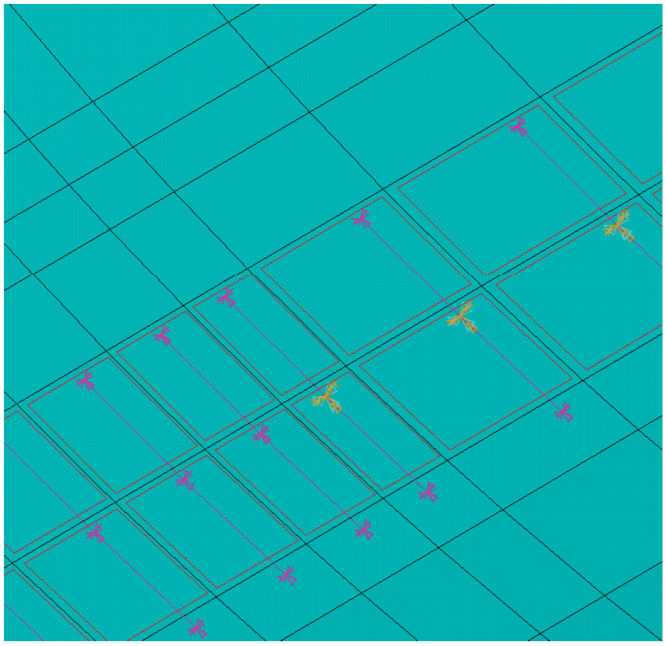

Figure 3.9.1-7
Dead Weight Simulation in EOS-*HSM*

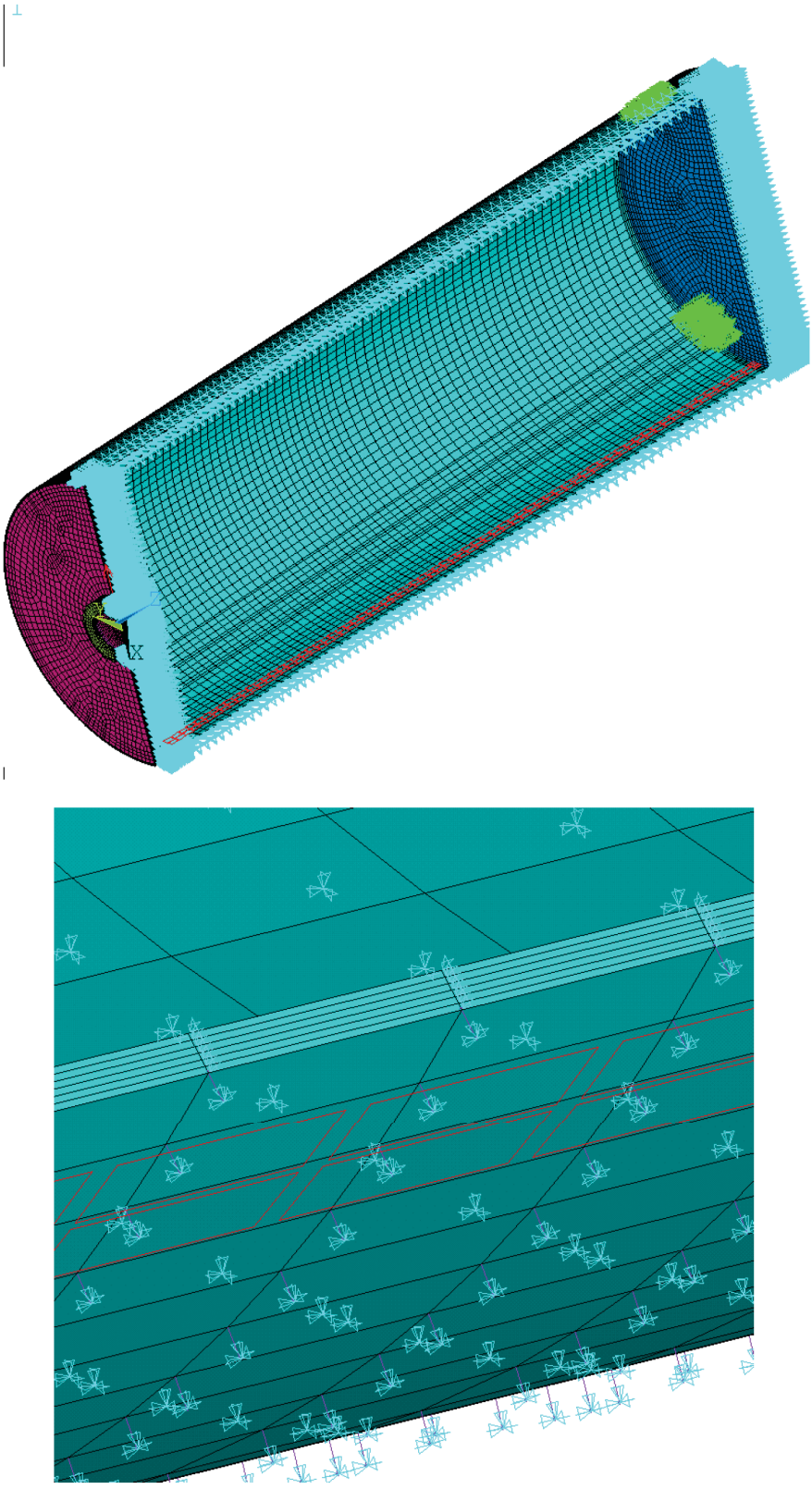

Figure 3.9.1-8
Dead Weight Simulation in EOS-TC

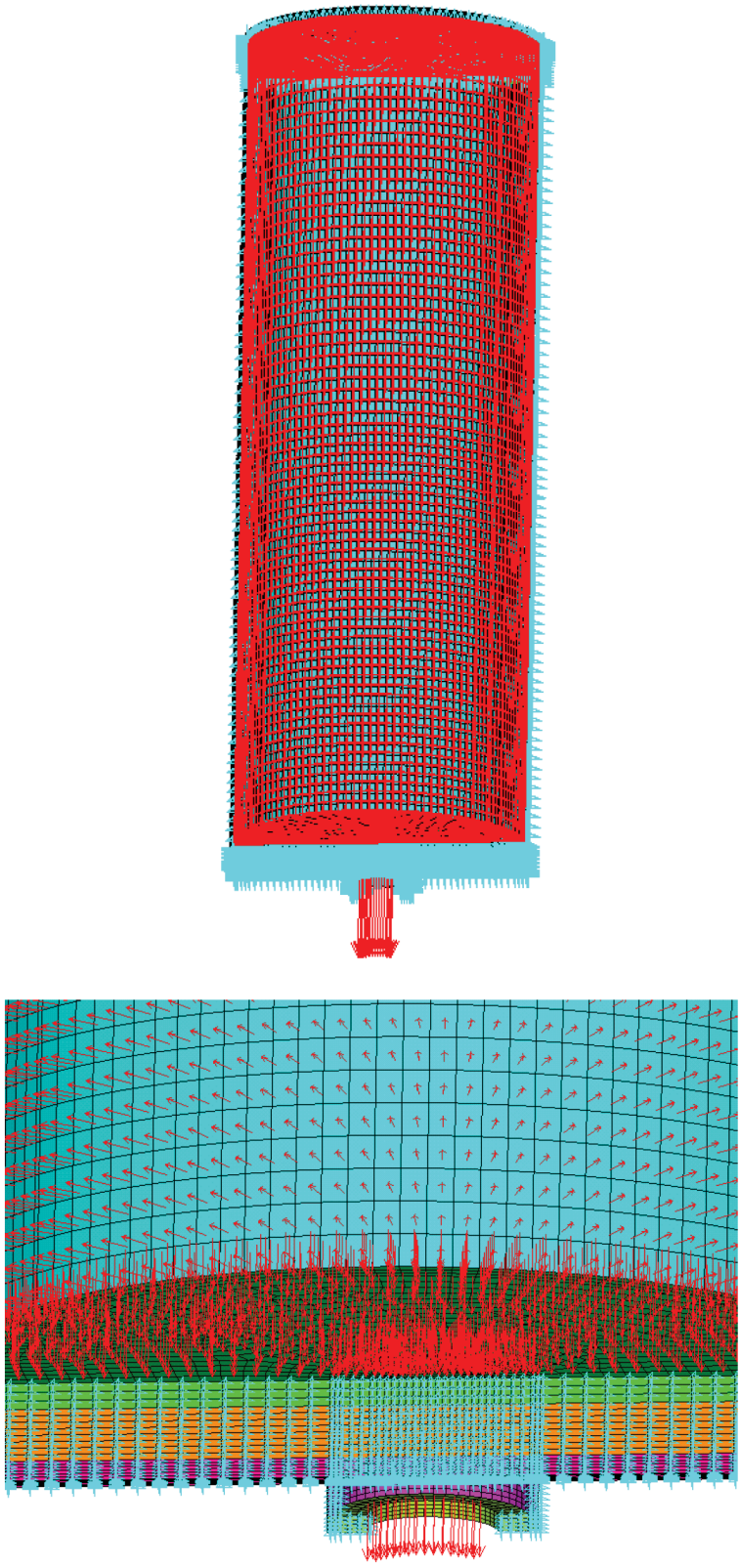

Figure 3.9.1-9
***Pull* Load with Internal Pressure**

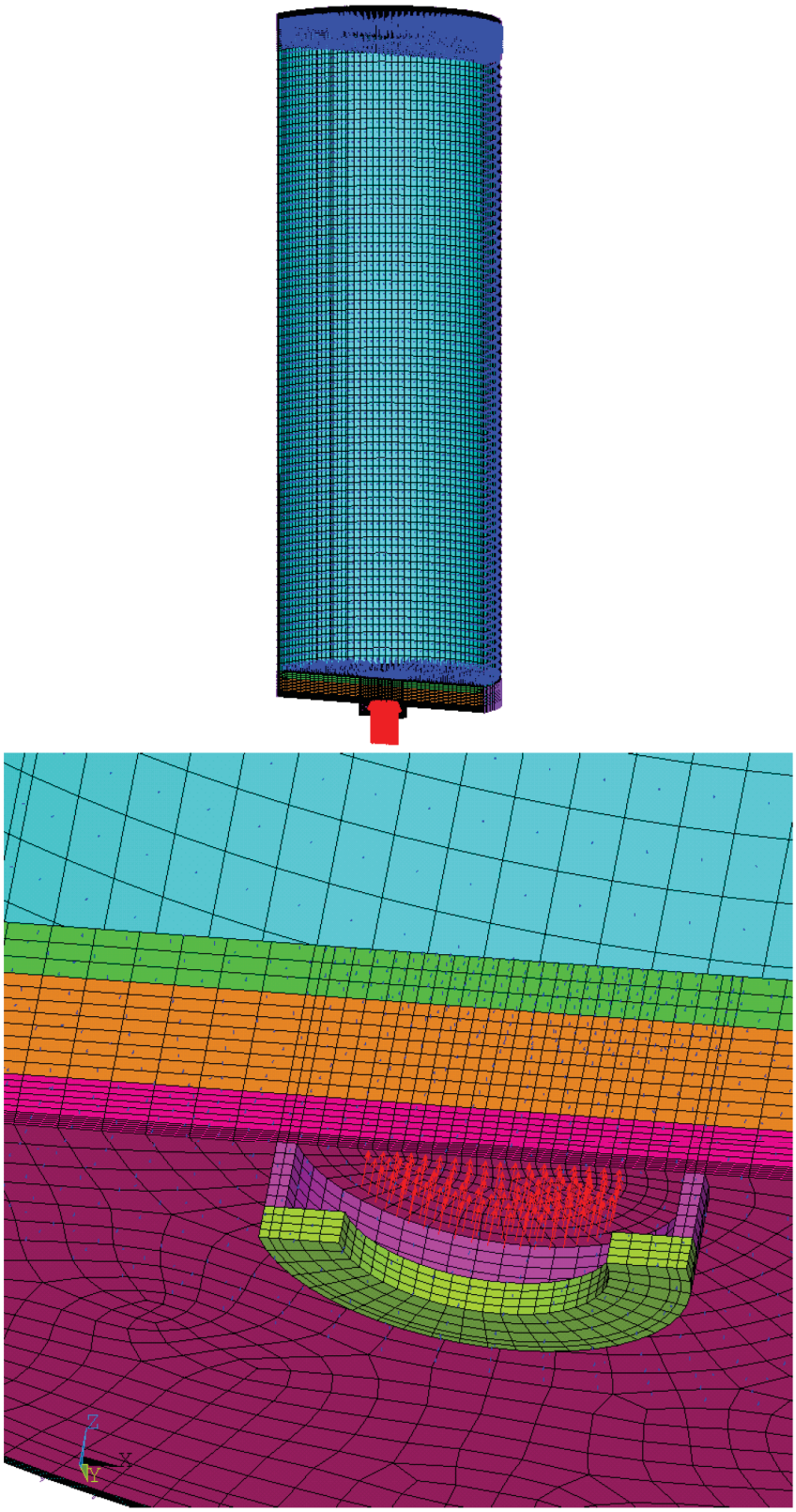

Figure 3.9.1-10
Push Load with Internal Pressure

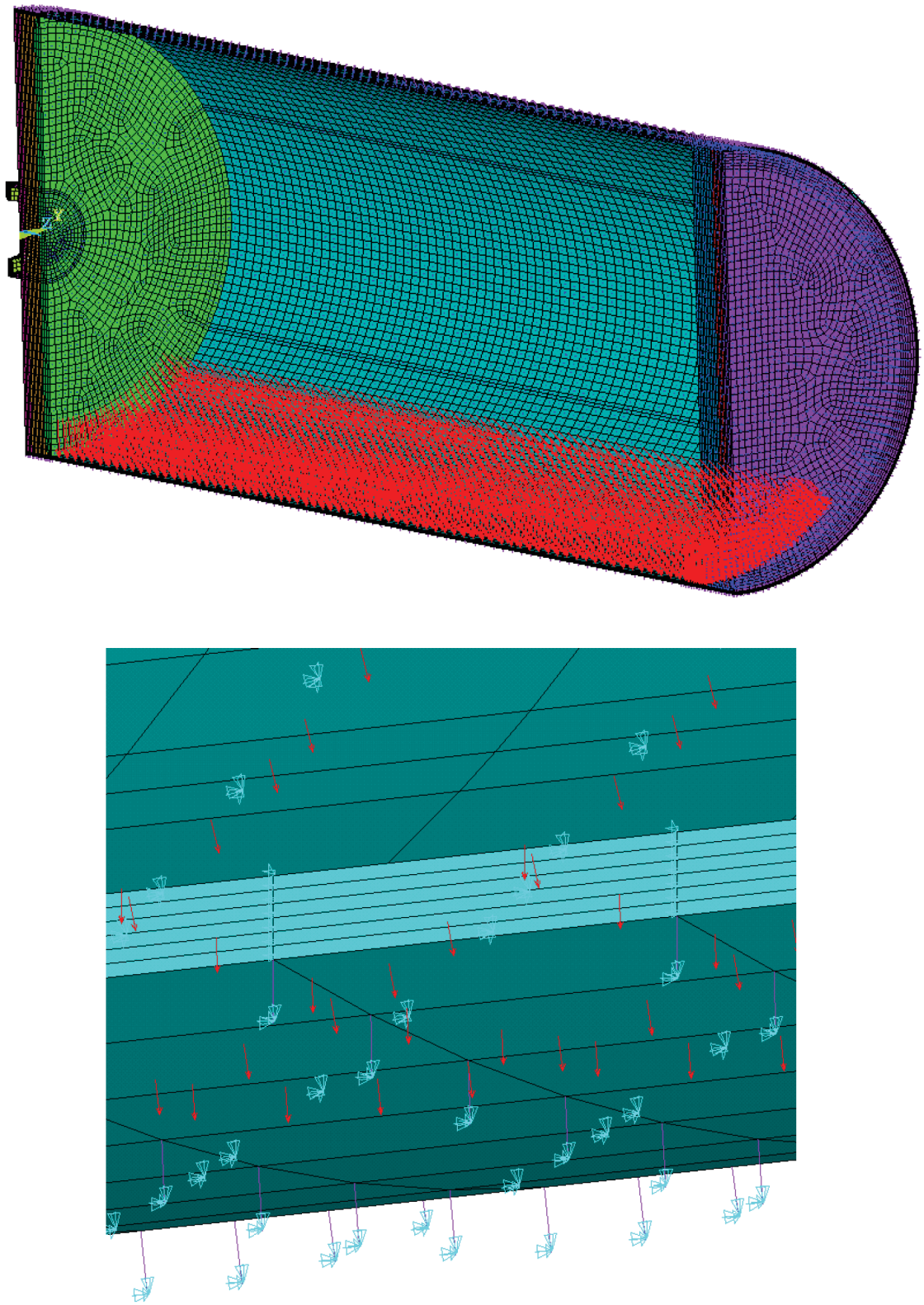

Figure 3.9.1-11
Side Drop Away from Cask Rail

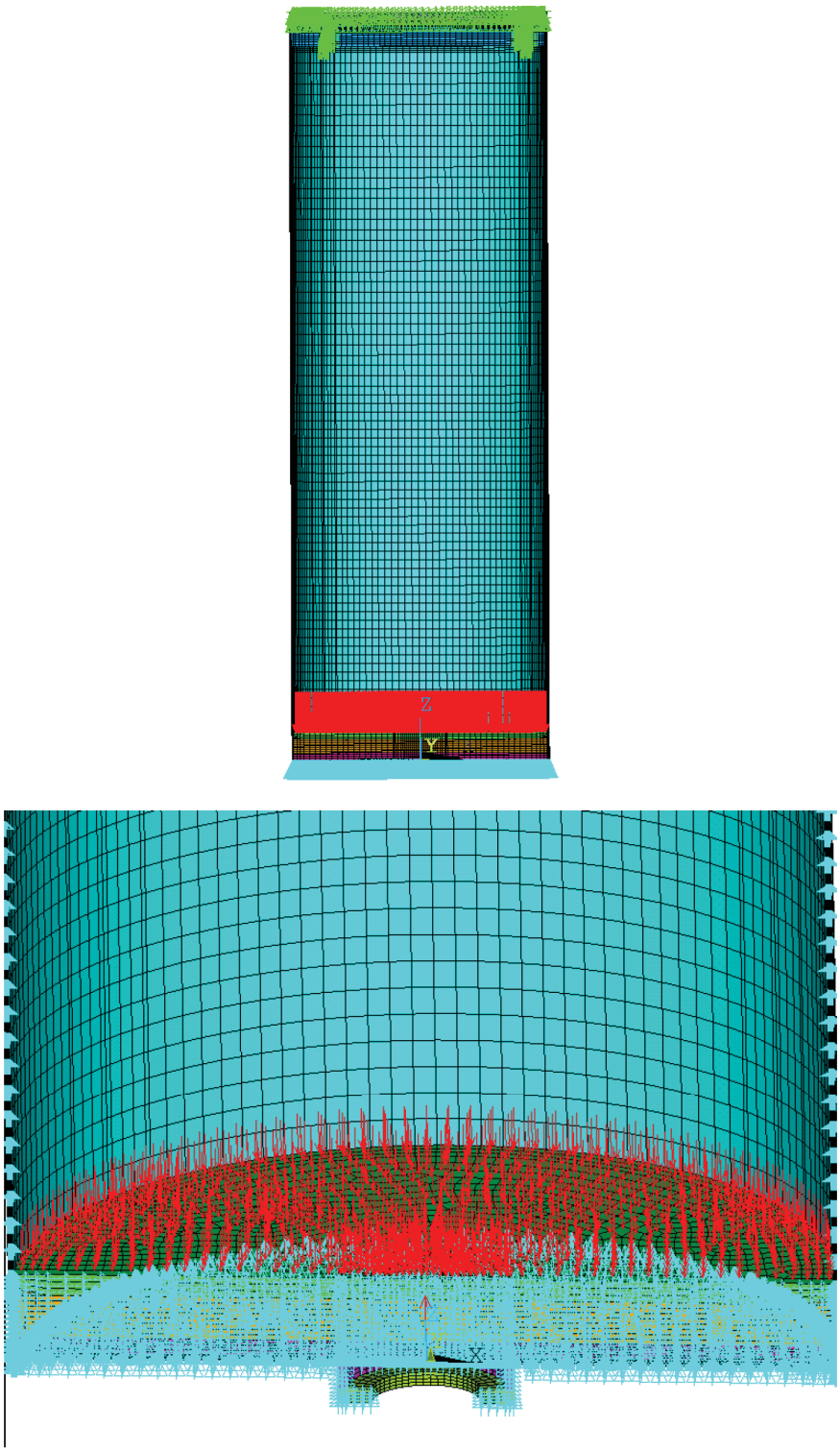

Figure 3.9.1-12
Bottom End Drop

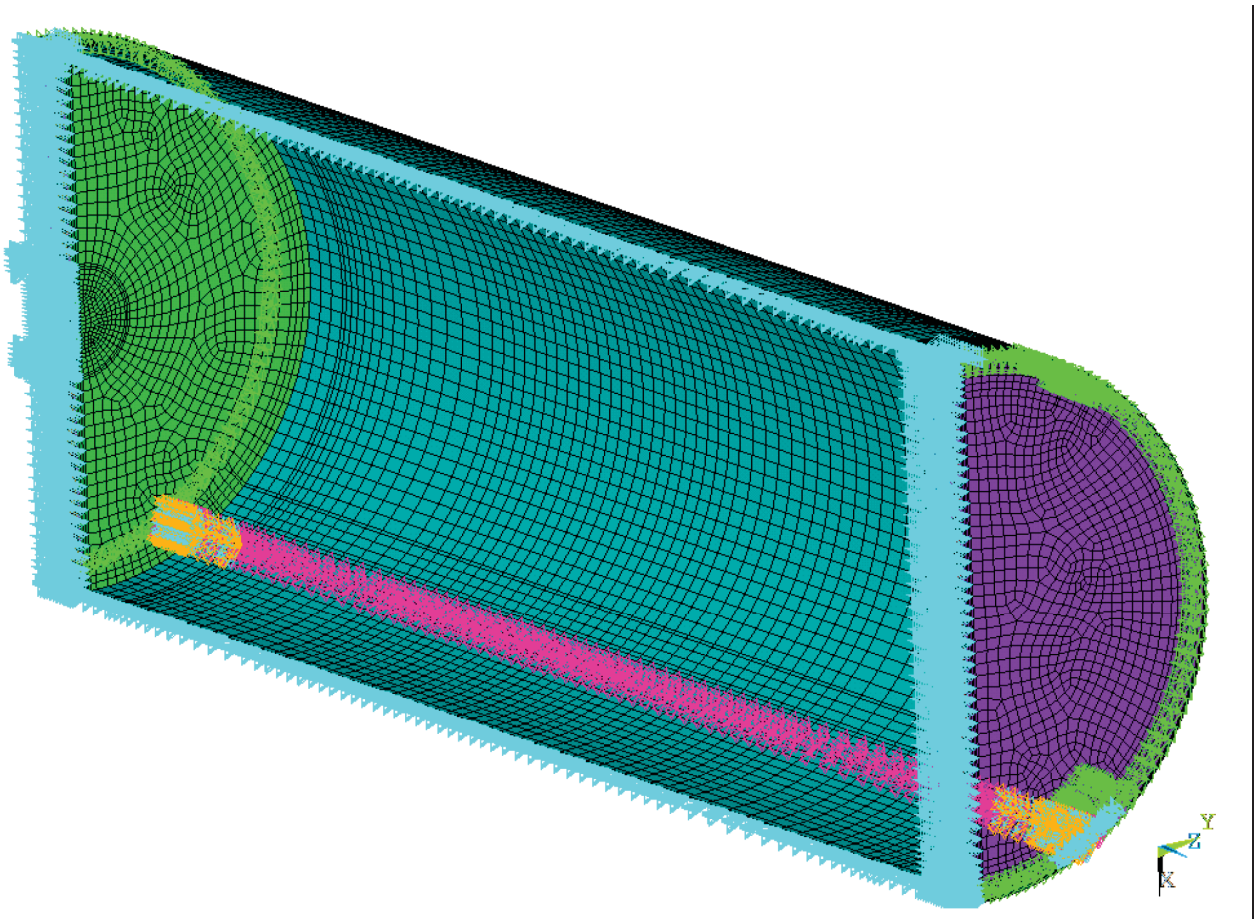

Figure 3.9.1-13
High Seismic in EOS-HSM Simulation

Proprietary Information on Pages 3.9.1-60 through 3.9.1-65
Withheld Pursuant to 10 CFR 2.390

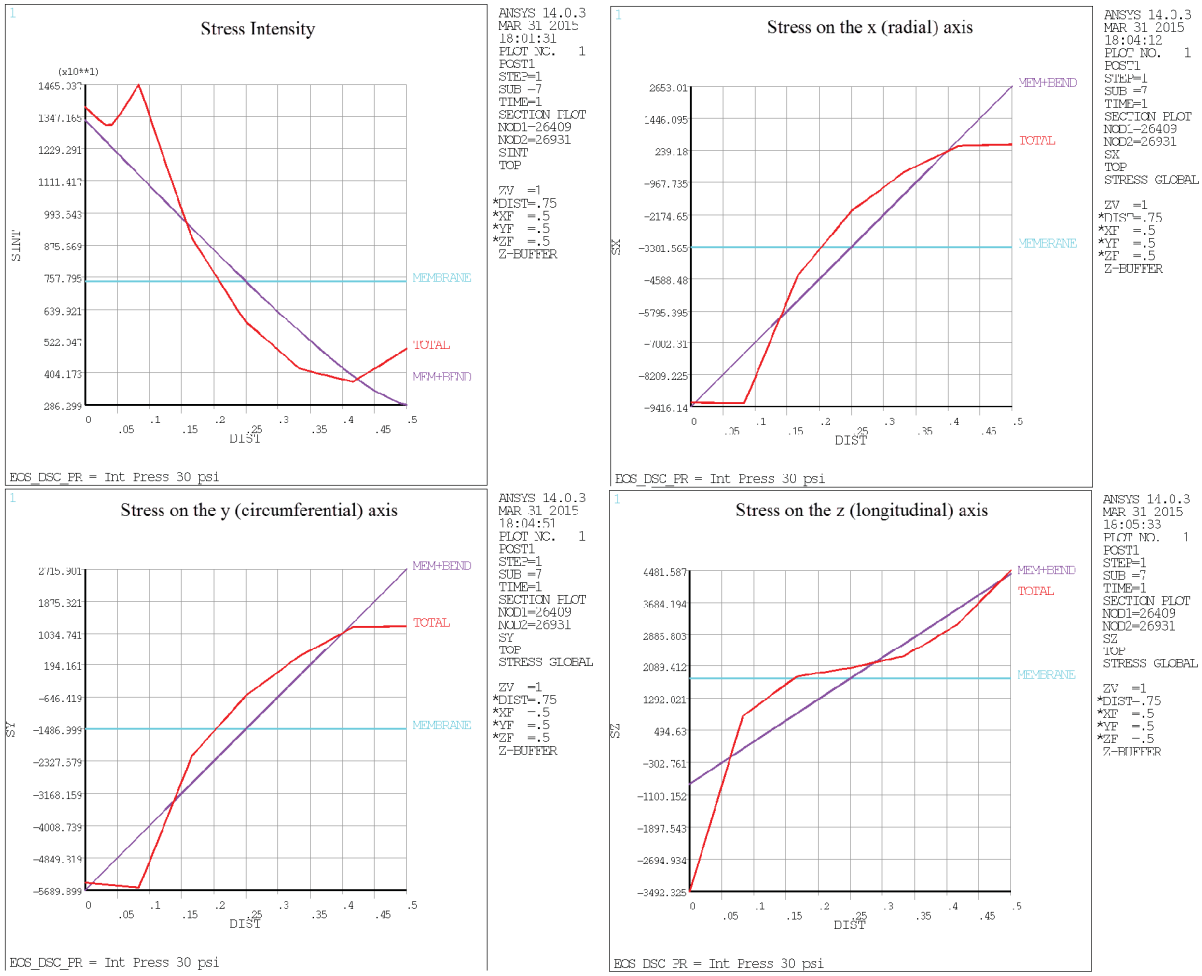

Figure 3.9.1-20
Maximum Membrane (S_{INT}, S_x, S_y, S_z) for Normal, Internal Pressure Load Case

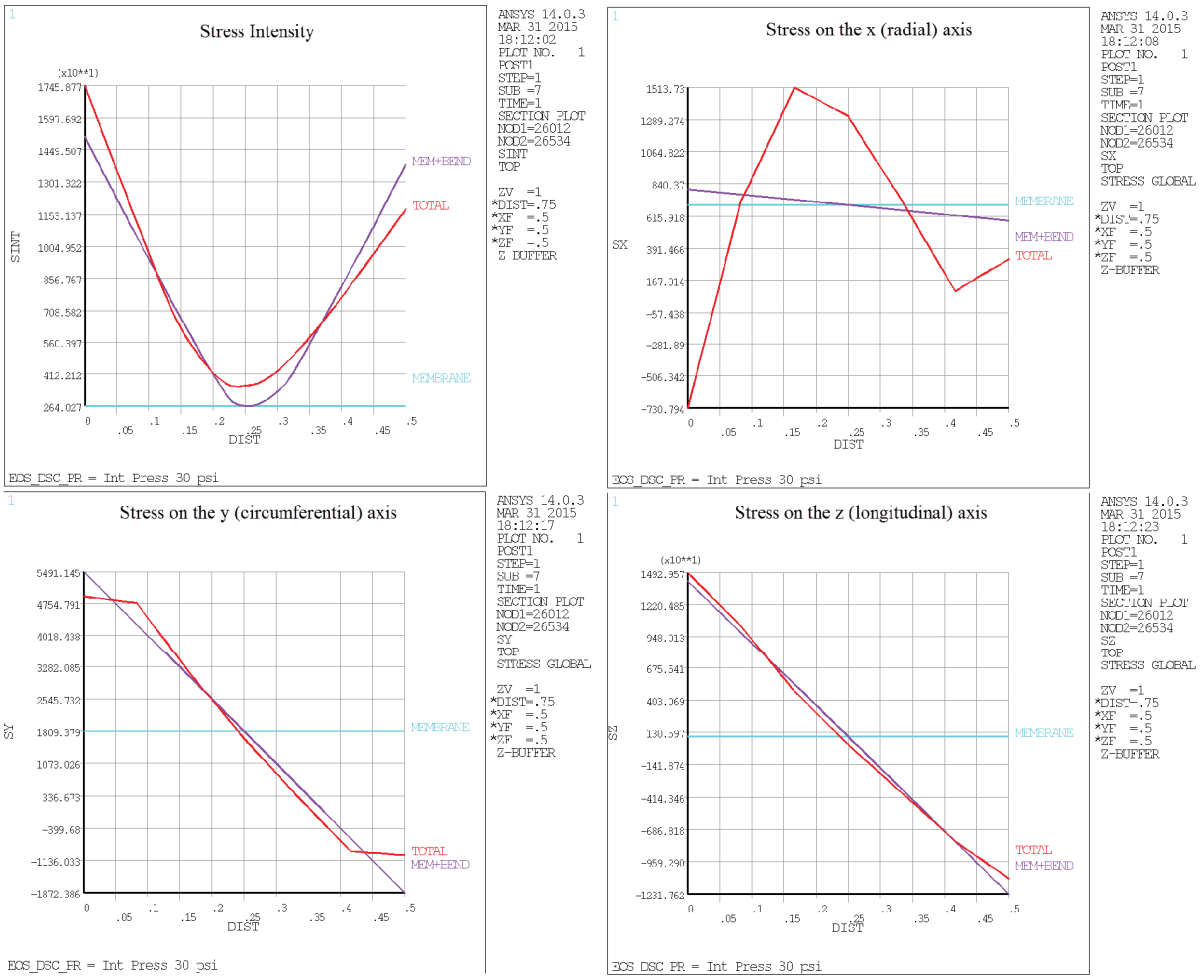

Figure 3.9.1-21
Maximum Membrane + Bending (S_{INT}, S_x, S_y, S_z) for Normal, Internal Pressure Load Case

APPENDIX 3.9.2
EOS-37PTH AND EOS-89BTH BASKET STRUCTURAL ANALYSIS

Table of Contents

List of Tables

List of Figures

3.9.2 EOS-37PTH AND EOS-89BTH BASKET STRUCTURAL ANALYSIS

This appendix evaluates the structural integrity of the EOS-37PTH and EOS-89BTH DSC basket for normal, off-normal, and side and end drop accident loads.

3.9.2.1 EOS-37PTH Basket Structural Evaluation for Normal/Off-Normal Loads

This section evaluates the structural integrity of the EOS-37PTH DSC basket for normal and off-normal loads. Onsite transfer conditions in the TC108, TC125, and TC135 transfer cask (TC) and storage conditions in the EOS-HSM are considered.

3.9.2.1.1 General Description

The EOS-37PTH DSC consists of a shell assembly that provides confinement and shielding, and an internal basket assembly that locates and supports the FAs. The basket is made up of interlocking, slotted plates to form an egg-crate type structure. The egg-crate structure forms a grid of 37 fuel compartments that house PWR spent fuel assemblies (SFAs). A typical stack-up of grid plates is composed of a structural steel plate, an aluminum plate for heat transfer and a neutron absorber plate (neutron poison) for criticality.

[

]

The basket structure is open at each end and therefore, when the EOS-TC is oriented vertically, longitudinal FA loads are applied directly to the cover plates/shield plugs of the DSC shell assembly and not to the basket assembly. When the EOS-TC is oriented horizontally, longitudinal FA loads from handling may be at least partially transferred to the basket assembly due to friction. The FAs are laterally supported in the basket's fuel compartments. The basket is laterally supported by the basket transition rails and the DSC inner shell.

The minimum open dimension of each fuel compartment cell is sized to allow storage of the applicable fuel, which provides clearance around the FAs. The length of the DSC shell/basket assemblies can be customized to accommodate different FA lengths. The basket length is less than the DSC cavity length to allow for thermal expansion and tolerances.

[

]

The DSC shell and basket assemblies are detailed in Section 1.3.

3.9.2.1.2 Key Dimensions and Materials

The key basket dimensions and materials are per Drawings EOS01-1010-SAR and EOS01-1011-SAR (Section 1.3.1).

The key DSC dimensions and materials are per Drawing EOS01-1001-SAR (Section 1.3.1).

The key EOS-TC dimensions are per Drawings in Section 1.3.4.

3.9.2.1.3 Material Properties

The mechanical properties of structural materials used for the basket assembly as a function of temperature are shown in Chapter 8.

3.9.2.1.4 Temperature Data

Temperature data from the thermal analyses in Chapter 4 at the axial location of hottest temperatures are considered for the thermal stress analysis and component evaluations. A bounding temperature gradient is used in the thermal stress analysis.

3.9.2.1.5 Fuel Data

Chapter 2 provides design characteristics for the types of pressurized water reactor (PWR) FAs to be considered. A bounding distributed weight of 11.0 lbs/in. in the active fuel region is considered in the deadweight and handling analyses.

3.9.2.1.6 Methodology

ANSYS 10.0A1 [3.9.2-2] is used for the evaluation of side loads and thermal loads. Hand calculations are performed to conservatively calculate the stresses due to the axial handling loads. Axial loads are combined with the corresponding side loads, as applicable. Load conditions for the vertical orientation of the DSC/TC are not controlling. Therefore, only the horizontal orientation is evaluated. However, the temperature gradient applied in the thermal analysis bounds the gradients applicable to both the horizontal and vertical orientations (see Section 3.9.2.1.6.1.4).

3.9.2.1.6.1 Finite Element Model

3.9.2.1.6.1.1 Analysis Model Description for Side Loads

In consideration of continuous support of the basket grid structure by the transition rails along the entire length, a 6-inch slice of the basket assembly is modeled, consisting of one-half the widths (basket axial direction) of the basket plates. One end of the 6-inch long model is at the symmetry plane of the horizontal plates and is at the free edges of the vertical plates. The opposite end of the 6-inch long model is at the symmetry plane of the vertical plates and is at the free edges of the horizontal plates. Symmetry boundary conditions (UY = ROTX = ROTZ = 0) are defined at the symmetry planes of the grid plates and at both cut faces of the transition rails and steel angle plates. Geometry plots of the ANSYS model are shown in Figure 3.9.2-1 through Figure 3.9.2-7.

The top and bottom regions of the basket assembly use grid plates with widths as small as 6 inches. The resulting ligaments at the 3-inch deep slots are only 3 inches wide, which is one-half of 6-inch wide ligaments for grid plates in the middle region. However, the tributary width for loading from fuel is also one-half of the tributary width for plates in the middle region, and the fuel distributed load is smaller at the ends since it is away from the active fuel region. Furthermore, the temperatures are lower at the top and bottom of the basket assembly. Therefore, the top and bottom regions of the basket assembly are bounded by the analyzed middle region.

The steel grid plates and the DSC shell are modeled using ANSYS Shell181 elements. No structural credit is taken for the poison plates or for the aluminum plates. The mass of the poison plates and aluminum plates is accounted for by increasing the density of the adjacent steel grid plates. Reinforcing steel angle plates in the R45 transition rails are also modeled using ANSYS Shell181 elements. The aluminum transition rails are modeled using ANSYS Solid185 elements.

Contact between the grid plates at the slots is modeled using ANSYS Conta178 elements (without friction). Initial gaps are defined for the contact elements based on the thickness stack-up of the steel, poison, and aluminum plates in each slot. Similarly, contact between the grid plates and the aluminum transition rails are modeled using ANSYS Conta178 elements (without friction). The initial gaps between the plates and the transition rails are considered closed. This implies that the unmodeled "sandwiched" aluminum, and poison plates are assumed to transfer loads normal to the plates. For stability and convergence purposes, soft springs (Combin14) are modeled coincident with the contact elements.

Bolts connecting the transition rails to the grid plates are modeled using ANSYS Beam4 elements. Nodes on the bolt elements are coupled to nodes on the grid plates, aluminum transition rails, and reinforcing steel angle plates in the rails, as applicable. At one end of each bolt, a contact element (Conta178) is defined in the axial direction of the bolt. The couples and contact element are defined so that only tension loads are transferred through the bolts (due to oversized bolt holes).

Similarly, tie rods for the R90 transition rail assemblies are modeled using ANSYS Beam4 elements. For loading other than thermal, the ends of tie rods are connected to the transition rails in the same manner as for the bolts, so that only tension loads are transferred. One Belleville spring washer is used at each end of the tie rods to allow for thermal growth of the R90 aluminum rail assemblies. Therefore, nonlinear Combin39 spring elements are used in lieu of the contact elements only for the thermal analyses (see Section 3.9.2.1.6.1.2). The thermal loading basically compresses the washer, so the tie rods behave like tension-only for other loads.

The DSC shell, when fully welded with cover plates, is much stiffer than the basket and therefore, for static analyses of the basket for small load levels such as deadweight and on-site handling loads, the DSC shell is considered to be rigid. Gaps between the basket and the DSC cylindrical shell are modeled using ANSYS Conta178 elements (without friction). Each gap element contains two nodes; one on each surface of the structures. Initial gaps are based on a basket outside diameter of 74.10 inches and a DSC inside diameter of 74.50 inches, and the side load orientation. Initial gaps are adjusted in consideration of the radial thermal growth of the basket relative to the growth of the DSC shell.

To consider bounding conditions, two sets of analyses are performed. The first set of analyses defines nominal gaps for a basket thermal growth, relative to the DSC shell, approximated to be 0.05 inches. The second set of analyses adjusts the gaps for a basket minimum thermal growth, relative to the DSC shell, of 0.0158 inch, calculated based on average temperatures of the basket and DSC shell at the hottest cross-section per Chapter 4.

Side loads due to transfer handling bound the loads applicable to storage in the EOS-HSM for which only deadweight is applicable. As discussed earlier, the DSC shell, when fully welded with cover plates, is much stiffer than the basket and therefore, for static analyses of the basket for small load levels such as deadweight and on-site handling loads, the DSC shell is considered to be rigid. Therefore the impact of the rail location is insignificant and one model envelopes the configuration when the DSC is inside the EOS-TC and EOS-HSM.

3.9.2.1.6.1.2 Analysis Model Description for Thermal Loads

The basket assembly thermal stress model is similar to the side-loaded model except that it excludes the DSC cylindrical shell (which does not restrain the thermal growth of the basket). One Belleville spring washer is used at each end of the tie rods to allow for thermal growth of the R90 aluminum rail assemblies. Therefore, nonlinear Combin39 spring elements are used in lieu of contact elements at one end of each tie rod for the thermal analyses. The force-deflection input is determined using data associated with the spring washer.

Boundary conditions for the transition rails and rail angle plates are removed from one end of the model to avoid fictitious thermal stresses that would occur if both ends were restrained. Two thermal cases are considered in consideration of the boundary conditions for the transition rails and rail angle plates: restraint at y = 0 inch (near end restraint), and restraint at y = 6 inches(far end restraint). Although the maximum stress results from these two cases are effectively the same, the results are combined with the deadweight and handling cases using ANSYS load combinations to preclude the conservatism of adding maximum stresses regardless of location. The consideration of two sets of boundary conditions for thermal ensures that the correct maximum stress in combination with deadweight and handling stress is obtained.

3.9.2.1.6.1.3 Material Properties in Analyses

The modeled components of the basket and DSC are based on lower bound material properties. The material properties used for stress analyses (except thermal stress analyses) are based on bounding average temperature values at the hottest section for off-normal transfer in a horizontal EOS-TC. Elastic analyses are used for all normal and off-normal conditions.

3.9.2.1.6.1.4 Loads

Load cases are based on the loads described in Chapter 2.

For side loading, the fuel weight load is modeled conservatively using a pressure load equivalent to the applicable acceleration, or G-load, times the FA weight divided by the basket fuel compartment area associated with the active fuel region length and the fuel compartment width between slots (8.79 inches). A fuel load of 11.0 lbs/in acting on the fuel compartment width between slots is applied to bound the load distribution in the active fuel region for all PWR fuel types identified in Chapter 2. Figure 3.9.2-8 shows the application of fuel weight pressure loads to the model.

For 0° and 180° side load orientations, the equivalent fuel assembly pressure acts only on the horizontal plates. For 90° and 270° side load orientations, the equivalent fuel assembly pressure acts only on the vertical plates. For other orientations, the equivalent FA pressure acts perpendicular to the horizontal and vertical plates, proportioned based on the Cosine and Sine of the orientation angle.

Based on the handling load combination required per Chapter 2, the following bounding normal side load conditions (DSC and basket in horizontal position) are evaluated:

- DW + 1g Vertical = 2.0g Vertical at $\theta = 180°$
- DW + 0.5g Vert. + 0.5g Transverse = 1.58g at $\theta_{198} = 198.43°$ *
- DW + 1.0g Transverse = 1.414g at $\theta_{225} = 225.0°$ *

* $\theta_{198} = 180° + \text{Tan}^{-1}(0.5 / 1.5) = 198.43°$; $\theta_{225} = 180° + \text{Tan}^{-1}(1.0 / 1.0) = 225°$

Thermal stress analyses are based on a bounding temperature profile. The temperature profile used is represented by the following equation, labeled "EOS Basket Analysis" in Figure 3.9.2-9:

$$T(x) = -0.3952\ x^2 + 3.4661\ x + 790.29$$

Where,

T(x) = Basket temperature as a function of radius, x.

Figure 3.9.2-9 shows the raw temperature data (versus radius) for one load case from the thermal analyses, labeled "EOS-37PTH in EOS-TC125, Grid Plates, LC # 6" (worst-case temperature condition for steepness of radial temperature gradient). A comparison of the curves shows that the curve labeled as "EOS Basket Analysis," which gives the temperatures versus radius used in the basket thermal stress analysis herein, provides the bounding steeper gradient.

3.9.2.1.6.2 Criteria

The basis for allowable stresses is obtained from Chapter 8 and ASME Section III, Division 1, Subsection NG [3.9.2-1]. The criteria are summarized in Chapter 3, Table 3-2. Allowable stresses for the threaded fasteners, used to connect the transition rails to the basket grid structure, are from Chapter 8 and Section NG-3230 of [3.9.2-1]. The criteria are summarized in Table 3.9.2-1. The component allowable stress values are summarized in Table 3.9.2-2. The allowable stresses are based on material properties at 700 °F for the grid plates and 550 °F for the transition rails, angle plates, bolts and tie rods. These temperatures bound the average temperatures at the hottest section for the grid plates and transition rails, respectively, summarized in Chapter 4 for off-normal transfer in a horizontal EOS-TC.

3.9.2.1.6.3 Creep Evaluation for Long Term Storage

The aluminum R90 rails are designed to resist the bearing loads due to the deadweight of the loaded basket for 80 years while stored in the EOS-HSM. For long-term creep effects, where loading on the aluminum transition rail redistributes over time, an average bearing stress is an appropriate value to consider.

Conservatively, it is assumed that the entire weight of the basket is resisted by the three pieces of a single aluminum R90 rail. The 1g deadweight load from the entire weight of a 6-inch long portion of the basket is approximately 3,416 lb. The area of the corresponding 6-inch long portion of the R90 rail that resists the load is approximately = 156 in^2. However, credit for the outer portion of the width of the rail is excluded by conservatively considering only half of the rail width. The corresponding bearing stress is calculated as follows:

Basket 1g vertical bearing stress = Load / Area = 43.8 psi, or, 0.044 ksi.
(on aluminum R90 transition rail)

The individual compartment load at each SFA location on the supporting aluminum plate gives a much lower bearing stress. Using a conservative width of only 8 inches for a compartment gives:

SFA 1g vert. bearing stress = (Load / length) / Width = 1.375 psi, or, 0.0014 ksi.
(on aluminum plate)

The allowable bearing stresses are provided in Chapter 8, and based on Reference [3.9.2-3]; they represent the stress in Aluminum 1100 to produce a strain of 0.01 in 550,000 hours (approximately 63 years). However, the creep strain curve is so flat that the values at 80 years are approximately the same. The allowable bearing stress for Aluminum 1100 represents a conservative lower bound. The initial temperature values (time = 0) and the corresponding allowable bearing stresses in the basket aluminum components, to limit creep strain to 0.01, are as follows:

- 0.254 ksi in the hottest aluminum plate, with a starting temperature of 680 °F
- 0.758 ksi in the hottest R90 rail, with a starting temperature of 470 °F
- 0.876 ksi in a less than hottest R90 rail, based on a starting temperature of 440 °F

From Chapter 4 for normal conditions (applicable to long-term storage conditions) at the hottest cross-section of the basket, the average R90 transition rail temperature is not more than 469 °F, which is less than the above temperature of 470 °F for the hottest R90 rail. Similarly, from Chapter 4, for normal conditions, the hottest basket plate temperature is not more than 668 °F, which is less than the above temperature of 680 °F for the hottest aluminum plate. Based on this comparison of temperatures, and since the heat dissipation rate for the EOS-37PTH basket is better than that for the basket temperature data (temperature versus time) used in Reference [3.9.2-3], the allowable creep stresses given above are applicable to the aluminum components of the EOS-37PTH basket.

3.9.2.1.7 Results

3.9.2.1.7.1 Results for On-Site DW+Handling and Thermal Stress Analysis

Combined results for basket component stress results for normal condition deadweight + handling loads and thermal stress analysis are shown in Table 3.9.2-3. The tabulated results show that all stresses meet the corresponding Code limits.

ANSYS Force Summation Comparison

An ANSYS force summation for the basket components only, for the 2g deadweight plus handling load combination, is compared to the expected load as shown below:

Force Summation: F_z = -6,831.256 lb
(in vertical direction (z), length of model is 6 inches)
Expected Load:
Basket weight / length w/o spent fuel: = 167.2 lb/in
Basket wt. w/o spent fuel (6” long) = 1,003 lb.
Spent fuel weight (6” long) = (11 lb/in) (6” length of basket) (37 SFAs)
= 2,442 lb.
Total weight of the basket, with spent fuel (6” long) = 3,445 lb (for 1g)
Expected Load at 2g (in vertical direction) = 6,890 lb.

The ANSYS load of 6,831 is within 1% of the hand-calculated weight load and therefore, is acceptable.

Similarly, the ANSYS 1g load is 3,416 lb, or half of the ANSYS 2g load, as expected.

3.9.2.1.7.2 Aluminum Components – Long Term Storage Deadweight Bearing Stress

The aluminum R90 rails are designed to resist the bearing loads due to the deadweight of the loaded basket for 80 years while stored in the EOS-HSM. A review of the R90 transition rail stresses in Figure 3.9.2-11 shows that for the 1g deadweight loading, the R90 rail carries most of the loading. The aluminum R45 rails take some of the bearing load but are not controlling. The stresses shown in Figure 3.9.2-11 are unaveraged stresses that include local and peak effects. However, for long-term creep effects, where loading on the aluminum transition rail redistributes over time, an average bearing stress is a more appropriate value to consider. The stresses calculated in Section 3.9.2.1.6.3 are compared to allowable stress values that are reduced to limit the effect due to creep.

Comparison of Aluminum Bearing Stress to Allowable Creep Stress from Section 3.9.2.1.6.3:

Component	Bearing Stress	Allowable Creep Stress	Stress/Allowable Ratio
Alum. Rail	0.044 ksi	0.758 ksi	0.0580
Alum. Plate	0.0014 ksi	0.254 ksi	0.0055

3.9.2.1.8 Conclusions

Finite element analyses and hand calculations for the EOS-37PTH basket assembly are performed for all normal and off-normal on-site conditions. Controlling stress intensities are reported in Table 3.9.2-3. A comparison of stress intensities to the corresponding allowable values indicate that all load conditions and combinations show acceptable stress levels, as applicable.

3.9.2.2 EOS-89BTH Basket Structural Evaluation for Normal/Off-Normal Loads

The basis for the fuel compartment allowable stress values is the ASME Code, Section III, Subsection NG (Reference [3.9.2-1]), as given in Chapter 8.

3.9.2.2.1 General Description

The EOS-89BTH DSCs consists of a shell assembly that provides confinement and shielding, and an internal basket assembly that locates and supports the FAs. The basket is made up of interlocking slotted plates to form an egg-crate type structure. The egg-crate structure forms a grid of 89 fuel compartments that house boiling water reactor (BWR) SFAs. A typical stack-up of grid plates is composed of a structural steel plate, an aluminum plate for heat transfer and a neutron absorber plate (neutron poison) for criticality.

The DSC shell and basket assemblies are detailed in drawings in Section 1.3.2.

The descriptions in Section 3.9.2.1.1 of the transition rails and basket are also applicable to the EOS-89BTH DSC.

3.9.2.2.2 Key Dimensions and Materials

The key basket dimensions and materials are per Drawings EOS01-1020-SAR and EOS01-1021-SAR Section 1.3.2.

The key DSC dimensions and materials are per Drawing EOS01-1001-SAR (Section 1.3.2):

The key EOS-TC dimensions are per the drawings in Section 1.3.4.

3.9.2.2.3 Material Properties

The mechanical properties of structural materials used for the basket assembly and canister as a function of temperature are shown in Chapter 8.

3.9.2.2.4 Temperature Data

Temperature data from the EOS-89BTH thermal analyses and from the EOS-37PTH thermal analyses in Chapter 4, at the axial location of hottest temperatures, are considered herein for the thermal stress analysis and component evaluations. The conservative temperature gradient used herein for the thermal stress analysis bounds the gradients for the EOS-89BTH basket. See Section 3.9.2.1.6.1.4 for further discussion.

3.9.2.2.5 Fuel Data

Chapter 2 provides design characteristics for the types of BWR FAs to be considered. A maximum FA weight of 705 lbs is used. A distributed weight of 705 lbs / 150 in. = 4.7 lbs/in is considered to be bounding in the active fuel region for the deadweight and handling analyses.

3.9.2.2.6 Methodology

Same as Section 3.9.2.1.6.

3.9.2.2.6.1 Finite Element Model

3.9.2.2.6.1.1 Analysis Model Description for Side Loads

Geometry plots of the ANSYS model are shown in Figure 3.9.2-12 through Figure 3.9.2-18. All other details of the analysis model description are the same as Section 3.9.2.1.6.1.1.

3.9.2.2.6.1.2 Analysis Model Description for Thermal Loads

Same as Section 3.9.2.1.6.1.2.

3.9.2.2.6.1.3 Material Properties in Analyses

Same as Section 3.9.2.1.6.1.3.

3.9.2.2.6.1.4 Loads

Load cases are based on the loads described in Chapter 2.

For side loading, the fuel weight load is modeled conservatively using a pressure load equivalent to the applicable acceleration, or g-load, times the FA weight divided by the basket fuel compartment area associated with the active fuel region length and the fuel compartment width between slots (5.85 inches). A fuel load of 4.7 lbs/in acting on the fuel compartment width between slots is applied to bound the load distribution in the active fuel region for all BWR fuel types identified in Chapter 2. Figure 3.9.2-19 shows the application of fuel weight pressure loads to the model.

For 0° and 180° side load orientations, the equivalent FA pressure acts only on the horizontal plates. For 90° and 270° side load orientations, the equivalent fuel assembly pressure acts only on the vertical plates. For other orientations, the equivalent FA pressure acts perpendicular to the horizontal and vertical plates, proportioned based on the Cosine and Sine of the orientation angle.

Based on the handling load combination, the following bounding normal side load conditions (DSC and basket in horizontal position) are evaluated:

- - DW + 1g Vertical = 2.0g Vertical at $\theta = 180°$
- - DW + 0.5g Vert. + 0.5g Transverse = 1.58g at $\theta_{198} = 198.43°$ *
- - DW + 1.0g Transverse = 1.414g at $\theta_{225} = 225.0°$ *

* $\theta_{198} = 180° + \text{Tan-1}(0.5 / 1.5) = 198.43°$; $\theta_{225} = 180° + \text{Tan-1}(1.0 / 1.0) = 225°$

Thermal stress analyses are made based on a bounding temperature profile. The temperature profile used is represented by the following equation labeled "EOS Basket Analysis" in Figure 3.9.2-9:

$$T(x) = -0.3952\ x^2 + 3.4661\ x + 790.29$$

Where,

T(x) = Basket temperature as a function of radius, x.

Due to the lower heat load in the EOS-89BTH DSC compared to the EOS-37PTH DSC, limited analyses are run in Chapter 4 to demonstrate that the maximum fuel cladding temperatures for the EOS-89BTH will be bounded by those for the EOS-37PTH. However, resulting maximum EOS-89BTH basket component temperatures are in some cases shown to be greater than for the EOS-37PTH basket component temperatures.

Figure 3.9.2-20 shows that although the EOS-89BTH grid plate temperatures are slightly greater than the EOS-37PTH grid plate temperatures, the gradients are similar. As shown in these figures and in comparison plots for other thermal cases, the analyzed temperature profile has a steeper temperature gradient than that for the raw data. Therefore, it can be concluded that the conservative temperature gradient used herein for the thermal stress analysis will bound the gradients for the EOS-89BTH basket. Figure 3.9.2-21 shows the bounding temperature profile applied to the ANSYS model.

3.9.2.2.6.2 Criteria

The basis for allowable stresses is obtained from Chapter 8 and ASME Section III, Division 1, Subsection NG (Reference [3.9.2-1]). The criteria are summarized in Chapter 3, Table 3-2.

Allowable stresses for the threaded fasteners, used to connect the transition rails to the basket grid structure, are from Chapter 8 and Section NG-3230 of [3.9.2-1]. The criteria are summarized in Table 3.9.2-1. The component allowable stress values are summarized in Table 3.9.2-2. The allowable stresses are based on material properties at 700 °F for the grid plates (except where noted otherwise) and 550 °F for the transition rails, angle plates, bolts and tie rods. These temperatures bound the average temperatures at the hottest section for the grid plates and transition rails, respectively, summarized in Chapter 4 for transfer in a horizontal EOS-TC (non-accident).

3.9.2.2.6.3 Creep Evaluation for Long Term Storage

The aluminum R90 rails are designed to resist the bearing loads due to the deadweight of the loaded basket for 80 years while stored in the EOS-HSM. For long-term creep effects, where loading on the aluminum transition rail redistributes over time, an average bearing stress is an appropriate value to consider.

Conservatively assuming that the entire weight of the basket is resisted by the three pieces of a single aluminum R90 rail, the 1g deadweight load from the entire weight of a 6-inch long portion of the basket is approximately 3,462 lb. The area of the corresponding 6-inch long portion of the R90 rail that resists the load is approximately = 102 in^2. However, credit for the outer portion of the width of the rail is excluded by conservatively considering only half of the rail width. The corresponding bearing stress is calculated as follows:

Basket 1g vert. bearing stress = Load / Area = 67.9 psi, or, 0.068 ksi. (on aluminum R90 transition rail)

The individual compartment load at each SFA location on the supporting aluminum plate gives a much lower bearing stress. Using a conservative width of only 5 inches for a compartment gives:

SFA 1g vert. bearing stress = (Load / length) / Width = 0.940 psi, or, 0.00094 ksi. (on aluminum plate)

The allowable bearing stresses are provided in Section 3.9.2.1.6.3. The initial temperature values (time = 0) and the corresponding allowable bearing stresses in the basket aluminum components, to limit creep strain to 0.01, are as follows:

- 0.254 ksi in the hottest aluminum plate, with a starting temperature of 680 °F
- 0.758 ksi in the hottest R90 rail, with a starting temperature of 470 °F
- 0.876 ksi in a less than hottest R90 rail, based on a starting temperature of 440 °F

From Chapter 4, for normal conditions (applicable to long-term storage conditions) at the hottest cross-section of the basket, the average R90 transition rail temperature is not more than 446 °F, which is less than the above temperature of 470 °F for the hottest R90 rail. Similarly, from Chapter 4, for normal conditions, the hottest basket plate temperature is not more than 676 °F, which is less than the above temperature of 680 °F for the hottest aluminum plate. Based on this comparison of temperatures, and since the heat dissipation rate for the EOS-89BTH basket is better than that for the basket temperature data (temperature versus time) used in Reference [3.9.2-3], the allowable creep stresses given above are applicable to the aluminum components of the EOS-89BTH basket.

3.9.2.2.7 Results

3.9.2.2.7.1 Results for On-Site DW+Handling and Thermal Stress Analysis

Combined results with controlling stress ratios for normal condition deadweight + handling loads and thermal analysis are shown in Table 3.9.2-4. The tabulated results show that all stresses meet the corresponding Code limits.

ANSYS Force Summation Comparison

An ANSYS force summation for the basket components only, for the 2g deadweight plus handling load combination, is compared to the expected load as shown below:

Force Summation: F_z = -6,923.822 lb (in vertical direction (z), length of model is 6")
Expected Load:
Basket weight / length w/o spent fuel = (19,300 + 637 + 1,110 + 3,980) / 166.0 + 1,720 / 175.0
= 160.6 lb/in
Basket wt. w/o spent fuel (6" long) = (160.6) (6") = 964 lb.
Spent fuel weight (6" long) = (4.7 lb/in) (6" length of basket) (89 SFAs)
= 2,510 lb.

Total weight of the basket, with spent fuel (6" long) = 964 + 2,510 = 3,474 lb (for 1g)
Expected Load at 2g (in vertical direction) = 2 (3,474) = 6,948 lb.

The ANSYS load of 6,924 is within 0.4% of the hand-calculated weight load and therefore, is acceptable.

Similarly, the ANSYS 1g load is 3,462 lb, or half of the ANSYS 2g load, as expected.

3.9.2.2.7.2 Aluminum Components – Long Term Storage Deadweight Bearing Stress

The aluminum R90 rails are designed to resist the bearing loads due to the deadweight of the loaded basket for 80 years while stored in the EOS-HSM. A review of the R90 transition rail stresses in Figure 3.9.2-22 shows that for the 1g deadweight loading, the R90 rail carries most of the loading. The aluminum R45 rails take some of the bearing load but are not controlling. The stresses shown in Figure 3.9.2-22 are unaveraged stresses that include local and peak effects. However, for long-term creep effects, where loading on the aluminum transition rail redistributes over time, an average bearing stress is a more appropriate value to consider.

The stresses calculated in Section 3.9.2.2.6.3 are compared to allowable stress values that are reduced to limit the effect due to creep.

Comparison of Aluminum Bearing Stress to Allowable Creep Stress from Section 3.9.2.2.6.3:

Component	Bearing Stress	Allowable Creep Stress	Stress/Allowable Ratio
Alum. Rail	0.068 ksi	0.758 ksi	0.0897
Alum. Plate	0.00094 ksi	0.254 ksi	0.0037

3.9.2.2.7.3 Conclusions

Finite element analyses and hand calculations for the EOS-89BTH basket assembly are performed for all normal and off-normal on-site conditions. Controlling stress intensities are reported in Table 3.9.2-4. A comparison of stress intensities to the corresponding allowable values indicate that all load conditions show acceptable stress levels, as applicable.

3.9.2.3 EOS-37PTH Basket Structural Evaluation for On-Site Accident Drop Loads

This section evaluates the structural integrity of the EOS-37PTH DSC basket for on-site accident side and end drop loads. On-site transfer conditions in the EOS-TC108, EOS-TC125, or EOS-TC135 are considered for thermal properties used in the side drop load analyses.

3.9.2.3.1 General Description

Same as Section 3.9.2.1.1.

3.9.2.3.2 Key Dimensions and Materials

Same as Section 3.9.2.1.2.

3.9.2.3.3 Material Properties

Same as Section 3.9.2.1.3.

3.9.2.3.4 Temperature Data

Same as Section 3.9.2.1.4.

3.9.2.3.5 Fuel Data

Chapter 2 provides design characteristics for the types of pressurized water reactor (PWR) FAs to be considered. A bounding distributed weight of 11.0 lbs/in. in the active fuel region is considered for the on-site accident side drop analyses.

3.9.2.3.6 Methodology

ANSYS 10.0A1 [3.9.2-2] is used for the evaluation of on-site accident side drop loads. Hand calculations are performed to conservatively calculate the stresses due to the on-site axial end drop loads. Stresses due to the end drop loads are not controlling. Therefore, only the side drop load analysis results are presented.

3.9.2.3.6.1 Finite Element Model

3.9.2.3.6.1.1 Analysis Model Description for Side Loads

In consideration of continuous support of the basket grid structure by the transition rails along the entire length, a 6-inch slice of the basket assembly is modeled, consisting of one-half the widths of the basket plates. One end of the 6-inch long model is at the symmetry plane of the horizontal plates and is at the free edges of the vertical plates. The opposite end of the 6-inch long model is at the symmetry plane of the vertical plates and is at the free edges of the horizontal plates. Symmetry boundary conditions (UY = ROTX = ROTZ = 0) are defined at the symmetry planes of the grid plates and at both cut faces of the transition rails and steel angle plates. Geometry plots of the ANSYS model are shown in Figure 3.9.2-1 through Figure 3.9.2-8 (180 degree drop orientation shown).

The top and bottom regions of the basket assembly use grid plates with widths as small as 6 inches. The resulting ligaments at the 3-inch deep slots are only 3 inches wide, which is one-half of 6-inch wide ligaments for grid plates in the middle region. However, the tributary width for loading from fuel is also one-half of the tributary width for plates in the middle region, and the fuel distributed load is smaller at the ends since it is away from the active fuel region. Furthermore, the temperatures are lower at the top and bottom of the basket assembly. Therefore, the top and bottom regions of the basket assembly are bounded by the analyzed middle region.

The steel grid plates and the DSC shell are modeled using ANSYS Shell181 elements. No structural credit is taken for the poison plates or for the aluminum plates. The mass of the poison plates and aluminum plates is accounted for by increasing the density of the adjacent steel grid plates. Reinforcing steel angle plates in the R45 transition rails are also modeled using ANSYS Shell181 elements. The aluminum transition rails are modeled using ANSYS Solid185 elements.

Contact between the grid plates at the slots is modeled using ANSYS Conta178 elements (without friction). Initial gaps are defined for the contact elements based on the thickness stack-up of the steel, poison, and aluminum plates in each slot. Similarly, contact between the grid plates and the aluminum transition rails are modeled using ANSYS Conta178 elements (without friction). The initial gaps between the plates and the transition rails are considered closed. This implies that the unmodeled "sandwiched" aluminum and poison plates are assumed to transfer loads normal to the plates. For stability and convergence purposes, soft springs (Combin14) are modeled coincident with the contact elements.

Bolts connecting the transition rails to the grid plates are modeled using ANSYS Beam4 elements. Nodes on the bolt elements are coupled to nodes on the grid plates, aluminum transition rails, and reinforcing steel angle plates in the rails, as applicable. At one end of each bolt, a contact element (Conta178) is defined in the axial direction of the bolt. The couples and contact elements are defined such that only tension loads are transferred through the bolts (due to oversized bolt holes). Similarly, tie rods for the R90 transition rail assemblies are modeled using ANSYS Beam4 elements. The ends of tie rods are connected to the transition rails in the same manner as for the bolts, such that only tension loads are transferred. The Belleville spring washers used at the ends of the tie rods are considered to be compressed by thermal loading so the tie rods behave as tension-only for other loads. Additional side drop analyses are performed without the connection bolts and tie rods (assumed to fail) to demonstrate that they are not needed for an accident drop.

Gaps between the basket and the DSC cylindrical shell are modeled using ANSYS Conta178 elements (without friction). Initial gaps are based on a basket outside diameter of 74.10 inches and a DSC inside diameter of 74.50 inches, and the side load orientation. Initial gaps are adjusted in consideration of the radial thermal growth of the basket relative to the growth of the DSC shell. Each gap element contains two nodes; one on each surface of the structures. The flexibility of the DSC shell is considered. Therefore, additional gap elements (ANSYS Conta178) are modeled between the DSC and the EOS-TC cask, where the gap nodes specified at the inner side of the cask are restrained in the three translational directions. Initial gaps are based on a DSC outside diameter of 75.50 inches and an EOS-TC inner shell diameter of 76.25 inches, and the side load orientation. Initial gaps are adjusted in consideration of the radial thermal growth of the DSC shell relative to the growth of the cask. Cask rails are simulated by using the difference between cask and DSC radii, combined with the rail thickness, as applicable, and using zero gap contact elements at the rails in initial contact with the DSC and non-zero gap contact elements elsewhere between the DSC and the cask.

To consider the stiffening effect of the DSC end plates on the cylindrical shell, a simplified, half-length model of the DSC shell was used to get more realistic cylindrical shell side drop deformations for gap calculations. The model includes a thick cover plate representing the two cover plates, and contact elements to the nodes at the inner diameter of the cask and cask rails are modeled as described above for the basket model. Symmetry boundary conditions (UY = ROTX = ROTZ = 0) are defined at the end of the model opposite of the cover plate (mid-length of the DSC shell). Elastic-plastic material properties at 400 °F are defined for the shell, based on a bilinear material stress-strain curve with a 1% tangent modulus. The average shell temperature of a horizontally oriented DSC in an EOS-TC for off-normal conditions is less than 435 °F so an approximate value of 400 °F was used. A uniform pressure is applied to a range +/-45 degrees from the bottom to represent the basket and fuel load. Internal pressure and the associated stress stiffening effects are conservatively not modeled. The resulting shell displacements at the symmetry plane of the cylindrical shell, for the upper 140 degrees (+/-70 degrees) opposite from the point of drop, are applied for 180° and 270° side drop load analyses. For the 225° side drop load analyses, the shell displacements at the upper 60 degrees (+/-30 degrees) opposite from the point of drop are applied. This credits the stiffening effect of the DSC end plates while allowing the shell to locally displace around the cask rails based on interaction with loading from the basket components.

3.9.2.3.6.1.2 Material Properties in Analyses

The modeled components of the basket and DSC are based on lower bound material properties. The material properties used for stress/strain analyses are based on representative average temperature values.

For elastic-plastic strain and buckling analyses, bilinear material stress-strain curves are used with a 1% tangent modulus for all materials except the bolts and tie rods. This is consistent with previous licensed basket designs.

3.9.2.3.6.1.3 Loads

Load cases are based on the loads described in Chapter 2.

A 65 inch side drop is considered in various orientations to ensure the adequacy of the design under on-site accident side drop conditions. A side drop load of 60g is evaluated to bound the acceleration predicted in Appendix 3.9.3. A 75g end drop is also considered to conservatively envelop the effects of a 65-inch corner drop.

For side loading, the fuel weight load is modeled conservatively using a pressure load equivalent to the applicable acceleration, or G-load, times the fuel assembly weight divided by the basket fuel compartment area associated with the active fuel region length and the fuel compartment width between slots (8.79 inches). A fuel load of 11.0 lbs/in. acting on the fuel compartment width between slots is applied to bound the load distribution in the active fuel region for all PWR fuel types. Figure 3.9.2-8 shows the application of fuel weight pressure loads to the model (for a 180° side drop orientation).

For 0° and 180° side load orientations, the equivalent fuel assembly pressure acts only on the horizontal plates. For 90° and 270° side load orientations, the equivalent fuel assembly pressure acts only on the vertical plates. For other orientations, the equivalent fuel assembly pressure acts perpendicular to the horizontal and vertical plates, proportioned based on the Cosine and Sine of the orientation angle.

The following accident side drop load conditions (DSC and basket in horizontal position) are evaluated:

- 180° Side Drop on Rails
  (due to symmetry, this also covers the 0° Side Drop)
- 270° Side Drop away from Rails
  (due to symmetry, this also covers the 90° Side Drop)
- 225° Side Drop on Rails
  (due to symmetry, this also covers other multiples of 45° Side Drop)

3.9.2.3.6.2 Criteria

The basis for allowable strains is obtained from Chapter 8. The strain criteria are discussed and summarized in Section 3.1.1.1.1.

The basket grid plate strain criteria are summarized in Table 3.9.2-5. The threaded fasteners, used to connect the transition rails to the basket grid structure, are not required to be evaluated because they are considered to fail (with analyses and calculations confirming that they are not needed for accident condition drops).

Section 3.9.3.3.2 demonstrates that uncontrolled crack propagation in the basket plates is not an issue for the AISI 4130 material.

3.9.2.3.7 Results

3.9.2.3.7.1 Results for Analysis of 60g Accident Side Loading

60g accident side drop loads are analyzed using the ANSYS model described in Section 3.9.2.3.6.1.1. Accident condition equivalent static elastic-plastic analyses are performed for computing the strains.

The fuel weight load is modeled conservatively using a pressure load equivalent to the applicable acceleration, or G-load, times the maximum fuel assembly weight per length (11.0 lbs/in) divided by the fuel compartment width (8.79 inches).

At the 180° side load orientation, the equivalent 1g fuel assembly pressure, acting only on the horizontal plates, P_{180h}, is calculated as follows:

P_{180h} = 11.0 lbs/in / (8.79") = 1.2514 psi

At the 270° side load orientation, 1g acting only on the vertical plates:

P_{270v} = 11.0 lbs/in / (8.79") = 1.2514 psi

At 225° (45 degrees from bottom), 1g acting on the horizontal and vertical plates:

$P_{225h} = P_{225v} = P_{180h} \sin(45°)$ = 0.8849 psi

The ANSYS unit (1g) accelerations, indicating direction of load, are:

180-degree	acel, 0, 0, 1
270-degree	acel, 1, 0, 0
225-degree	acel, 0.7071, 0, 0.7071

For side load analyses, the equivalent fuel assembly pressure loads and accelerations above are multiplied by the corresponding side load acceleration value (e.g., 60g).

Displacements, stresses, strains and forces for each converged load step are saved to ANSYS files.

Basket grid plate strain results for accident condition 60g side drop loads are shown in Table 3.9.2-6. Results with controlling strain ratios are shown in Table 3.9.2-7. An ANSYS strain contour plot corresponding to the bounding strain values is shown in Figure 3.9.2-23. The tabulated results show that all strains meet the corresponding allowable strain limits. As demonstrated in Section 3.9.3.3.2, uncontrolled crack propagation in the grid plates is not an issue for the 4130 material.

Analyses are run to 75g. The program stops at the load substep that fails to result in a converged solution, if convergence to 75g does not occur. The last converged load step is considered the buckling load. The buckling load values are compared with 60g, the required g-load for accident conditions, with results shown in Table 3.9.2-8. All analyses complete the 75g load step.

Stresses and strains in the aluminum basket transition rails are not explicitly evaluated. All analyzed drop conditions include the case where the connecting bolts and tie rods are assumed to fail, to demonstrate that the connection to the aluminum is not needed to maintain basket strains within the allowable strain limits. Therefore, the only significant stress in the basket aluminum rails is a bearing type stress where the transition rail is compressed between the basket grid plates and the inside surface of the EOS-DSC. Since bearing stresses are not required to be evaluated for accident conditions, no further evaluation of the basket transition rails is required.

ANSYS Force Summation Comparison

An ANSYS force summation for the basket components only, for the 60g side drop, is compared to the expected load as shown below:

From the ANSYS results for the 60g load step:

Force Summation: Fz = -204,896.4 lb
(in vertical direction (z), length of model is 6 inches)

Expected Load:

Basket weight / length w/o spent fuel:

= (18,900 + 1,080) / (181.5 - 0.9) + (983 + 4,790 + 4,370) / (181.5 - 1.25 - 0.9)

= 167.2 lb/in.

Basket wt. w/o spent fuel (6 inches long) = (167.2) (6 inches) = 1,003 lb.

Spent fuel weight (6" long) = (11 lb/in) (6-inch length of basket) (37 SFAs) = 2,442 lb.

Total weight of the basket, with spent fuel (6 incheslong) = 1,003 + 2,442 = 3,445 lb (for 1g)

Expected Load at 60g (in vertical direction) = 60 (3,445) = 206,700 lb.

The ANSYS load of 204,896 is very similar to the hand-calculated weight load (within 1%) and therefore, is acceptable.

3.9.2.3.7.2 75g Accident End Drop Loading Calculations

Compressive stress associated with the 75g end drop condition is calculated using conservative loads and geometry. For the 75g end drop load condition, the steel grid plates are assumed to carry their own weight plus the weight of all of the aluminum components. The fuel assembly loads are applied directly to the cover plates/shield plugs of the DSC shell assembly and not to the basket assembly. The basket weight considered below bounds the weight summarized in Chapter 3, Table 3-6. The axial stress calculated below represents the general membrane stress in the steel grid plates. The local bearing and peak stresses at the intersections of the slots are not required to be evaluated for accident conditions. There is no significant out-of-plane bending in the grid plates for the 75g end drop condition.

75g axial load:

$\sigma_{Axial\text{-}75g} = 75 (W_{basket}) / A_S$ (conservative to use full basket weight)

$W_{basket} = 36.0$ kips (conservative)

Section Area, A_S = summation of plate lengths and thicknesses (from plate details), conservatively excluding slot widths and extensions beyond the last slot of each plate.

$A_S = 4[0.281"(7)(8.80") + 0.281"(7)(8.80") + 0.281"(5)(8.80") + 0.313"(3)(8.80")]$

$= 221.0 \text{ in}^2$

Therefore,

$\sigma_{Axial\text{-}75g} = 75 (36.0) / 221.0$

$= 12.22$ ksi

This stress value is low (below yield), such that the 75g end drop load condition strains do not control and no further evaluation is required.

3.9.2.3.7.3 Adjacent Fuel Compartment Relative Displacements

Maximum relative perpendicular displacement from one fuel compartment plate to another is determined from the ANSYS results for the accident side drops. These differences are addressed in the criticality evaluations to ensure that the fuel assembly array pitch does not significantly change due to the accident side drop. The sketch below indicates the sign convention and typical locations where displacements are extracted.

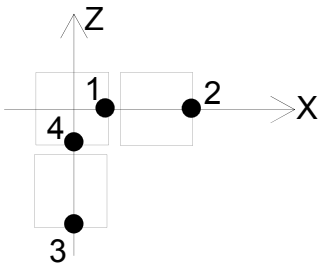

The relative displacements are calculated as follows:

$\Delta_{UX} = UX_2 - UX_1$

$\Delta_{UZ} = UZ_4 - UZ_3$

Maximum relative displacements for those adjacent compartments that have moved closer together are tabulated in Table 3.9.2-9. Relative displacements that indicate fuel compartments have moved away from one another are ignored. The summary table includes results for analyses with bolts and tie rods modeled and for analyses without bolts and tie rods modeled.

3.9.2.3.7.4 Conclusions

Finite element analyses and hand calculations for the EOS-37PTH basket assembly are performed for all accident side and end drop on-site conditions. Controlling strains are reported in Table 3.9.2-7. A comparison of strains to the corresponding allowable values indicates that all load conditions show acceptable results.

As demonstrated in Section 3.9.3.3.2, uncontrolled crack propagation in the grid plates is not an issue for the 4130 material.

3.9.2.4 EOS-89BTH Basket Structural Evaluation for On-Site Accident Drop Loads

This section evaluates the structural integrity of the EOS-89BTH DSC basket for on-site accident side and end drop loads. On-site transfer conditions in the EOS-TC108, EOS-TC125, or EOS-TC135 are considered for thermal properties used in the side drop load analyses.

3.9.2.4.1 General Description

Same as Section3.9.2.2.1.

3.9.2.4.2 Key Dimensions and Materials

Same as Section3.9.2.2.2.

3.9.2.4.3 Material Properties

Same as Section 3.9.2.2.3.

3.9.2.4.4 Temperature Data

Same as Section3.9.2.2.4.

3.9.2.4.5 Fuel Data

Chapter 2 provides design characteristics for the types of BWR FAs to be considered. A maximum FA weight of 705 lbs is used. A distributed weight of 705 lbs / 150 in. = 4.7 lbs/in is considered to be bounding in the active fuel region for the on-site accident side drop analyses.

3.9.2.4.6 Methodology

ANSYS 10.0A1 [3.9.2-2] is used for the evaluation of on-site accident side drop loads. Hand calculations are performed to conservatively calculate the stresses due to the on-site axial end drop loads. Stresses due to the end drop loads are not controlling. Therefore, only the side drop load analysis results are presented.

3.9.2.4.6.1 Finite Element Model

3.9.2.4.6.1.1 Analysis Model Description for Side Loads

Geometry plots of the ANSYS model are shown in Figure 3.9.2-12 through Figure 3.9.2-18. All other details of the analysis model description are the same as Section 3.9.2.3.6.1.1.

3.9.2.4.6.1.2 Material Properties in Analyses

Same as Section 3.9.2.3.6.1.2.

3.9.2.4.6.1.3 Loads

Load cases are based on the loads described in Chapter 2.

A 65 inch side drop is considered in various orientations to ensure the adequacy of the design under on-site accident side drop conditions. A side drop load of 60g is evaluated to bound the acceleration predicted in Appendix 3.9.3. A 75g end drop is also considered to conservatively envelop the effects of a 65 inch corner drop.

For side loading, the fuel weight load is modeled conservatively using a pressure load equivalent to the applicable acceleration, or G-load, times the fuel assembly weight divided by the basket fuel compartment area associated with the active fuel region length and the fuel compartment width between slots (5.85 inches). A fuel load of 4.7 lbs/in acting on the fuel compartment width between slots is applied to bound the load distribution in the active fuel region for all BWR fuel types. Figure 3.9.2-19 shows the application of fuel weight pressure loads to the model (for a 180° side drop orientation).

For 0° and 180° side load orientations, the equivalent fuel assembly pressure acts only on the horizontal plates. For 90° and 270° side load orientations, the equivalent fuel assembly pressure acts only on the vertical plates. For other orientations, the equivalent fuel assembly pressure acts perpendicular to the horizontal and vertical plates, proportioned based on the Cosine and Sine of the orientation angle.

The following accident side drop load conditions (DSC and basket in horizontal position) are evaluated:

- 180° Side Drop on Rails
  (due to symmetry, this also covers the 0° Side Drop)
- 270° Side Drop away from Rails
  (due to symmetry, this also covers the 90° Side Drop)
- 225° Side Drop on Rails
  (due to symmetry, this also covers other multiples of 45° Side Drop)

3.9.2.4.6.2 Criteria

The basis for allowable strains is obtained from Chapter 8. The strain criteria are discussed and summarized in Section 3.1.1.1.1.

The basket grid plate strain criteria are summarized in Table 3.9.2-5. The threaded fasteners, used to connect the transition rails to the basket grid structure, are not required to be evaluated because they are considered to fail (with analyses and calculations confirming that they are not needed for accident condition drops).

Section 3.9.3.3.2 demonstrates that uncontrolled crack propagation in the basket plates is not an issue for the AISI 4130 material.

3.9.2.4.7 Results

3.9.2.4.7.1 Results for Analysis of 60g Accident Side Loading

60g accident side drop loads are analyzed using the ANSYS model described in Section 3.9.2.4.6.1.1. Accident condition equivalent static elastic-plastic analyses are performed for computing the strains.

The fuel weight load is modeled conservatively using a pressure load equivalent to the applicable acceleration, or G-load, times the maximum fuel assembly weight per length (4.7 lbs/in) divided by the fuel compartment width (5.85 inches).

At the 180° side load orientation, the equivalent 1g fuel assembly pressure, acting only on the horizontal plates, P_{180h}, is calculated as follows:

P_{180h} = 4.7 lbs/in / (5.85 inches) = 0.8034 psi

At the 270° side load orientation, 1g acting only on the vertical plates:

P_{270v} = 4.7 lbs/in / (5.85 inches) = 0.8034 psi

At 225° (45 degrees from bottom), 1g acting on the horizontal and vertical plates:

$P_{225h} = P_{225v} = P_{180h} \sin(45°)$ = 0.5681 psi

The ANSYS unit (1g) accelerations, indicating direction of load, are:

180-degree	acel, 0, 0, 1
270-degree	acel, 1, 0, 0
225-degree	acel, 0.7071, 0, 0.7071

For side load analyses, the equivalent fuel assembly pressure loads and accelerations above are multiplied by the corresponding side load acceleration value (e.g., 60g).

Displacements, stresses, strains and forces for each converged load step are saved to ANSYS files.

Basket grid plate strain results for accident condition 60g side drop loads are shown in Table 3.9.2-10. Results with controlling strain ratios are shown in Table 3.9.2-11. ANSYS strain contour plots corresponding to the bounding strain values are shown in Figure 3.9.2-24 and Figure 3.9.2-23

EOS-37PTH Basket 180 Degree 60g Side Drop (without bolts / tie rods) – Grid Plates, $\varepsilon_m + \varepsilon_b$ (von Mises Plastic Strain, in/in)

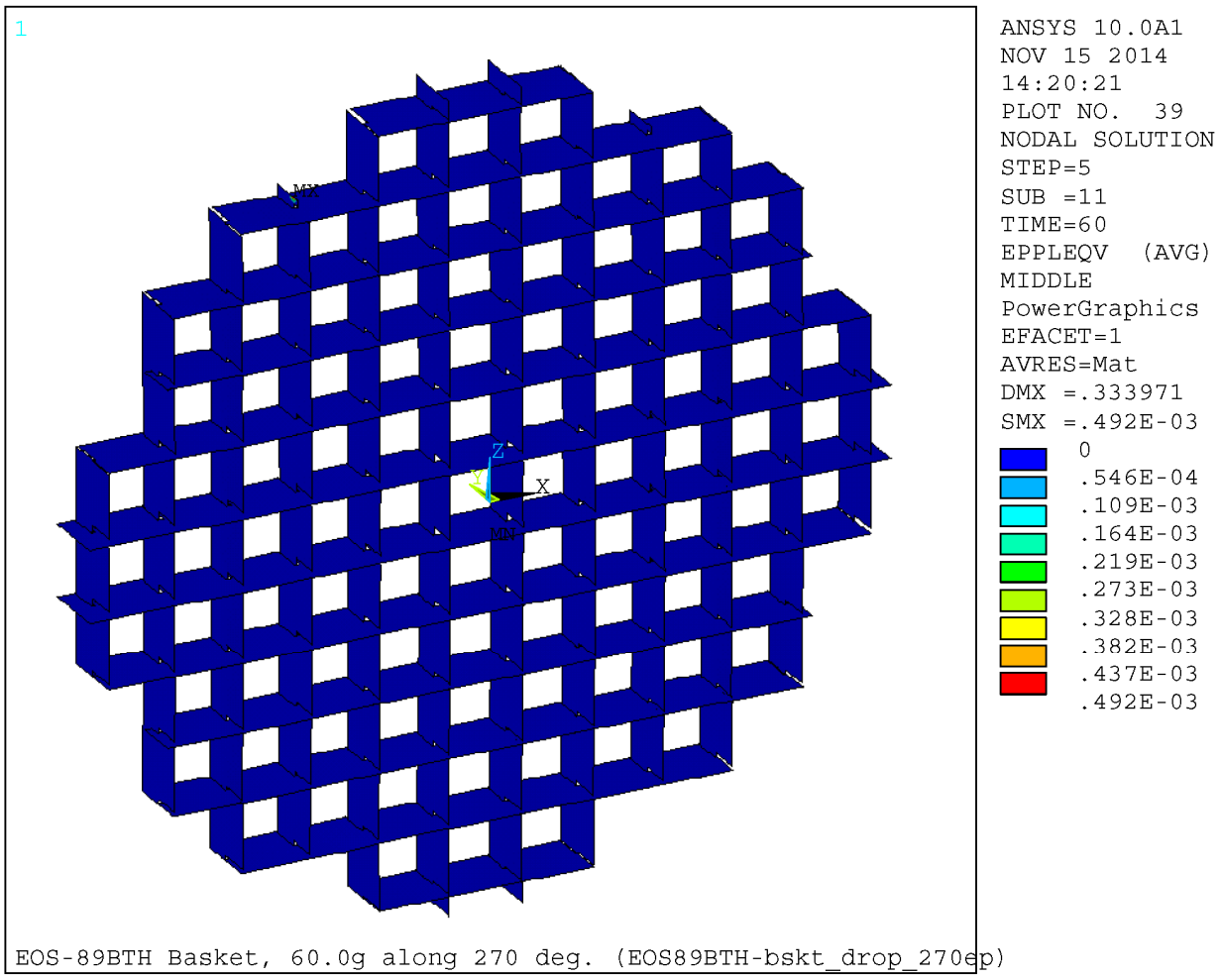

Figure 3.9.2-24
EOS-89BTH Basket 270 Degree 60g Side Drop (with bolts / tie rods) – Grid Plates, ε_m (von Mises Plastic Strain, in/in)

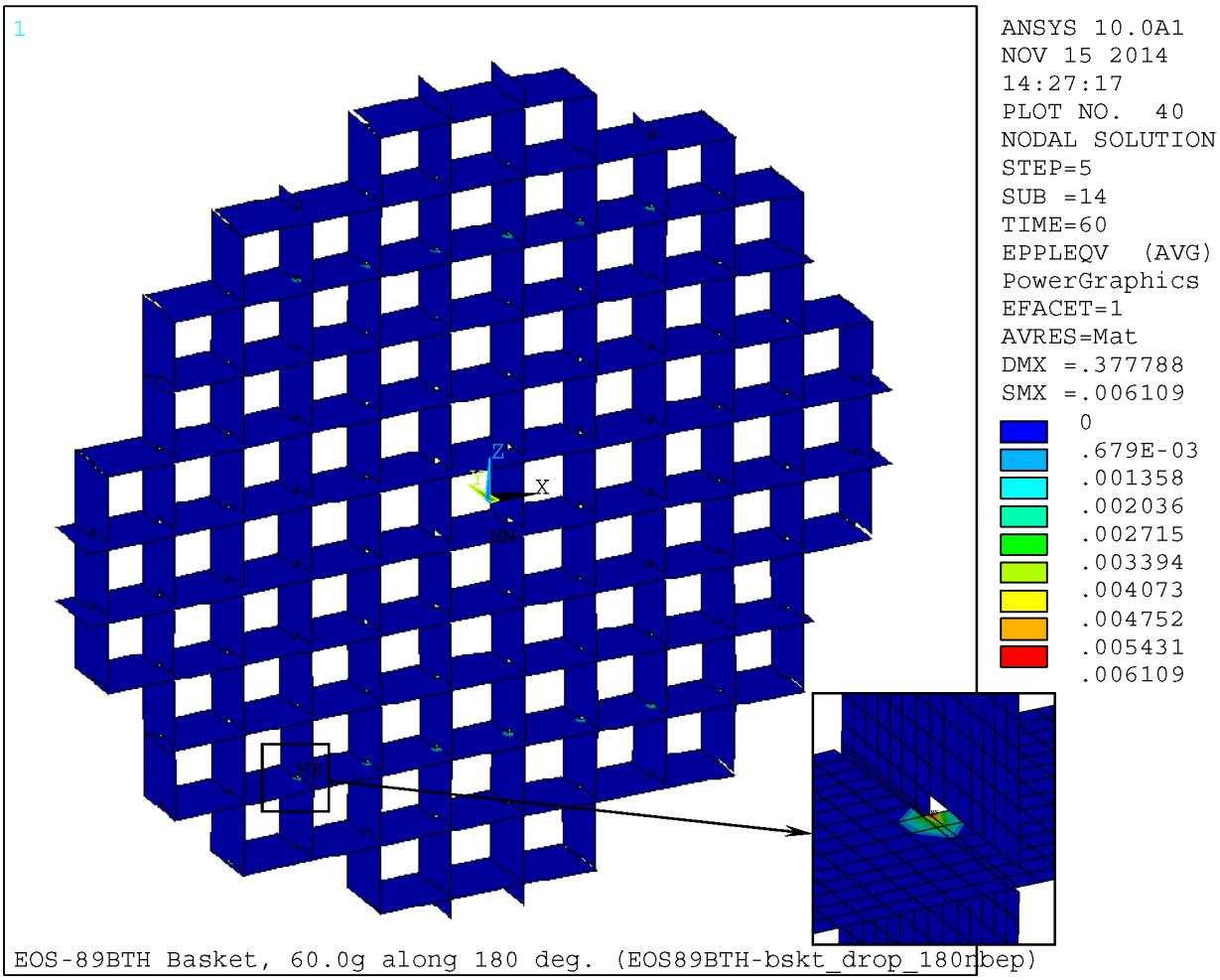

Figure 3.9.2-25. The tabulated results show that all strains meet the corresponding allowable strain limits. As demonstrated in Section 3.9.3.3.2, uncontrolled crack propagation in the grid plates is not an issue for the 4130 material.

Analyses are run to 75g. The program stops at the load substep that fails to result in a converged solution, if convergence to 75g does not occur. The last converged load step is considered the buckling load. The buckling load values are compared with 60g, the required g-load for accident conditions, with results shown in Table 3.9.2-8. All analyses complete the 75g load step.

Stresses and strains in the aluminum basket transition rails are not explicitly evaluated. All analyzed drop conditions include the case where the connecting bolts and tie rods are assumed to fail, to demonstrate that the connection to the aluminum is not needed to maintain basket strains within the allowable strain limits. Therefore, the only significant stress in the basket aluminum rails is a bearing type stress where the transition rail is compressed between the basket grid plates and the inside surface of the EOS-DSC. Since bearing stresses are not required to be evaluated for accident conditions, no further evaluation of the basket transition rails is required.

ANSYS Force Summation Comparison

An ANSYS force summation for the basket components only, for the 60g side drop, is compared to the expected load as shown below:

From the ANSYS results for the 60g load step:

Force Summation: Fz = -207,687.2 lb
(in vertical direction (z), length of model is 6 inches)

Expected Load:

Basket weight / length w/o spent fuel:

= (19,300 + 637 + 1,110 + 3,980) / 166.0 + 1,720 / 175.0

= 160.6 lb/in

Basket wt. w/o spent fuel (6 inches long) = (160.6) (6 inches) = 964 lb.

Spent fuel weight (6 inches long) = (4.7 lb/in) (6-inch length of basket) (89 SFAs) = 2,510 lb.

Total weight of the basket, with spent fuel (6 inches long) = 964 + 2,510 = 3,474 lb (for 1g)

Expected Load at 60g (in vertical direction) = 60 (3,474) = 208,440 lb.

The ANSYS load of 207,687 is very similar to the hand-calculated weight load (within 0.4%) and therefore, is acceptable.

3.9.2.4.7.2 75g Accident End Drop Loading Calculations

Compressive stress associated with the 75g end drop condition is calculated using conservative loads and geometry. For the 75g end drop load condition, the steel grid plates are assumed to carry their own weight plus the weight of all of the aluminum components. The fuel assembly loads are applied directly to the cover plates/shield plugs of the DSC shell assembly and not to the basket assembly. The basket weight considered below bounds the weight summarized in Chapter 3, Table 3-7. The axial stress calculated below represents the general membrane stress in the steel grid plates of the holddown ring, for which the plate cross-sectional area is less than other sections of the basket. The local bearing and peak stresses at the intersections of the slots are not required to be evaluated for accident conditions. There is no significant out-of-plane bending in the grid plates for the 75g end drop condition.

75g axial load:

$\sigma_{Axial\text{-}75g} = 75 (W_{basket}) / A_S$ (conservative to use full basket weight)

$W_{basket} = 32.0$ kips (conservative)

Section Area, A_S = summation of plate lengths and thicknesses

The shortest length (top or bottom) of each holddown ring plate is considered, rounded down to the nearest tenth of an inch. The area is reduced by 10% to conservatively account for slots.

$A_S = 0.90(2)[0.250"(69.9") + 0.1875"(46.7") + 0.250"(69.9") + 0.250"(44.8") + 0.250"(19.1") + 0.250"(19.1")]$

$= 116.0$ in^2

Therefore,

$\sigma_{Axial\text{-}75g} = 75 (32.0) / 116.0$

$= 20.69$ ksi

This stress value is low (below yield), such that the 75g end drop load condition strains do not control and no further evaluation is required.

3.9.2.4.7.3 Adjacent Fuel Compartment Relative Displacements

Maximum relative perpendicular displacement from one fuel compartment plate to another is determined from the ANSYS results for the accident side drops. These differences are addressed in the criticality evaluations to ensure that the fuel assembly array pitch does not significantly change due to the accident side drop. The sketch below indicates the sign convention and typical locations where displacements are extracted.

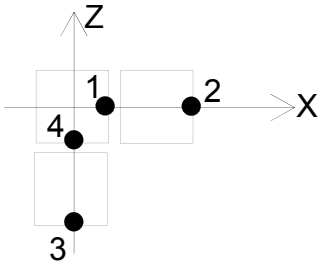

The relative displacements are calculated as follows:

$\Delta_{UX} = UX_2 - UX_1$

$\Delta_{UZ} = UZ_4 - UZ_3$

Maximum relative displacements for those adjacent compartments that have moved closer together are tabulated in Table 3.9.2-13. Relative displacements that indicate fuel compartments have moved away from one another are ignored. The summary table includes results for analyses with bolts and tie rods modeled and for analyses without bolts and tie rods modeled.

3.9.2.4.7.4 Conclusions

Finite element analyses and hand calculations for the EOS-89BTH basket assembly are performed for all accident side and end drop on-site conditions. Controlling strains are reported in Table 3.9.2-11. A comparison of strains to the corresponding allowable values indicates that all load conditions show acceptable results.

As demonstrated in Section 3.9.3.3.2, uncontrolled crack propagation in the grid plates is not an issue for the 4130 material.

3.9.2.5 References

3.9.2-1 American Society of Mechanical Engineers, “ASME Boiler and Pressure Vessel Code,” Section III, Division 1, Subsection NG, 2010 Edition thru 2011 Addenda.

3.9.2-2 ANSYS Computer Code and User’s Manual, Release 10.0.

3.9.2-3 AREVA TN Technical Report, "Evaluation of Creep of NUHOMS® Basket Aluminum Components under Long Term Storage Conditions", E-25768, Rev. 0 (Structural Integrity Associates, Inc. File No. TNI-20Q-302, Rev. 0).

Table 3.9.2-1
Threaded Fastener Stress Design Criteria (Normal / Off-Normal)

Stress Category	Allowable Stresses
	Normal / Off-Normal [1]
Primary + Secondary Membrane $P_m + Q_m$ [2]	$\min(0.9\ S_y, 2/3\ S_u)$
Primary + Secondary Shear $P_m + Q_m$ [3][6]	$0.6\ S_y$
Primary + Secondary Bearing $P_m + Q_m$ [4]	$2.7\ S_y$
Primary Membrane P_m [2]	S_m
Primary Shear P_m [3]	$0.6\ S_m$
Primary + Secondary Membrane + Bending $P_m + Q_m + P_b + Q_b$ [5][6]	$\min(1.2\ S_y, 8/9\ S_u)$

(1) Classification and stress limits are as defined in ASME Code, Section III, Subsection NG [3.9.2-1].

(2) Averaged stress intensity on tensile stress area at threaded section.

(3) Averaged stress across shear area of threaded section.

(4) Averaged bearing stress under the fastener head.

(5) Stress intensity, excluding effects of stress concentrations.

(6) Not applicable to this evaluation; no significant thermal shear due to oversized/slotted holes, and no significant bending.

Table 3.9.2-2
Component Allowable Stresses (Normal / Off-Normal)

Component	Material	Temp. (°F)	Stress Category	Allowable Stress (ksi)
Steel Grid Plates	AISI 4130	700	P_m	24.96
			$P_m + P_b$	37.43
			$P_m + P_b + Q$	74.87
Rail Angle Plates	SA-516 Grade 70	550	P_m	20.00
			$P_m + P_b$	30.00
			$P_m + P_b + Q$	60.00
Transition Rails	Aluminum 6061	550	$P_m + P_b$	4.85
			$P_m + P_b + Q$	9.70
Bolts (1)	SA-193 Grade B7	550	Tension, P_m	28.95
			Tension, $P_m + Q_m$	78.21
			Shear, P_m	17.37
Tie Rods	SA-193 Grade B7	550	Tension, P_m	28.95
			Tension, $P_m + Q_m$	78.21

(1) For basket side loading, only tension loads are transferred through the bolts and tie rods due to oversized/slotted bolts holes that allow for thermal expansion.

Table 3.9.2-3
EOS-37PTH Basket Stress Summary – Enveloped DW + Handling + Thermal

Load Combination	Component	Stress Category	Maximum Stress (ksi) (1)	Allowable Stress (ksi)	Stress Ratio
Enveloping Results for Normal Conditions in the EOS-TC	Grid Plates (3)	P_m	4.61+0.25= 4.86	24.96	0.195
		$P_m + P_b$	23.95+0.25= 24.20	37.43	0.647
		$P_m + P_b + Q$	31.94	74.87	0.427
	Angle Plates	P_m	3.56	20.00	0.178
		$P_m + P_b$	4.63	30.00	0.154
		$P_m + P_b + Q$	12.75	60.00	0.213
	Transition Rails	$P_m + P_b$	2.72	4.85	0.560
		$P_m + P_b + Q$	8.57	9.70	0.883
	Bolts (2)(4)	P_m	12.24	28.95	0.423
		$P_m + Q_m$	44.61	78.21	0.570
	Tie Rods (2)	P_m	7.32	28.95	0.253
		$P_m + Q_m$	14.87	78.21	0.190

(1) $P_m + P_b + Q$ values are determined using ANSYS load combinations.

(2) Bolt and tie rod stresses listed are increased for the reduced area at the threads.

(3) Grid plate stresses include hand calculated stresses for 0.5g axial, where controlled by the DW + (0.5g Vert., 0.5g Trans., 0.5g Ax.) Handling load combination.

(4) Bolt maximum shear stress is 14.84 < 17.37, with a stress ratio of 0.854 per conservative hand calculation for axial handling.

Table 3.9.2-4
EOS-89BTH Basket Stress Summary – Enveloped DW + Handling + Thermal

Load Combination	Component	Stress Category	Maximum Stress (ksi) (1)	Allowable Stress (ksi)	Stress Ratio
Enveloping Results for Normal Conditions in the EOS-TC	Grid Plates (3)	P_m	4.30	24.96	0.172
		$P_m + P_b$	17.11+0.42 =17.53	37.43	0.468
		$P_m + P_b + Q$	23.23+0.42= 23.65	74.87	0.316
	Angle Plates	P_m	1.77	20.00	0.088
		$P_m + P_b$	2.58	30.00	0.086
		$P_m + P_b + Q$	12.52	60.00	0.209
	Transition Rails	$P_m + P_b$	4.47	4.85	0.921
		$P_m + P_b + Q$	11.77	9.70	1.214 (4)
	Bolts (2)(5)	P_m	6.15	28.95	0.212
		$P_m + Q_m$	24.47	78.21	0.313
	Tie Rods (2)	P_m	2.99	28.95	0.103
		$P_m + Q_m$	8.59	78.21	0.110

(1) $P_m + P_b + Q$ values are determined using ANSYS load combinations.

(2) Bolt and tie rod stresses listed are increased for the reduced area at the threads.

(3) Grid plate stresses include hand calculated stresses for 0.5g axial, where controlled by the DW + (0.5g Vert., 0.5g Trans., 0.5g Ax.) Handling load combination.

(4) This level of stress occurs only at very small locations at locations of bolts, and they are considered to be peak stresses. In addition, most of this stress is due to thermal, occurs during initial heat-up, is not cyclic and therefore, is not a fatigue concern. Stresses away from these small areas are significantly lower and well within the allowable stress.

(5) Bolt maximum shear stress is 14.92 < 17.37, with a stress ratio of 0.859 per conservative hand calculation for axial handling.

Table 3.9.2-5
Basket Grid Plate Accident Drop Strain Design Criteria

Strain Category	Allowable Strains (2)
	Accident (1)
Primary Membrane ε_m	1.0%
Primary Membrane + Bending $\varepsilon_m + \varepsilon_b$	3.0%
Primary + Peak $\varepsilon_m + \varepsilon_b + \varepsilon_F$	10.0% (3)
Compression or Buckling	Note 4

(1) Basket strain limits are described in Chapter 3.

(2) Plastic strain limits.

(3) Membrane + bending strains determined from the analyses conservatively include peak strain, such that the limit on primary + peak does not need to be evaluated.

(4) Determine the buckling load for each postulated drop orientation to demonstrate that the basket does not buckle within maximum drop load of 60g. Report the safety margin.

Table 3.9.2-6
EOS-37PTH Basket Grid Plate Strain Summary – Side Drops with and without Bolts and Tie Rods

Side Drop Load Case	Fastener Status	Strain (1) Category	Maximum Strain/Stress (in/in / ksi)	Allowable Strain/Stress (in/in / ksi)
60g, 180 deg. Side Drop	with Bolts/Tie Rods	ε_m	0.00000	0.01
		$\varepsilon_m + \varepsilon_b$	0.00797	0.03
	without (2) Bolts/Tie Rods	ε_m	0.00000	0.01
		$\varepsilon_m + \varepsilon_b$	0.00834	0.03
60g, 270 deg. Side Drop	with Bolts/Tie Rods	ε_m	0.00000	0.01
		$\varepsilon_m + \varepsilon_b$	0.00770	0.03
	without (2) Bolts/Tie Rods	ε_m	0.00000	0.01
		$\varepsilon_m + \varepsilon_b$	0.00807	0.03
60g, 225 deg. Side Drop	with Bolts/Tie Rods	ε_m	0.00000	0.01
		$\varepsilon_m + \varepsilon_b$	0.00400	0.03
	without (2) Bolts/Tie Rods	ε_m	0.00000	0.01
		$\varepsilon_m + \varepsilon_b$	0.00376	0.03

(1) Von Mises plastic strain.

(2) Bolts and tie rods are removed from the model for this analysis, assuming that they fail.

Table 3.9.2-7
EOS-37PTH Basket Grid Plate Strain Summary – Enveloped Accident Conditions

Load Combination	Strain (1) Category	Maximum Strain/Stress (in/in / ksi)	Allowable Strain/Stress (in/in / ksi)	Strain Ratio
Enveloping Results for Accident Conditions in the EOS-TC	ε_m	0.00000	0.01	0.000
	$\varepsilon_m + \varepsilon_b$	0.00834	0.03	0.278

(1) Von Mises plastic strain.

Table 3.9.2-8
EOS-37PTH Basket Buckling Analysis Results Summary

Load Condition	Last Converged Load (G)	Actual Max. Load (G)	Factor of Safety
60g 180 deg. drop, with bolts & tie rods	75.0 (1)	60.0	1.25
60g 270 deg. drop, with bolts & tie rods	75.0 (1)	60.0	1.25
60g 225 deg. drop, with bolts & tie rods	75.0 (1)	60.0	1.25
60g 180 deg. drop, without bolts & tie rods	75.0 (1)	60.0	1.25
60g 270 deg. drop, without bolts & tie rods	75.0 (1)	60.0	1.25
60g 225 deg. drop, without bolts & tie rods	75.0 (1)	60.0	1.25

(1) A maximum load of 75g was applied. Therefore, the buckling load and factor of safety may be greater.

Table 3.9.2-9
EOS-37PTH Basket Maximum Adjacent Fuel Compartment Relative Displacements

Load Condition	Drop Orientation	Maximum Absolute Relative Displacement (in)[1]			
		With Bolts & Tie Rods		Without Bolts & Tie Rods	
		Δ_{UX}	Δ_{UZ}	Δ_{UX}	Δ_{UZ}
60g Accident Side Drop	180°	0.039726	0.078975	0.062991	0.083127
	270°	0.075675	0.056695	0.077194	0.046207
	225°	0.069254	0.077784	0.069877	0.078839

(1) For displacements that indicate fuel compartments have moved closer together. Obtained from results for the 60g load step.

Table 3.9.2-10
EOS-89BTH Basket Grid Plate Strain Summary – Side Drops with and without Bolts and Tie Rods

Side Drop Load Case	Fastener Status	Strain (1) Category	Maximum Strain/Stress (in/in / ksi)	Allowable Strain/Stress (in/in / ksi)
60g, 180 deg. Side Drop	with Bolts/Tie Rods	ε_m	0.00000	0.01
		$\varepsilon_m + \varepsilon_b$	0.00595	0.03
	without (2) Bolts/Tie Rods	ε_m	0.00000	0.01
		$\varepsilon_m + \varepsilon_b$	0.00611	0.03
60g, 270 deg. Side Drop	with Bolts/Tie Rods	ε_m	0.00049	0.01
		$\varepsilon_m + \varepsilon_b$	0.00498	0.03
	without (2) Bolts/Tie Rods	ε_m	0.00000	0.01
		$\varepsilon_m + \varepsilon_b$	0.00491	0.03
60g, 225 deg. Side Drop	with Bolts/Tie Rods	ε_m	0.00000	0.01
		$\varepsilon_m + \varepsilon_b$	0.00264	0.03
	without (2) Bolts/Tie Rods	ε_m	0.00000	0.01
		$\varepsilon_m + \varepsilon_b$	0.00229	0.03

(1) Von Mises plastic strain.

(2) Bolts and tie rods are removed from the model for this analysis, assuming that they fail.

Table 3.9.2-11
EOS-89BTH Basket Grid Plate Strain Summary – Enveloped Accident Conditions

Load Combination	Strain (1) Category	Maximum Strain/Stress (in/in / ksi)	Allowable Strain/Stress (in/in / ksi)	Strain Ratio
Enveloping Results for Accident Conditions in the EOS-TC	ε_m	0.00049	0.01	0.049
	$\varepsilon_m + \varepsilon_b$	0.00611	0.03	0.204

(1) Von Mises plastic strain.

Table 3.9.2-12
EOS-89BTH Basket Buckling Analysis Results Summary

Load Condition	Last Converged Load (G)	Actual Max. Load (G)	Factor of Safety
60g 180 deg. drop, with bolts & tie rods	75.0 (1)	60.0	1.25
60g 270 deg. drop, with bolts & tie rods	75.0 (1)	60.0	1.25
60g 225 deg. drop, with bolts & tie rods	75.0 (1)	60.0	1.25
60g 180 deg. drop, without bolts & tie rods	66.975	60.0	1.12
60g 270 deg. drop, without bolts & tie rods	75.0 (1)	60.0	1.25
60g 225 deg. drop, without bolts & tie rods	75.0 (1)	60.0	1.25

(1) A maximum load of 75g was applied. Therefore, the buckling load and factor of safety may be greater.

Table 3.9.2-13
EOS-89BTH Basket Maximum Adjacent Fuel Compartment Relative Displacements

Load Condition	Drop Orientation	Maximum Absolute Relative Displacement (in)[1]			
		With Bolts & Tie Rods		Without Bolts & Tie Rods	
		Δ_{UX}	Δ_{UZ}	Δ_{UX}	Δ_{UZ}
60g Accident Side Drop	180°	0.021608	0.045477	0.022232	0.056033
	270°	0.032627	0.040907	0.040814	0.022854
	225°	0.031594	0.041521	0.027013	0.042423

(1) For displacements that indicate fuel compartments have moved closer together. Obtained from results for the 60g load step.

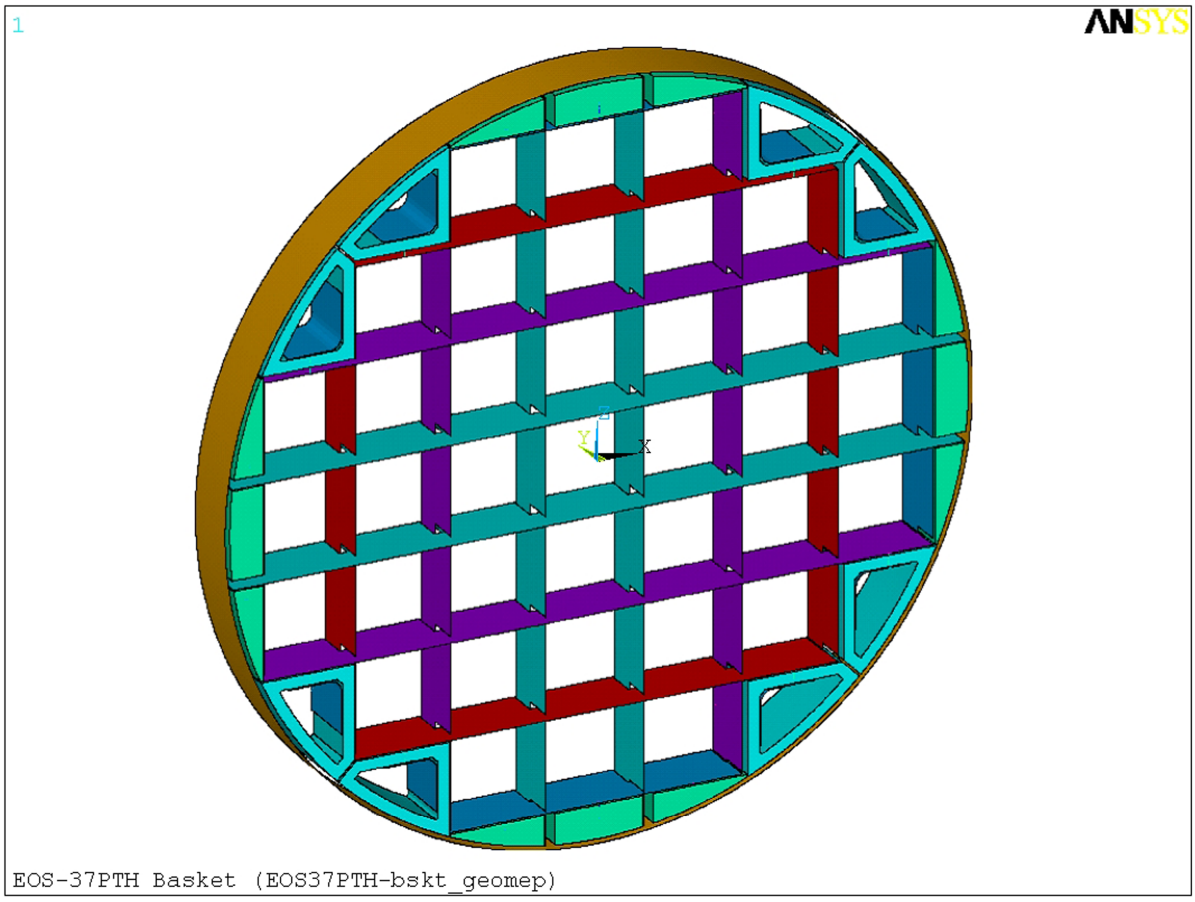

Figure 3.9.2-1
EOS-37PTH Basket Assembly ANSYS .Model (Components Only)
– Isometric View

Figure 3.9.2-2
EOS-37PTH Basket Assembly ANSYS Model (Components Only)
– Isometric View
Upper-Left Quadrant

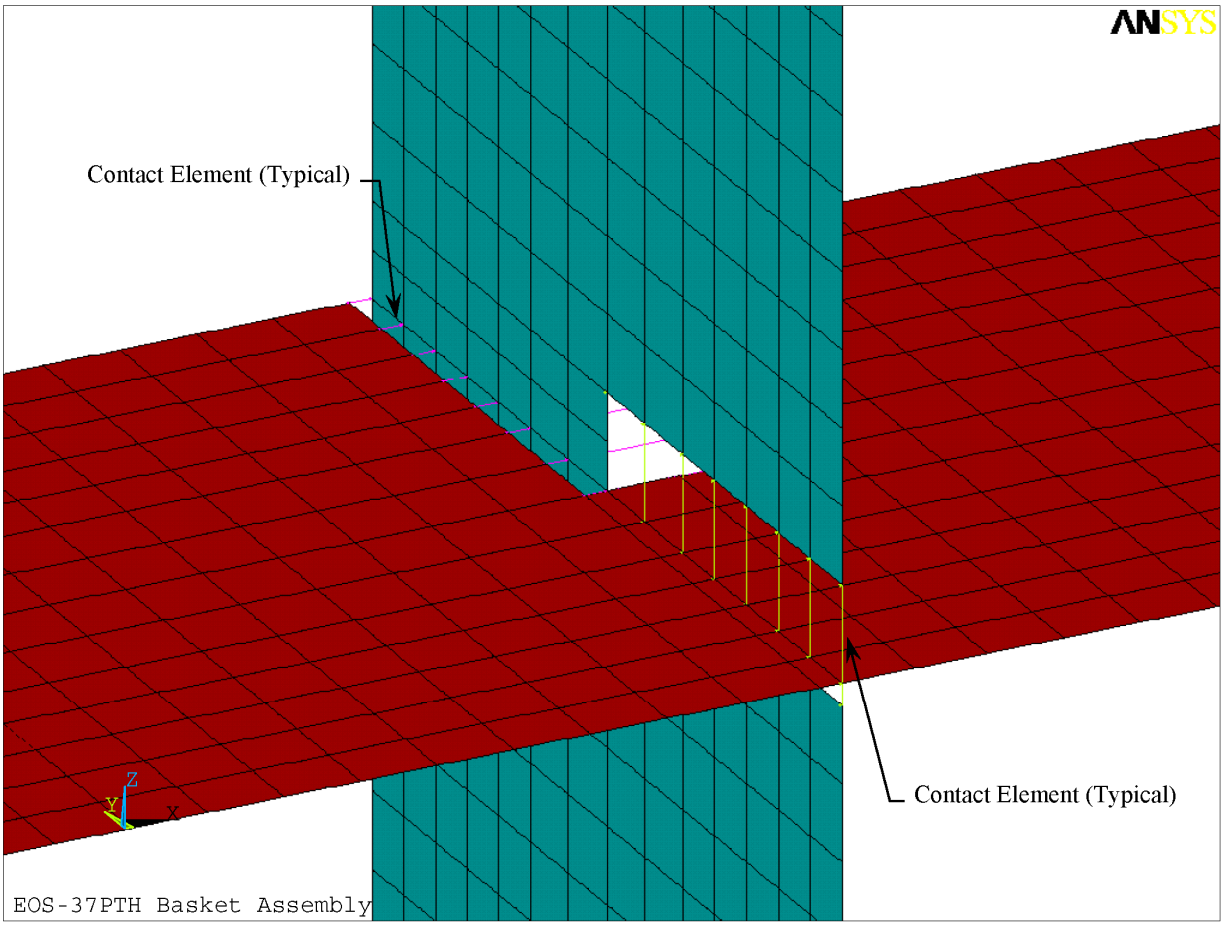

Figure 3.9.2-3
EOS-37PTH Basket Assembly Typical Grid Plate Intersection

Figure 3.9.2-4
EOS-37PTH Basket Assembly ANSYS Model (Components Only) – Front View

Figure 3.9.2-5
EOS-37PTH Basket Assembly ANSYS Model (Plate Thicknesses)
Lower Right Quadrant

Figure 3.9.2-6
EOS-37PTH Basket Assembly ANSYS Model (with Contact Elements) – Lower Right Quadrant

Figure 3.9.2-7
EOS-37PTH Basket Assembly ANSYS Model
−Transition Rail Bolt and Tie Rod Locations

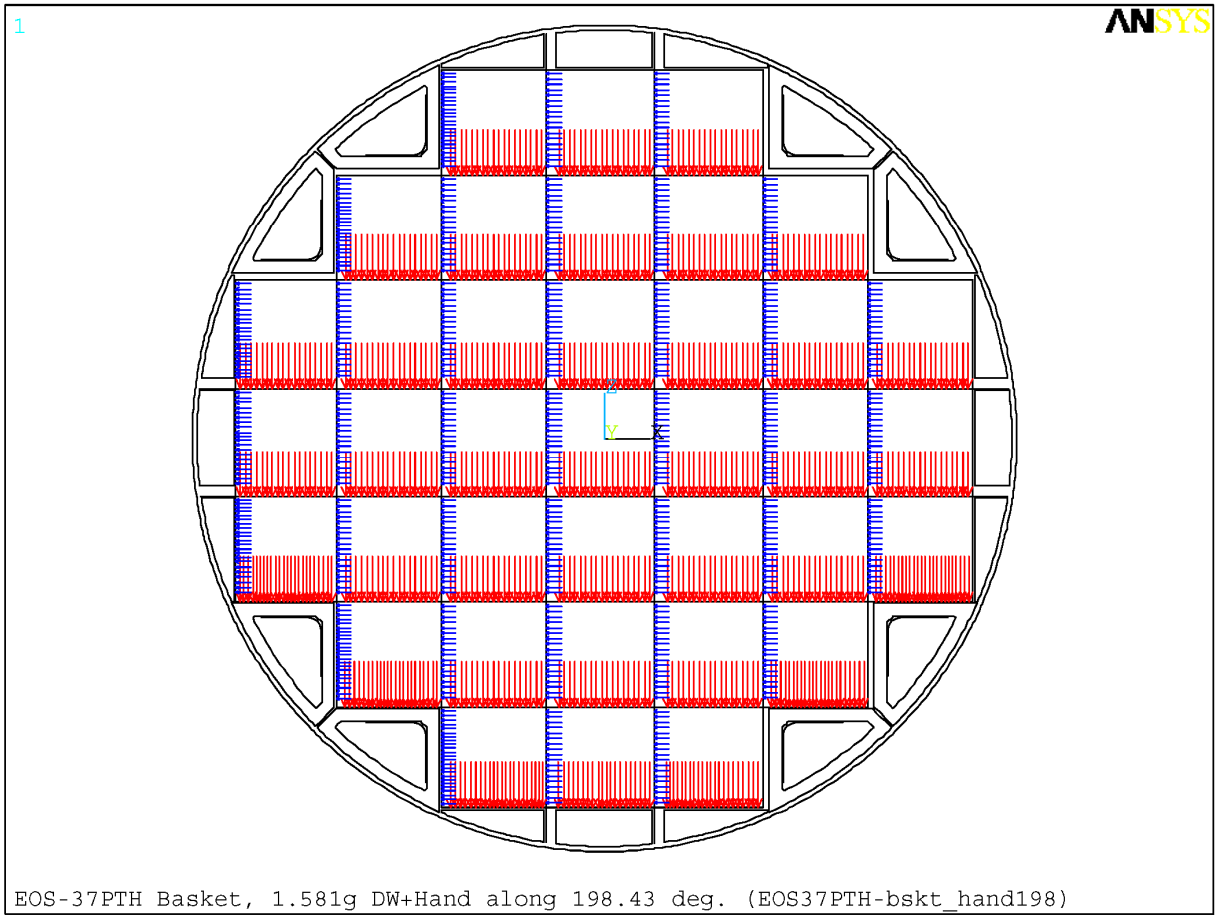

Figure 3.9.2-8
EOS-37PTH Basket Assembly ANSYS Model – Fuel Load Applied as Pressure

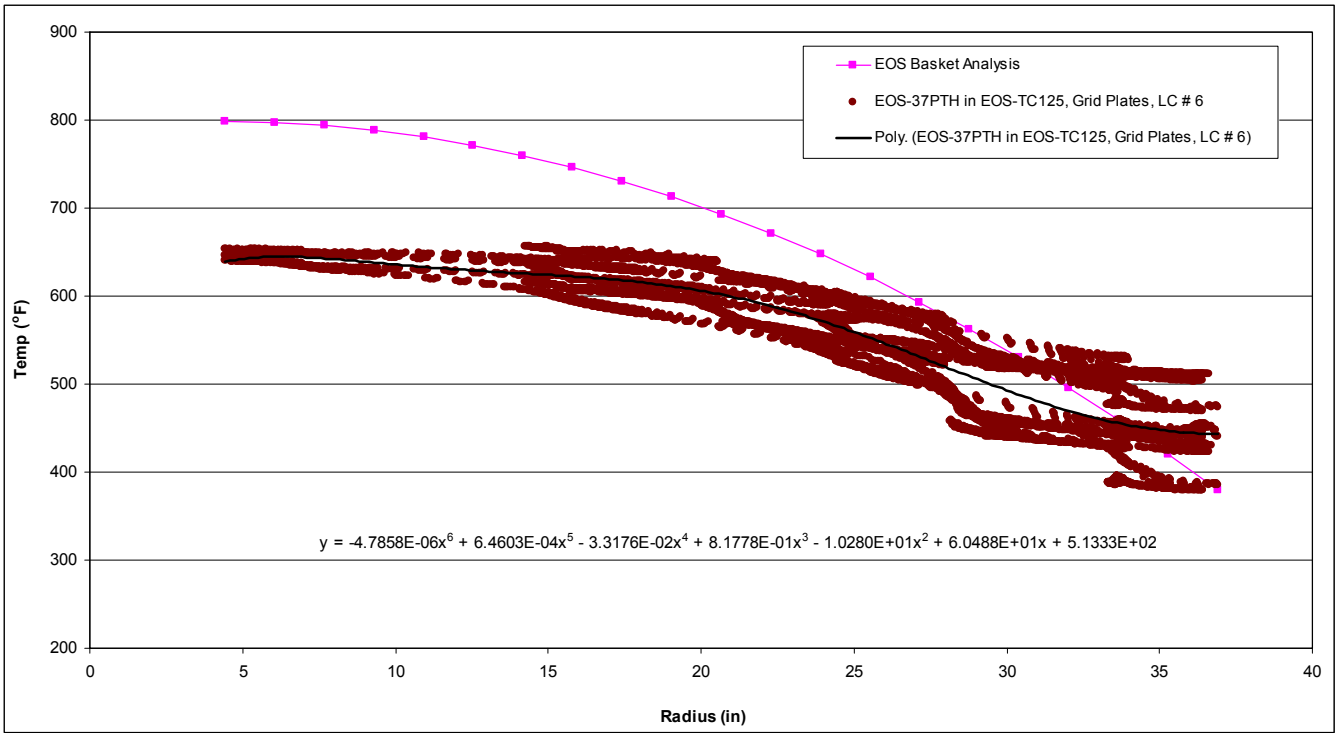

Figure 3.9.2-9
Comparison of Applied Temperature Profile to Data from Thermal Analysis for EOS-37PTH Basket Plates – Hottest Cross-Section, LC # 6, Horizontal, Off-Normal Hot Transfer in EOS-TC125, Outdoor

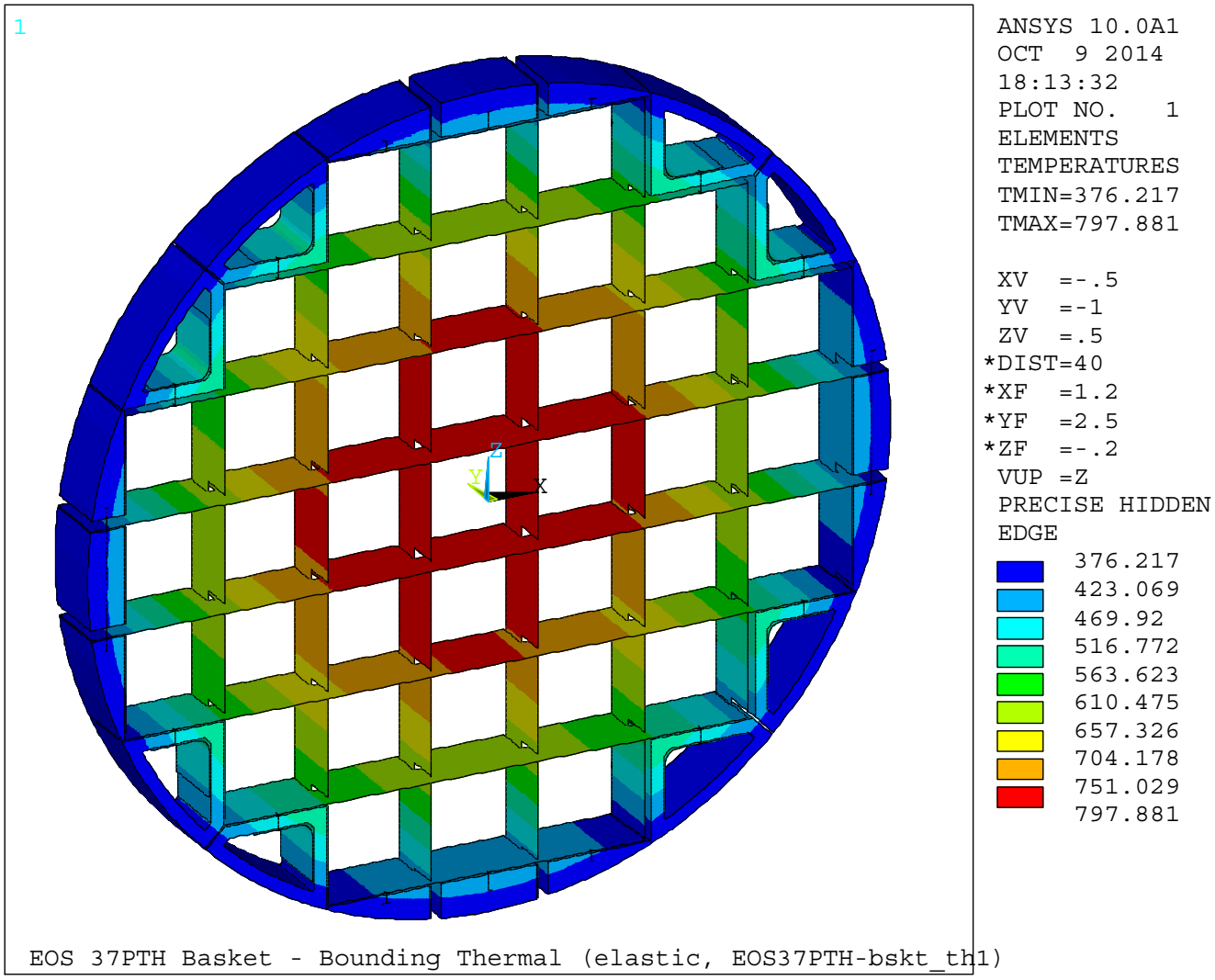

Figure 3.9.2-10
EOS-37PTH Basket Assembly ANSYS Model – Applied Bounding Thermal Profile

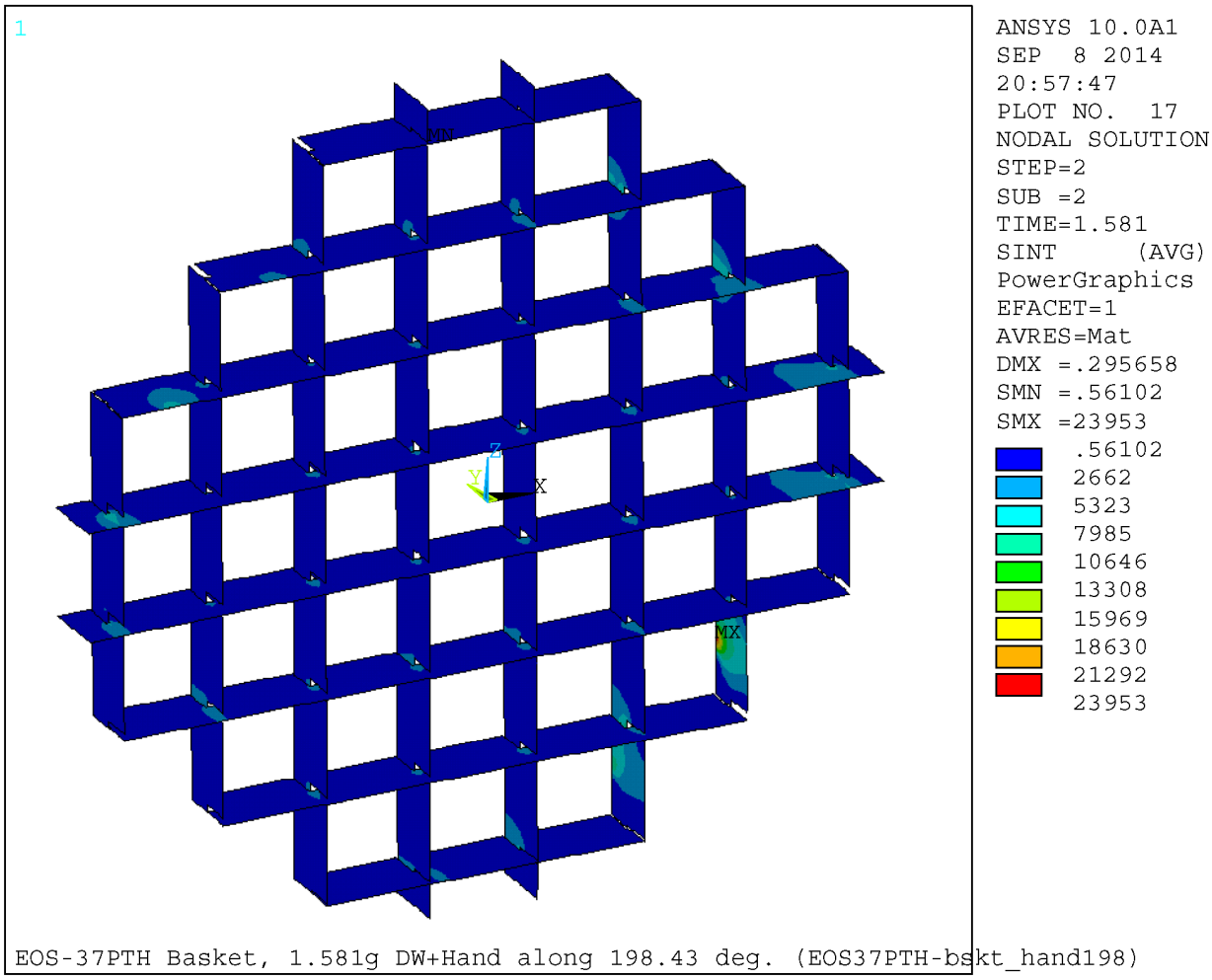

Figure 3.9.2-11
EOS-37PTH Basket 198.43 Degree 1.581g, DW + Handling – Grid Plates, $P_m + P_b$ (stress intensity, psi)

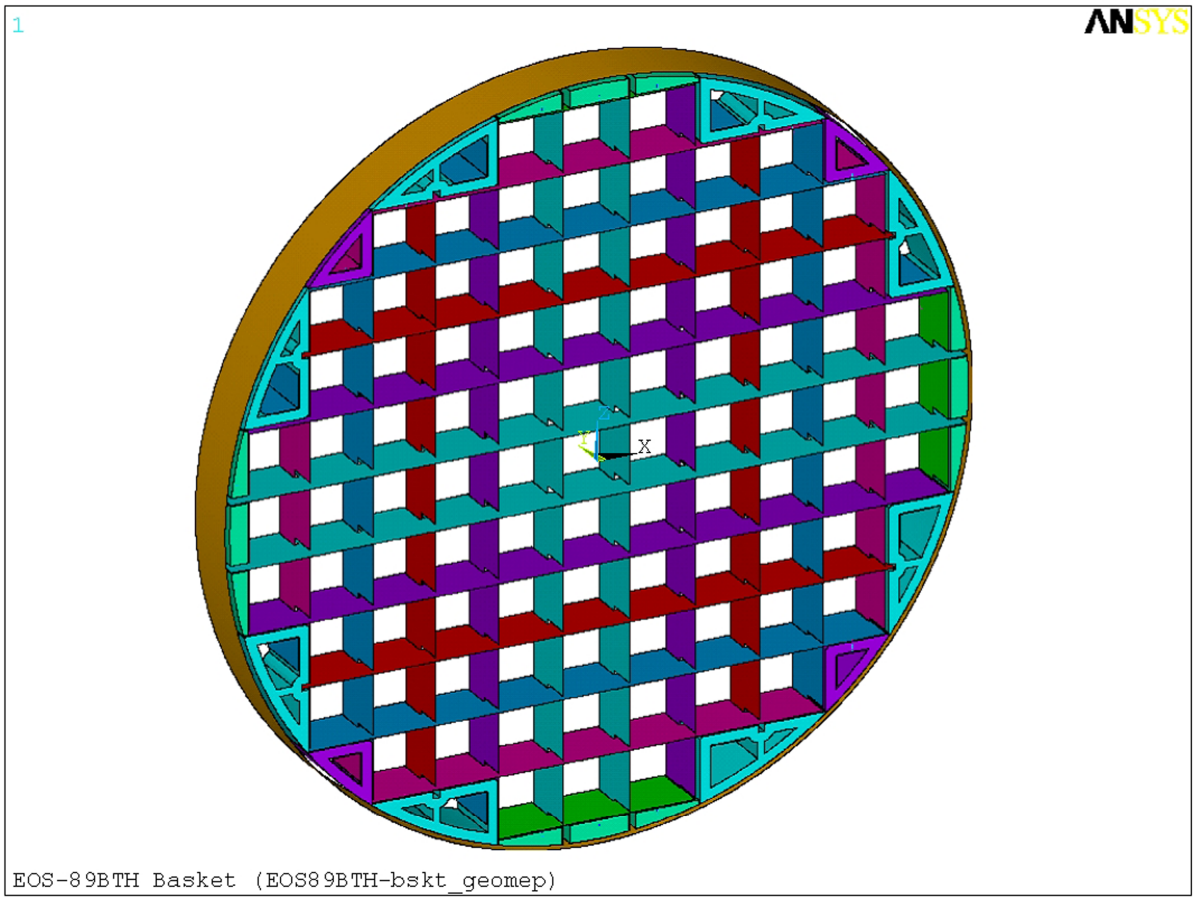

Figure 3.9.2-12
EOS-89BTH Basket Assembly ANSYS Model (Components Only) – Isometric View

Figure 3.9.2-13
EOS-89BTH Basket Assembly ANSYS Model (Components Only) –
Isometric View –
Upper-Left Quadrant

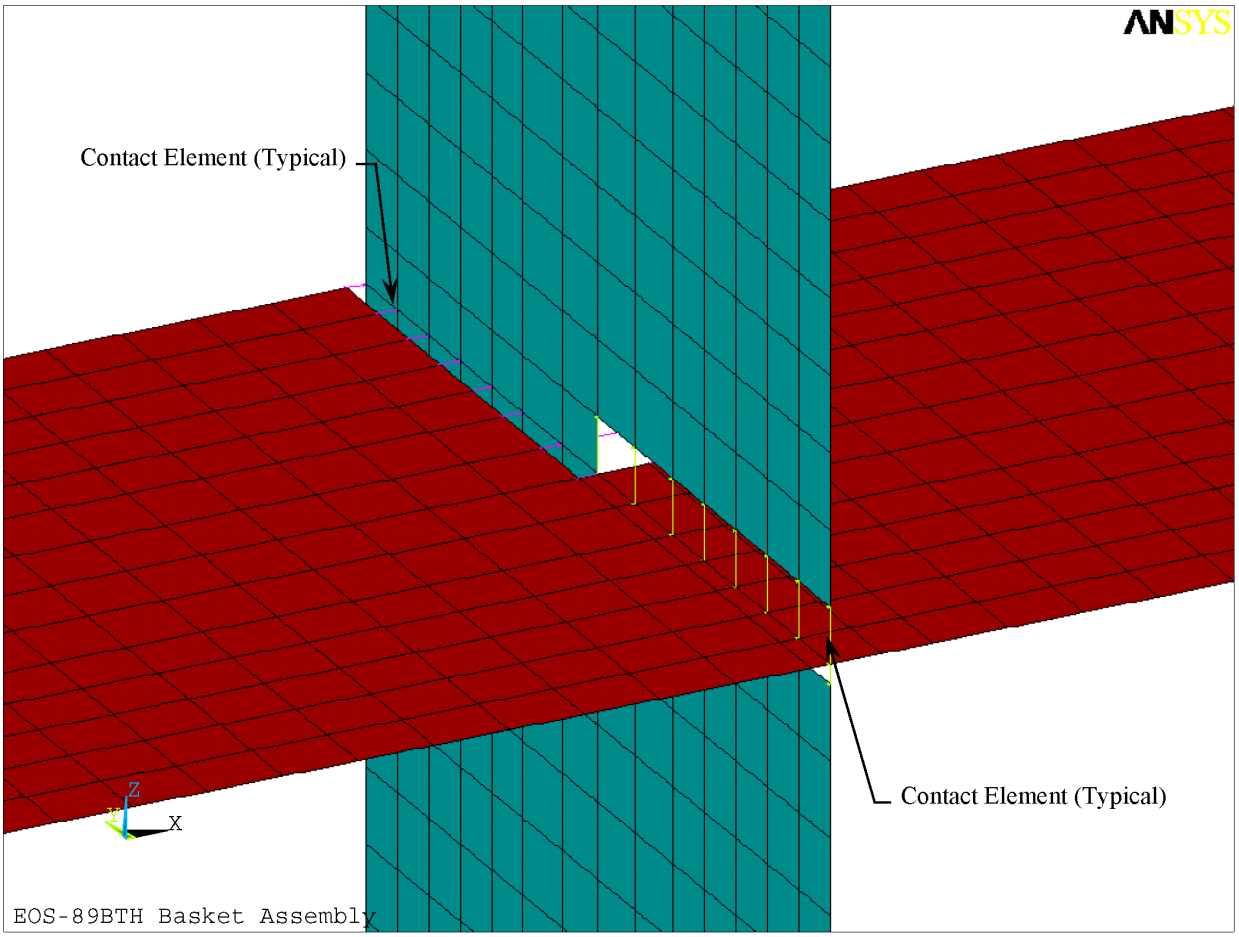

Figure 3.9.2-14
EOS-89BTH Basket Assembly Typical Grid Plate Intersection

Figure 3.9.2-15
EOS-89BTH Basket Assembly ANSYS Model (Components Only) – Front View

Figure 3.9.2-16
EOS-89BTH Basket Assembly ANSYS Model (Plate Thicknesses) –
Lower Right Quadrant

Figure 3.9.2-17
EOS-89BTH Basket Assembly ANSYS Model (with Contact Elements) – Lower Right Quadrant

Figure 3.9.2-18
EOS-89BTH Basket Assembly ANSYS Model –
Transition Rail Bolt and Tie Rod Locations

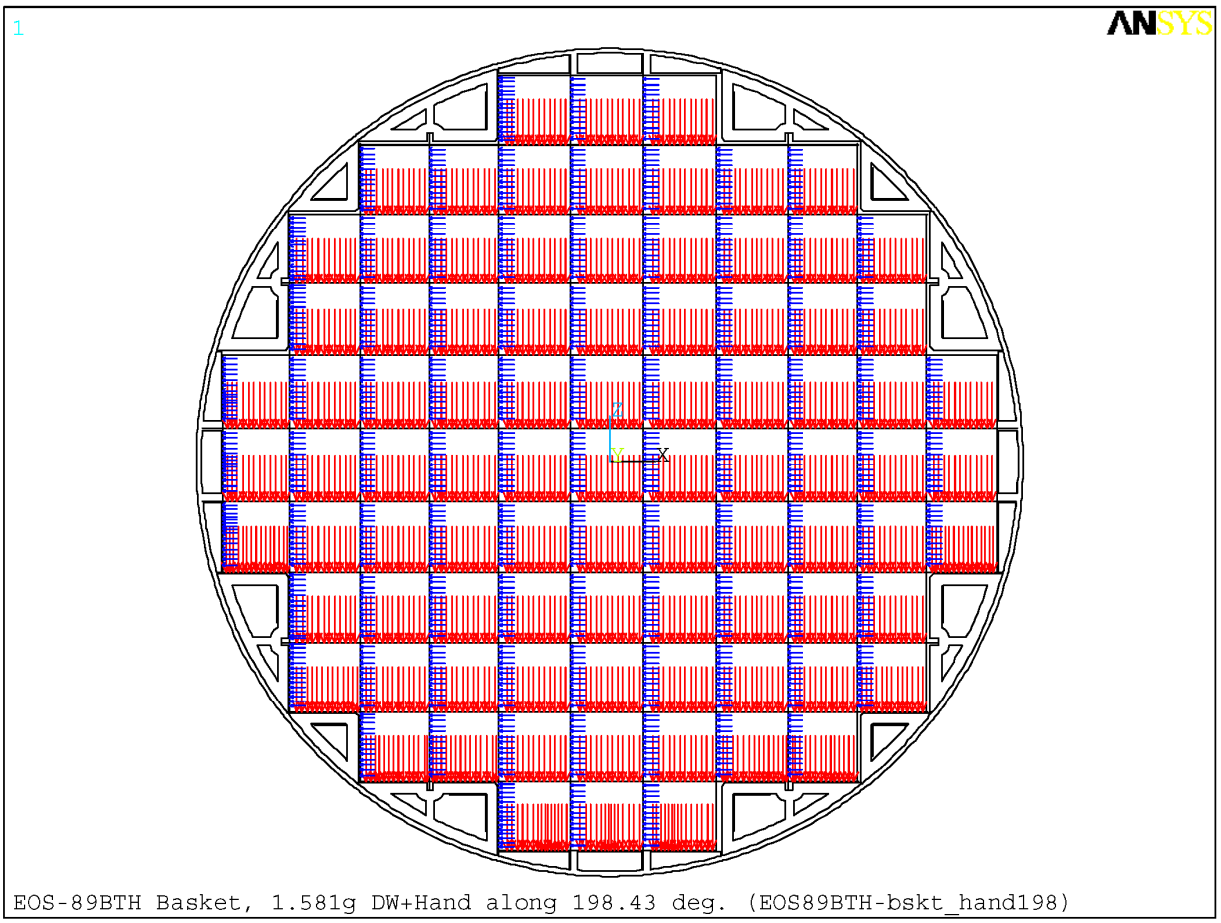

Figure 3.9.2-19
EOS-89BTH Basket Assembly ANSYS Model – Fuel Load Applied as Pressure

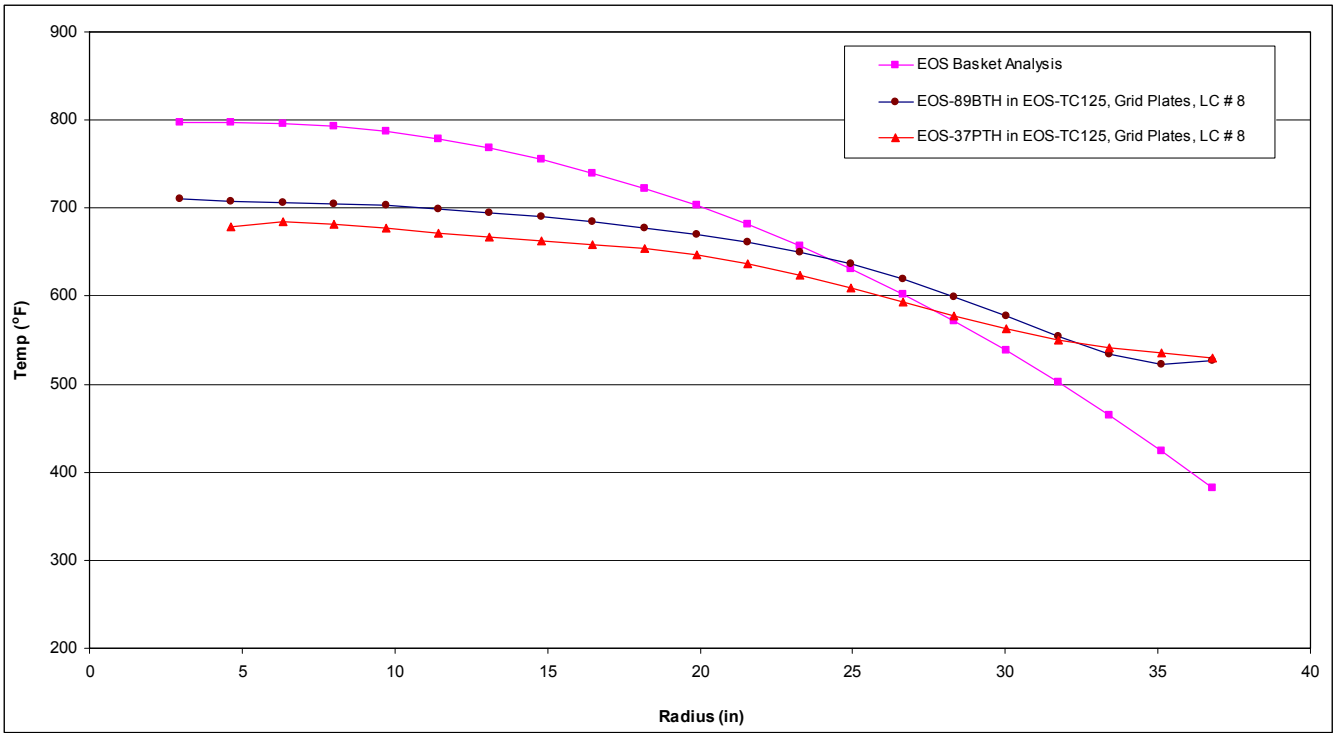

Figure 3.9.2-20
Comparison of EOS-89BTH and EOS-37PTH Temperatures (Curve Fits)
LC # 8, Vertical, Normal Hot Transfer in EOS-TC125, Indoor

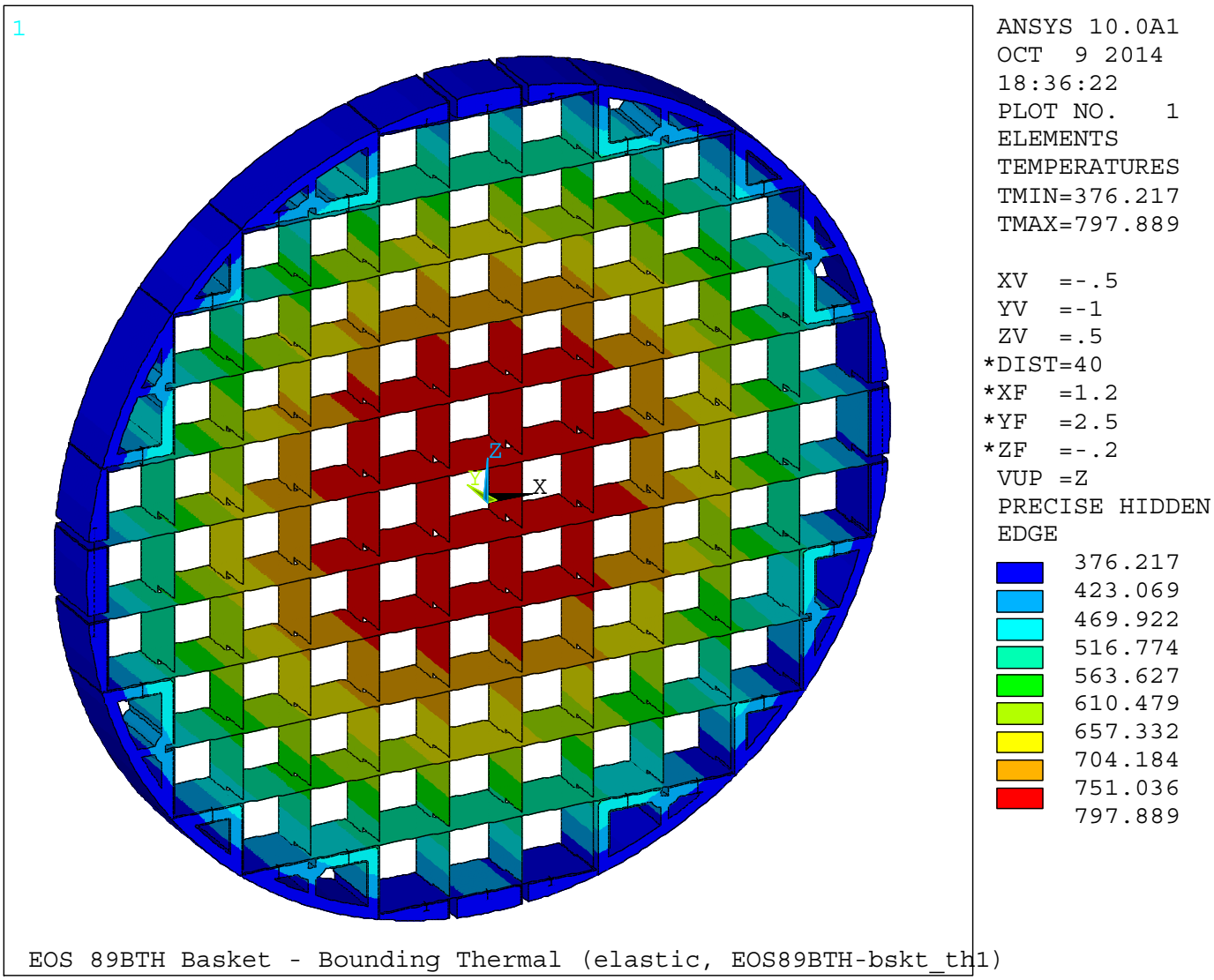

Figure 3.9.2-21
EOS-89BTH Basket Assembly ANSYS Model – Applied Bounding Thermal Profile

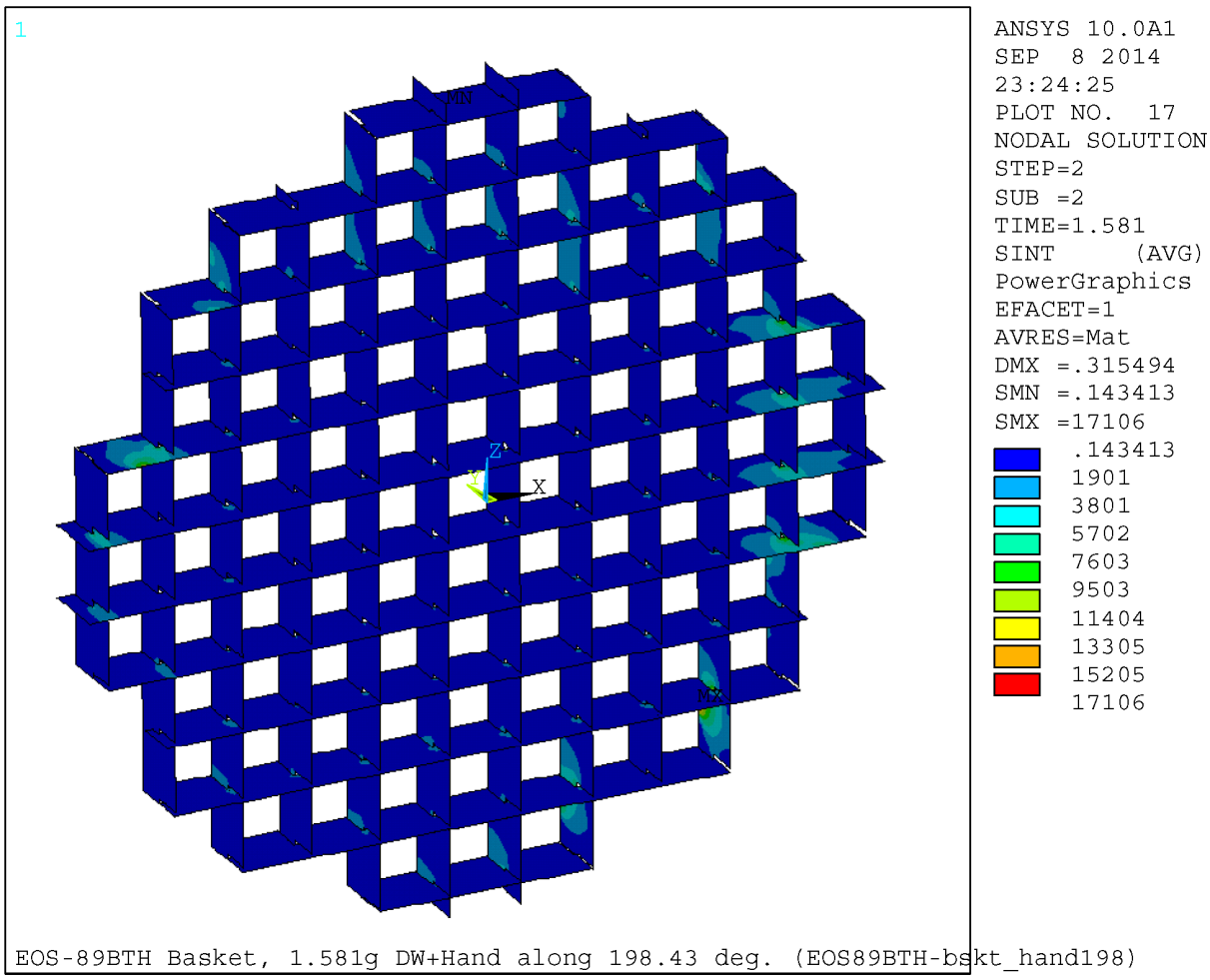

Figure 3.9.2-22
EOS-89BTH Basket 198.43 Degree 1.581g, DW + Handling
– Grid Plates, $P_m + P_b$ (stress intensity, psi)

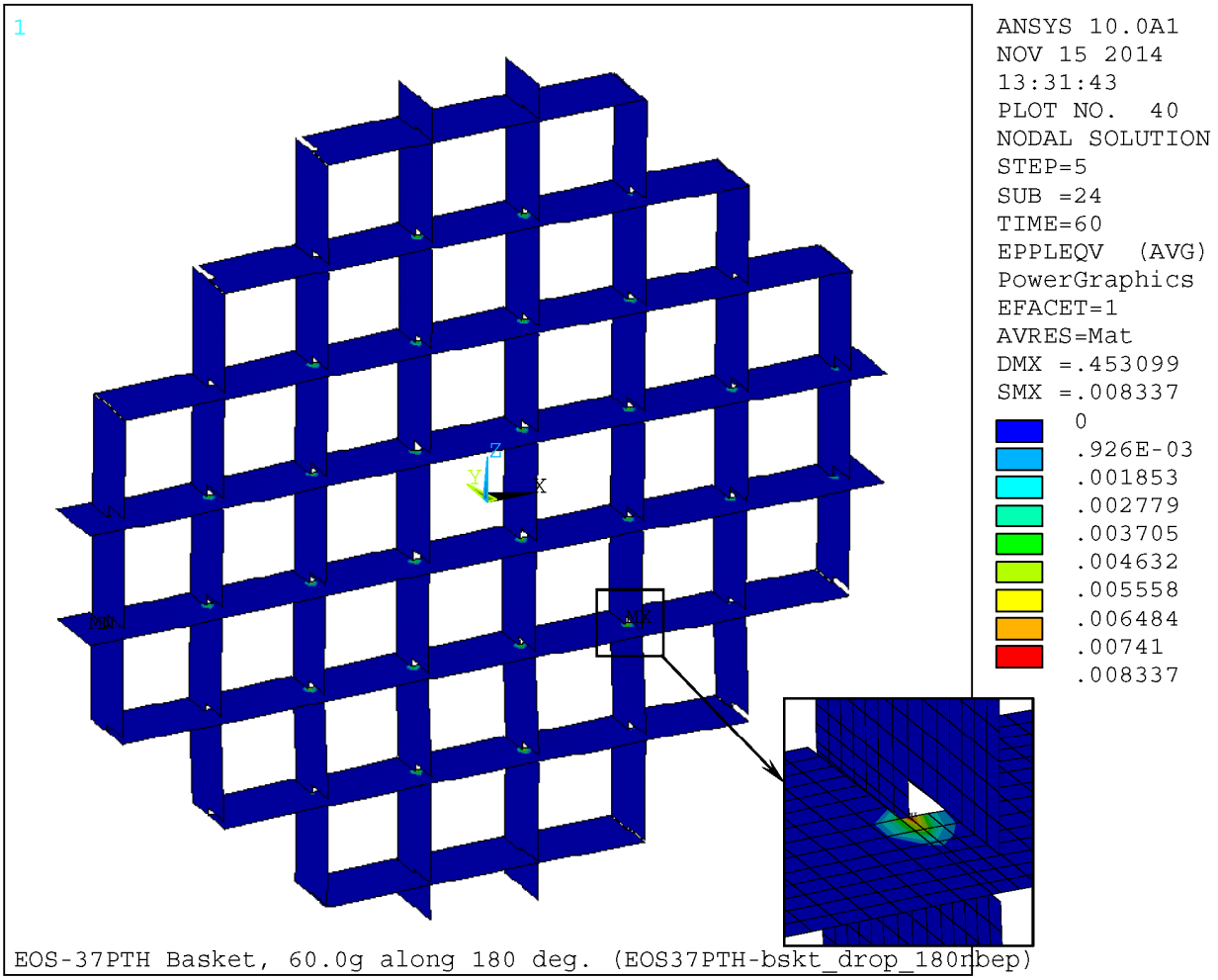

Figure 3.9.2-23
EOS-37PTH Basket 180 Degree 60g Side Drop (without bolts / tie rods) – Grid Plates, $\varepsilon_m + \varepsilon_b$ (von Mises Plastic Strain, in/in)

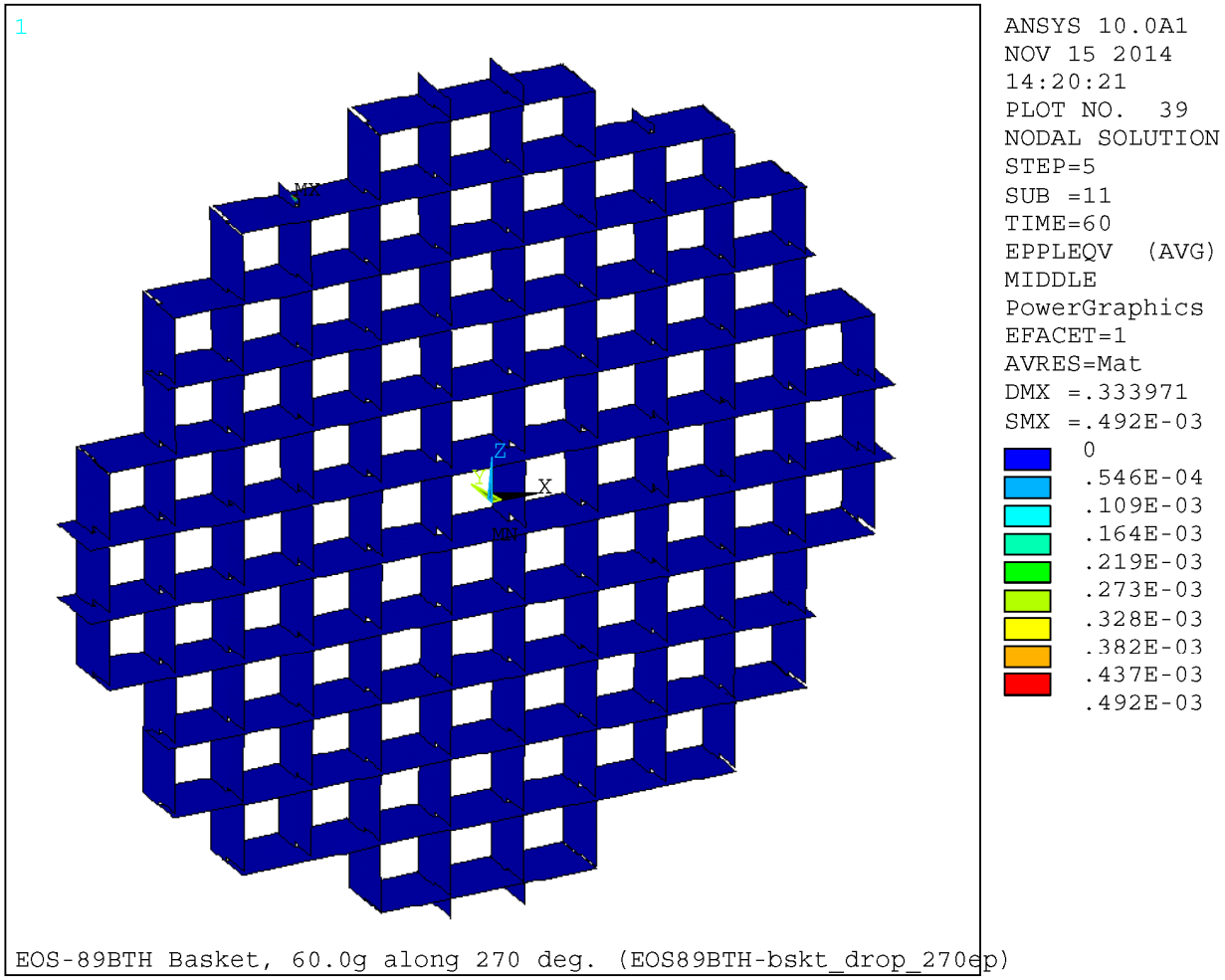

Figure 3.9.2-24
EOS-89BTH Basket 270 Degree 60g Side Drop (with bolts / tie rods) – Grid Plates, ε_m (von Mises Plastic Strain, in/in)

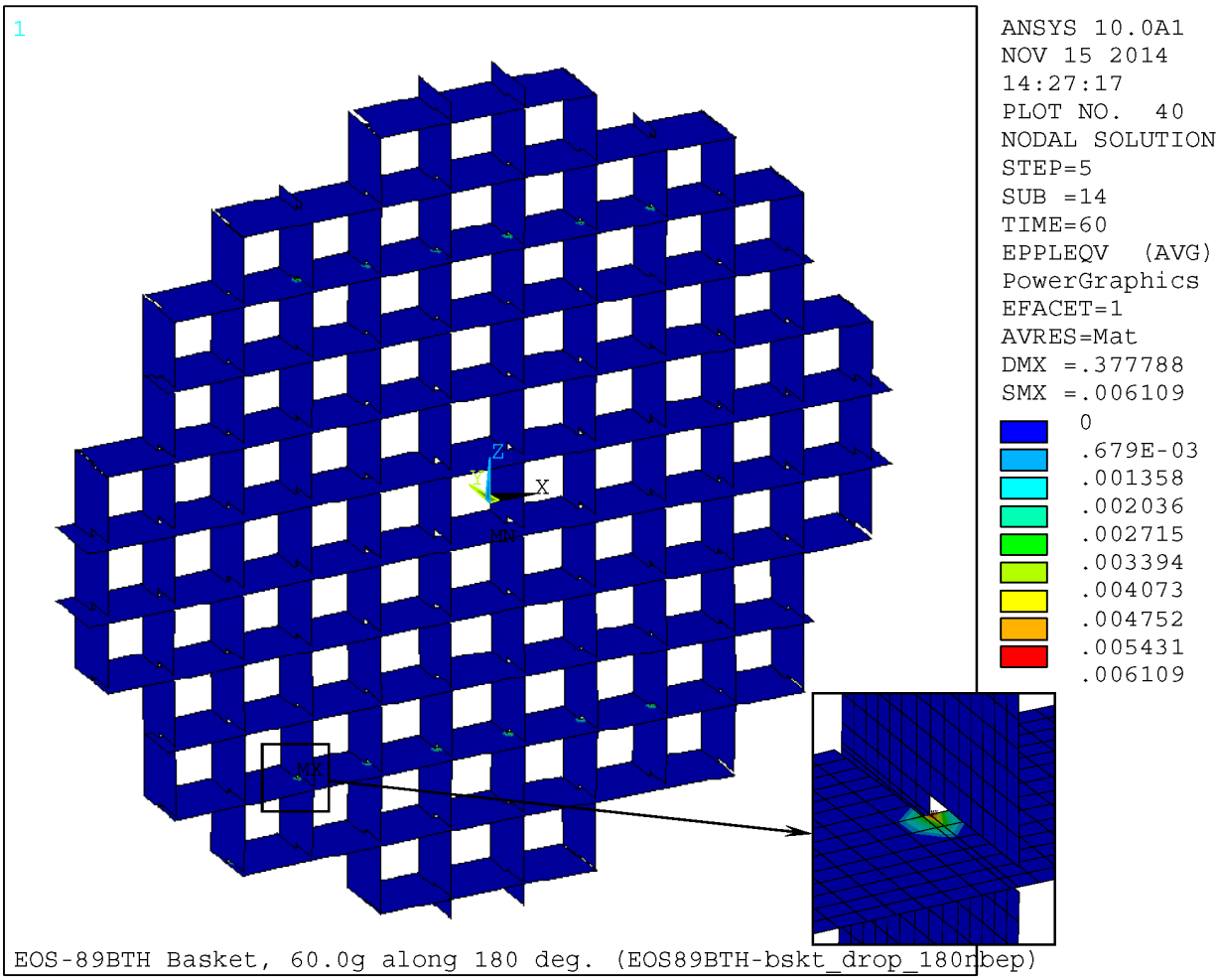

Figure 3.9.2-25
EOS-89BTH Basket 180 Degree 60g Side Drop (without bolts / tie rods) – Grid Plates, $\varepsilon_m + \varepsilon_b$ (von Mises Plastic Strain, in/in)